# Lateral MIMO-control of a bus

Enkuer, E.

*Award date:*
1998

Eindhoven University of Technology
Department of Electrical Engineering
Measurement and Control Group

# Lateral MIMO -control of a bus

by

E. Enkür

M.Sc. Thesis
carried out from may 1997 to April 1998
under supervision of Prof. dr. ir. P.P.J. van den Bosch and ir. D. de Bruin
date: April 1998

# *Abstract*

This project deals with the automatic control of the bus. The bus has to ride on a special road, a narrow lane which may not be accessed by any another traffic. To pre- define a reference trajectory some kind of a guiding system has to be used. In the road a (magnetic) guiding - line is placed to determine the lateral position of the bus with a magnetic sensor. Of course there are also other guiding systems such as, discrete markers along the road, vision systems (two cameras).
The controller that has to be designed must deal with many situations during driving.
If the bus has to make a curvature or it has to make a bus- stop and even in the presence of environmental disturbances like wind gusts or the condition of the road-surface (dry, wet, icy), the controller still has to cover in all this situations i.e. it must keep the bus on the track.
We have designed a MIMO, $H_\infty$-controller for the lateral position of the bus.
To design such a controller the following steps has to be taken.
First the dynamics of the bus are modeled. Therefore equations of motion of the vehicle (kinematics) and forces that occurs between road-tire contact are investigated. Some parameters of the bus are uncertain like the mass distribution (full , empty bus) or the road conditions mentioned above. All this gives rise to model perturbations and so different dynamics. The controller must then also stabilize the vehicle.
After modeling the vehicle a suitable controller-form has to be chosen, and simulations have to be carried out in order to check of the design specifications are met, followed by some conclusions and recommendations.

# Report on the study "lateral control of a bus"

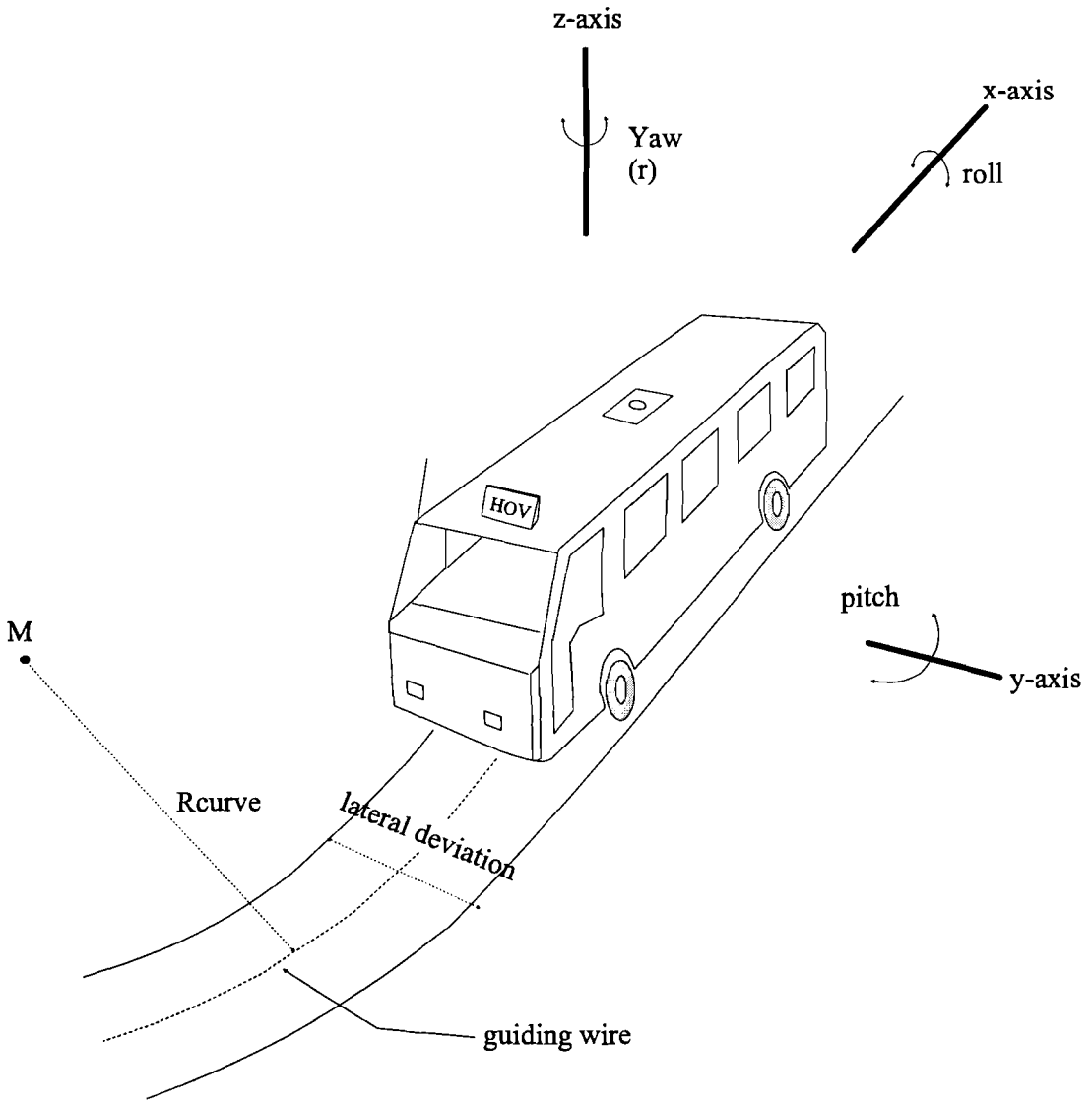


**Moving directions of the bus; We consider the Yaw- movement (r) and the lateral deviation from the guiding wire.**

# 1. Introduction

These days, the traffic on the roads grows with the time. As a consequence there is environmental pollution such as air- pollution and noise. The use of fuel especially in the city-traffic is enormous; the cars have to wait by the traffic lights, they have to accelerate or slow down. Of course there are also many accidents because of the still growing number of cars. All these mentioned aspects of traffic asks for a new concept of transportation.
To improve public transport, a new concept for public transport has been started. This project called the H.O.V. (High quality public transport) has to cope with the growing demands of transportation. If the traffic-flow can be automated completely then unfavorable aspects of the traffic mentioned above can be reduced. There are two control strategies that has to be worked to automate the traffic-flow; The first one is the longitudinal vehicle control (the distance between two vehicles) and the second one is the lateral control of the vehicle (lane keeping). An automatic control system to control the lateral and longitudinal position of a bus is described by: van den Bosch [1]. A feed-forward controller for the lateral position is described by: de Bruin [2].
In this work we will consider the lateral control of a vehicle. We have designed a MIMO, $H_\infty$-controller for the lateral position of the bus. The vehicle is an hybride bus, in this bus, the advantages of the tram and the bus are combined. The bus is powered by electro-motors who 's energy is supplied by a generator, which is coupled on a gas-motor. The bus consists of three carriages. We consider in this study only one (front) carriage, the tractor. All the wheels of the vehicle can be controlled independently by means of electronic controllers (Mechatronics= Mechanics and electronics). In this new concept many disciplines of engineering are involved.

This project deals with the automatic control of the bus. The bus has to ride on a special road, a narrow lane which may not be accessed by any another traffic. To pre- define a reference trajectory some kind of a guiding system has to be used. In the road a (magnetic) guiding - line is placed to determine the lateral position of the bus with a magnetic sensor. Of course there are also other guiding systems such as, discrete markers along the road, vision systems (two cameras).
The controller that has to be designed must deal with many situations during driving.
If the bus has to make a curvature or it has to make a bus- stop and even in the presence of environmental disturbances like wind gusts or the condition of the road-surface (dry, wet, icy), the controller still has to cover in all this situations i.e. it must keep the bus on the track.
To design such a controller the following steps has to be taken.
First the dynamics of the bus are modeled. Therefore equations of motion of the vehicle (kinematics) and forces that occurs between road-tire contact are investigated. Some parameters of the bus are uncertain like the mass distribution (full , empty bus) or the road conditions mentioned above. All this gives rise to model perturbations and so different dynamics. The controller must then also stabilize the vehicle.
After modeling the vehicle a suitable controller-form has to be chosen, and simulations have to be carried out in order to check of the design specifications are met, followed by some conclusions and recommendations.

# 2. Modeling of a 4WS-car.

To describe the (steering) dynamics of the four-wheel steered car we use the single-track model of Riekert- Schunk [4], this model is also used by Ackermann [5,6]. It is obtained by lumping the two front wheels into one wheel in the center line of the car. The same is done with the two rear wheels. Figure 2.1 gives a model representation of the vehicle. We assume that the vehicle can be seen as a rigid body see [7]

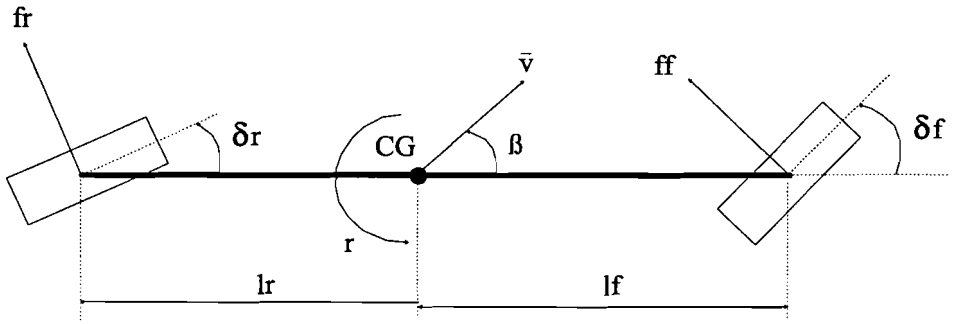


***Figure 2-1: Single track model for four wheel car steering***

*The variables in this figure are:*

CG= Center of gravity
$\delta_f$= front wheel steering angle
$\delta_r$= rear wheel steering angle
$\beta$= side slip angle between vehicle center line and velocity vector at the CG
r = vehicle jaw rate
$f_f$= lateral force generated by the front tire acting on the chassis
$f_r$= lateral force generated by the rear tire acting on the chassis
$l_f$= distance from CG to front axis
$l_r$= distance from CG to rear axis
l= vehicle wheel base, $l = l_f + l_r$
v= velocity of the vehicle

With this model representation, only automatic tracking of one point at the centerline of the vehicle is possible. In this case there is no information about the position of the whole centerline of the vehicle, the point used for tracking can be on the guiding line, but we do not know if the centerline is also on the track ('scharen' )
So we have to augment the model of Ackermann [6] with two tracking points to make automatic tracking possible [2].
In the next section, this will be discussed. Also the influences of disturbances are incorporated in the model .The roll and pitch dynamics are neglected in this model.
There are two coordinate systems used to refer the vehicles motion. One is the vehicle fixed coordinate system and the second is the world fixed coordinate system. For controller design we use the model in "vehicle directions" that is, the vehicle fixed coordinate system. To describe the vehicles motion to a certain reference trajectory (or reference point) we use a world fixed coordinate system. Figure 2.2 shows the coordinate frames.
Also coordinate systems are added to every wheel, but this will be treated later.
As mentioned above we assume the vehicle as a rigid body.

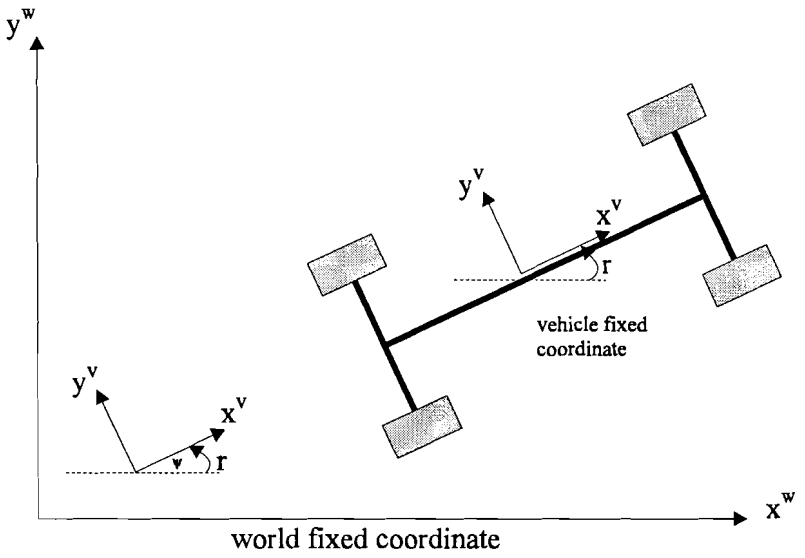


***Figure 2-2: The coordinate systems***

In this figure, we see that the vehicle coordinate system is rotated with an angle ψ in the given jaw-rate direction.

To derive a dynamic model of the vehicle, we need the laws of Newton and Euler. These equations are:

Newton's second law for translational motion : $m \cdot a^v = \Sigma F \quad [N]$

and for the rotational motion: $I \cdot \dot{\omega} = \Sigma M \quad [Nm]$

To use these laws we have to find expressions for the acceleration and the angular acceleration. In general for the acceleration of a rigid body this holds: At any time instant, the derivative of a linear velocity vector is linear acceleration, and the derivative of an angular velocity is angular acceleration, this can be put in the form of an "inertial frame" by using the transformation operator:

$$(d/dt)_I = (\frac{d}{dt})_I^v + \vec{\omega}\times$$

where × is the cross product.

By using this transformation operator the Newton's law becomes:

$$m \cdot \vec{a}^I = m \cdot [(\frac{d\vec{v}^v}{dt})_I + \vec{\omega} x \vec{v}^v)] = \vec{F} \qquad (2.2)$$

We define from now on the vehicle velocity v as: $v = |\vec{v}^v|$ and $\omega = |\vec{\omega}^v|$

## 2.1. Model of the guideline

To derive equations of motion we have to study, figure 2.3.

In this figure there are three velocities to be distinguished:

- velocity at the CG: v
- velocity at the front wheel: $v_f$
- velocity at the rear wheel : $v_r$

These velocities are build up at the tires by the longitudinal and lateral forces. Of course lateral forces depend on the steering angles, if the steering angles are becoming large, then also the lateral forces are getting larger. The steering angles are bounded as will be discussed later in the design specifications.
In the vehicle frame, the velocities and angular accelerations can be written as:

$$v = \begin{bmatrix} v \cdot \cos\beta \\ v \cdot \sin\beta \\ 0 \end{bmatrix} \quad \text{movement in the xy- plane, and} \qquad \omega = \begin{bmatrix} 0 \\ 0 \\ r \end{bmatrix}$$

The first element (top) of this vector is the longitudinal component of v and the second, is the lateral component.

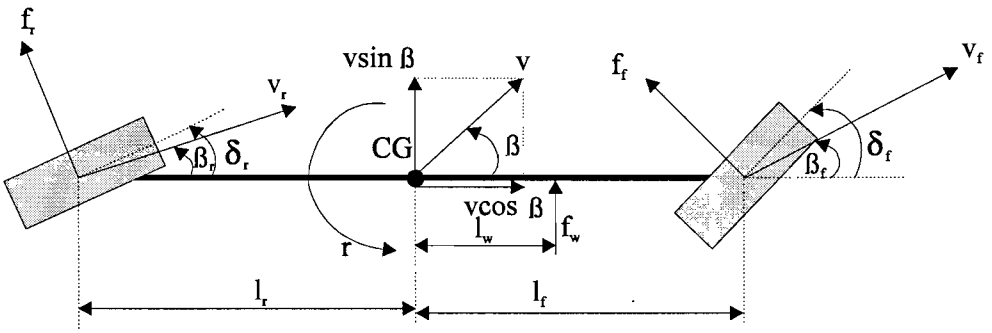


***Figure 2-3. Extended single track model***

In this figure $f_w$ is a disturbance force caused by the wind.
To calculate the *acceleration* in inertial frame we have to differentiate the velocities with (2.1) this results in

$$(\frac{dv}{dt})_I = (\frac{dv^v}{dt})_I + \omega \times v = \begin{bmatrix} \dot{v}\cos\beta - v\dot{\beta}\sin\beta \\ \dot{v}\sin\beta + v\dot{\beta}\cos\beta \\ 0 \end{bmatrix} + \begin{bmatrix} -rv\sin\beta \\ rv\cos\beta \\ 0 \end{bmatrix}$$

Now we can apply the Newton's law (2.2) which results for the longitudinal motion;

$$-mv(\dot{\beta} + r)\sin\beta + m\dot{v}\cos\beta = f_x \tag{2.3}$$

and for the lateral motion

$$mv(\dot{\beta} + r)\cos\beta + m\dot{v}\sin\beta = f_y \tag{2.4}$$

For the yaw- motion of the vehicle

$$J\dot{r} = m_z \tag{2.5}$$

We can combine (2.3), (2.4) and (2.5) to

$$\begin{bmatrix} mv(\dot{\beta}+r) \\ m\dot{v} \\ J\dot{r} \end{bmatrix} = \begin{bmatrix} -\sin\beta & \cos\beta & 0 \\ \cos\beta & \sin\beta & 0 \\ 0 & 0 & 1 \end{bmatrix} \begin{bmatrix} f_x \\ f_y \\ m_z \end{bmatrix} \tag{2.6}$$

with the forces $f_x$, $f_y$ and the torque $m_z$,

$$\begin{bmatrix} f_x \\ f_y \\ m_z \end{bmatrix} = \begin{bmatrix} -\sin\delta_f & -\sin\delta_r & 0 \\ \cos\delta_f & \cos\delta_r & 1 \\ l_f\cos\delta_f & -l_r\cos\delta_r & l_w \end{bmatrix} \begin{bmatrix} f_f \\ f_r \\ f_w \end{bmatrix} \tag{2.7}$$

From (2.7) we see that the wind force is acting on the vehicle in the lateral direction. The torque $m_z$ is caused by the lateral forces (front, rear) and wind force.
For small values of $\delta_f$, $\delta_r$ we can linearize (2.7) to

$$\begin{bmatrix} f_x \\ f_y \\ m_z \end{bmatrix} = \begin{bmatrix} -\delta_f & -\delta_r & 0 \\ 1 & 1 & 1 \\ l_f & -l_r & l_w \end{bmatrix} \begin{bmatrix} f_f \\ f_r \\ f_w \end{bmatrix} \tag{2.8}$$

with $f_f$, ($f_r$) the lateral forces generated by the front (rear) tire, acting on the chassis, figure 2.4 shows this. The second figure shows the directions of the dissolved forces.

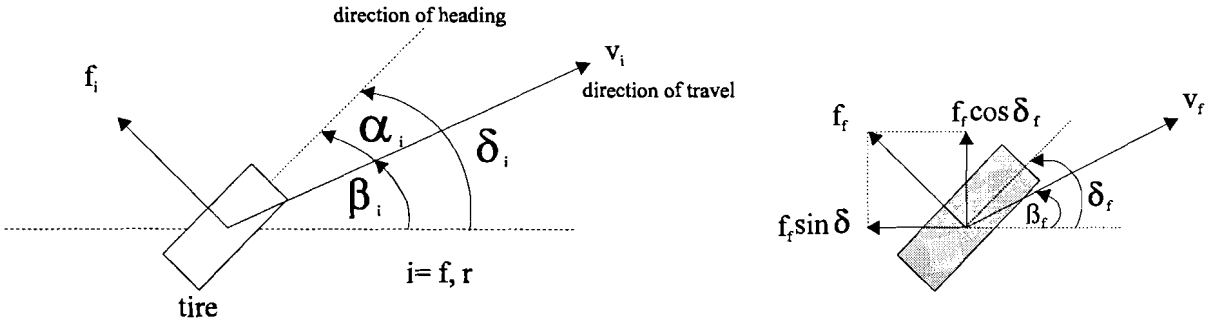


***Figure 2-4. Forces generated by the tires***

The lateral forces depend on the slip angles, $\alpha_f$ and $\alpha_r$. These are the angles between the direction of travel and the direction of heading of the wheels, Ackermann [6].

$$f_f = f_f(\alpha_f)$$
$$f_r = f_r(\alpha_r)$$

As can be seen in figure 2-3 , the velocity components in the longitudinal direction are equal, so:

$$v_r\cos\beta_r = v_f\cos\beta_f = v\cos\beta \tag{2.9}$$

$\beta$ is the angle between vehicle center and velocity vector at the CG. $\beta_f$ and $\beta_r$ are the angles between the centerline of the vehicle and the direction of travel as defined in figure 2-3
The lateral components depend on the jaw- rate r

$$v_f \sin\beta_f = v\sin\beta + l_f r \qquad (2.10)$$
$$v_r \sin\beta_r = v\sin\beta - l_r r$$

with (2.9) and (2.10) we can find expressions for side slip angles at the front and rear wheels:

$$\tan\beta_f = \tan\beta + \frac{l_f \cdot r}{v\cos\beta}$$
$$\tan\beta_r = \tan\beta - \frac{l_r \cdot r}{v\cos\beta}$$

If the side slip $\beta << 1$ then this can be linearized to

$$\beta_f = \beta + \frac{l_f \cdot r}{v}$$
$$\beta_r = \beta - \frac{l_f \cdot r}{v}$$

The local velocity $\vec{v}_f^{\,v}$ forms the (chassis) slip angle $\beta_f$ with the car body and tire slip angle $\alpha_f$ with the tire direction. If we use the expressions stated above for $\beta_f$ and $\beta_r$ then expressions for the slip angles become

$$\alpha_f = \delta_f - \beta_f = \delta_f - \beta - \frac{l_f \cdot r}{v}$$

and

$$\alpha_r = \delta_r - \beta_r = \delta_r - \beta + \frac{l_r \cdot r}{v}$$

The tire forces are linearized as

$$f_f = \mu \cdot C_f \cdot \alpha_f = \mu \cdot C_f(\delta_f - \beta - \frac{l_f \cdot r}{v})$$
$$f_r = \mu \cdot C_r \cdot \alpha_r = \mu \cdot C_r(\delta_r + \beta - \frac{l_r \cdot r}{v})$$

where the cornering stiffnesses $C_f$ and $C_r$ are the tire parameters, and $\mu$ is the road adhesion factor which models the road / tire contact. Values for $\mu$ are within the interval $\mu \in [0.1;1]$. Figure 2.5 shows the cornering forces against tire side slip angle.

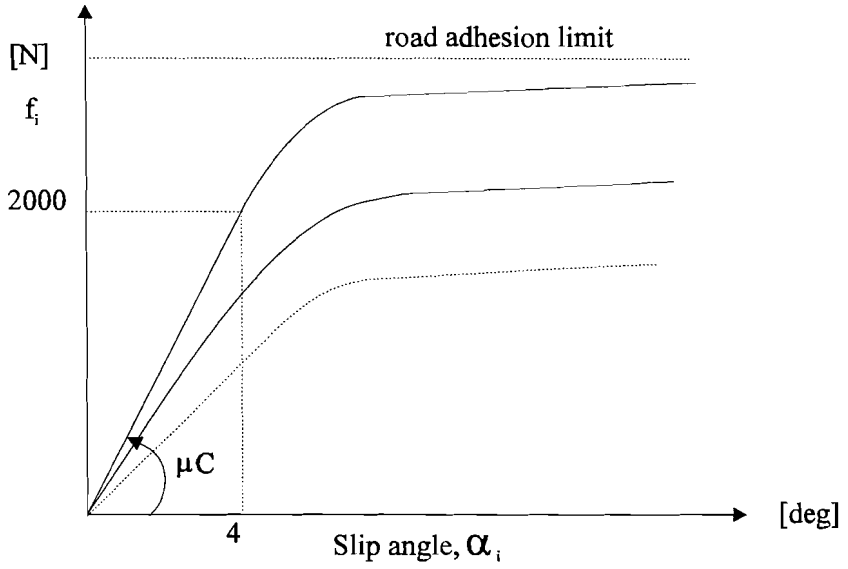


***Figure 2-5. Cornering forces***

The value of μ is 0.1 if the road is icy and 0.5 if the road is wet, for dry road this value is 1. Figure 2.5 shows also the linear area for the cornering forces, if we exceed this linear area ($\alpha \approx 4°$) and so enter the non- linear region then we must careful in the use of the linear tire model. In this case the nonlinear model of PACEJCA "the magic formula" can be used. See also Engelaar [3]

If $\beta << 1$, and v is constant (we consider only the lateral motion, $m\dot{v}=0$ in (2.6)), with the substitution of equations (2.7) and (2.8) in eq. 2.6 we have,

$$\begin{bmatrix} mv(\dot{\beta}+r) \\ J\cdot\dot{r} \end{bmatrix} = \begin{bmatrix} 1 & 1 & 1 \\ l_f & -l_r & l_w \end{bmatrix} \begin{bmatrix} f_f \\ f_r \\ f_w \end{bmatrix}$$

This is the single track model of car steering.

With $mv(\dot{\beta}+r)$ =$F_{\text{steering force}}$ and $J\cdot\dot{r}=m_z$ the torque which are generated by the lateral tire forces $f_f$ and $f_r$.

With the expressions for $f_f$ and $f_r$ substituted this becomes

$$\begin{bmatrix} mv(\dot{\beta}+r) \\ J\cdot\dot{r} \end{bmatrix} = \begin{bmatrix} 1 & 1 & 1 \\ l_f & -l_r & l_w \end{bmatrix} \begin{bmatrix} \mu\cdot C_f(\delta_f - \beta - \frac{l_f\cdot r}{v}) \\ \mu\cdot C_r(\delta_r - \beta + \frac{l_r\cdot r}{v}) \\ f_w \end{bmatrix}$$

this can be written as,

$$\dot{\vec{x}} = A\cdot\vec{x} + B\cdot\vec{u}$$

$$\begin{bmatrix} \dot{\beta} \\ \dot{r} \end{bmatrix} = \begin{bmatrix} a_{11} & a_{12} \\ a_{21} & a_{22} \end{bmatrix} \begin{bmatrix} \beta \\ r \end{bmatrix} + \begin{bmatrix} b_{11} & b_{12} & \frac{1}{mv} \\ b_{21} & b_{22} & \frac{l_w}{J} \end{bmatrix} \begin{bmatrix} \delta_f \\ \delta_r \\ f_w \end{bmatrix} \tag{2.8}$$

with the coefficients of the ***A*** - matrix,

$$a_{11} = \frac{-(c_r + c_f)}{\tilde{m}v} \qquad a_{12} = -1 + \frac{(c_r l_r - c_f l_f)}{\tilde{m}v^2}$$

$$a_{21} = \frac{(c_r l_r - c_f l_f)}{\tilde{J}} \qquad a_{22} = \frac{-(c_r l_r^2 + c_f l_f^2)}{\tilde{J}v}$$

and with the coefficients of the ***B*** - matrix,

$$b_{11} = \frac{c_f}{\tilde{m}v} \qquad b_{12} = \frac{c_r}{\tilde{m}v}$$

$$b_{21} = \frac{c_f l_f}{\tilde{J}} \qquad b_{22} = \frac{-c_r l_r}{\tilde{J}}$$

The vehicle mass is normalized by a road adhesion factor μ, i.e. $\tilde{m}=m/\mu$ is a "virtual mass". Similarly, the moment of inertia J is normalized as $\tilde{J}=J/\mu$.

We have now modeled the lateral and the yaw motion of the vehicle. Next, we have to model the vehicle's motion in circular cornering with respect to a certain reference line (guideline). This will be done in the next subsection. This subsection starts with describing the circular path.

## 2.2. The circular path

In order to study automation of car steering, the steering model is extended. The model must include not only velocities, but also the vehicle heading and the lateral position of the displacement sensor with respect to the reference path. In this extended model we use a linear model that is valid for small deviations from a stationary circular path. It is assumed that the reference consists of circular arcs. Figure 2.6 shows the transition from an arc with radius R1 and center M1 to an arc with radius R2 and center M2. At the transition point the tangent to the path is continuous. There is, however, a step change in the reference input from $R_{ref} = R_1$ to $R_{ref} = R_2$. For straight path segments the radius is $R_{ref} = \infty$.

It is more convenient to introduce the curvature $\rho_{ref} := 1 / R_{ref}$ as the input that generates the reference path.

The curvature is defined positive for left cornering and negative for right cornering.

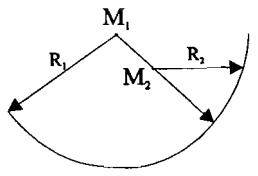


***Figure 2-6. The reference path is comprised of circular arcs.***

The vehicle motion in circular cornering can be modeled for small deviations from a stationary circular path.

Figure 2.7 shows the modified model for automatic tracking. In this model , $y_{CG}$ is the lateral deviation of the center of mass. The two tracking points $y_f$ and $y_r$ are the lateral deviations of the front and rear sensors respectively. There are two coordinate systems in this figure one earth-fixed coordinate system $(x_o,y_o)$ and the other is a vehicle fixed coordinate system $(x_v,y_v)$, which is rotated by the jaw angle $\psi$, $\psi_t$ is the angle between $x_o$ and the tangent to the path. The tangent to the path denoted by $V_t$ is rotated by a reference jaw angle $\psi_t$ ; $\Delta\psi=\psi-\psi_t$ is the angle between the path and the centerline of the vehicle and $f_w$ is the disturbance force due to wind.

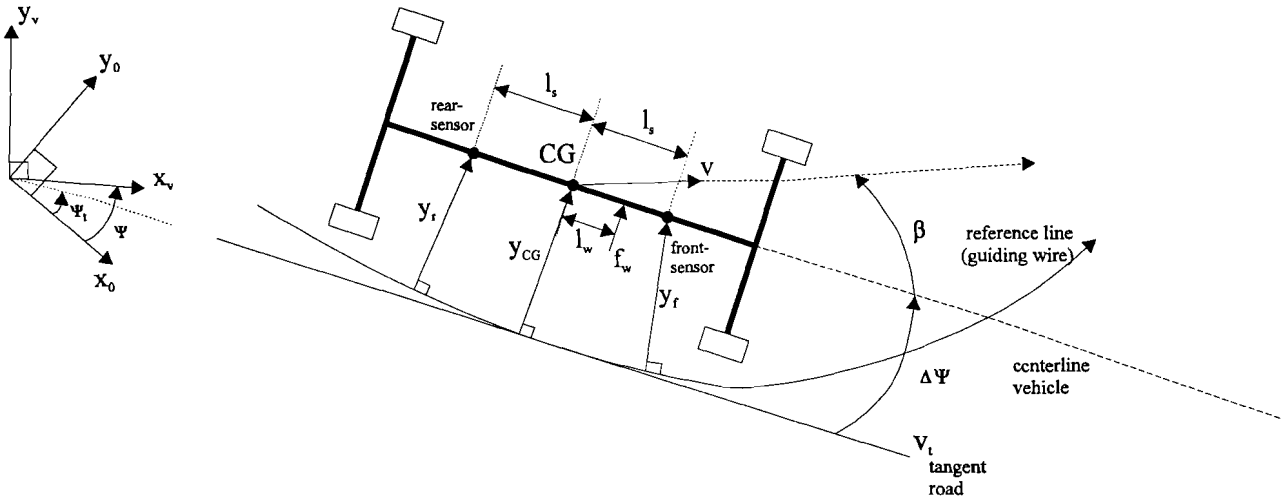


***Figure 2-7. Model for automatic track following.***

A model for the rate of change of $y_{CG}$ will now be developed . The component of the car velocity v that is perpendicular to $v_t$ is equal to the rate of change of $y_{CG}$. This perpendicular component is given by $v \sin(\beta+\Delta\psi)$ where $\beta$ is the car sideslip angle. With the linearization $\sin(\beta+\Delta\psi) \approx \beta+\Delta\psi$ the deviation $y_{CG}$ changes according to

$$\dot{y}_{CG} = v(\beta + \Delta\psi) \tag{2.9}$$

where, v is the vehicle's velocity. The front sensor is mounted at a distance $l_s$ in front of the CG while the rear sensor is mounted at a distance $l_s$ rear of the CG with $|l_s| << R_{ref}$ .

The measured displacement $y_{CG}$ from the guiding wire now changes both with $\dot{y}_{CG}$ and under the influence of the jaw rate $r=\dot{\psi}$ [rad/sec]. Taking this into account the velocity of the front sensor is,

$$\dot{y}_f = \dot{y}_{CG} + l_s(r - v \cdot \rho_{ref}) \tag{2.10}$$

where, $\rho_{ref}$ is the path curvature at CG. The same can be done for the rear sensor the velocity is then,

$$\dot{y}_r = \dot{y}_{CG} - l_s(r - v \cdot \rho_{ref}) \tag{2.11}$$

The angle $\Delta\psi$ will be obtained by integrating its derivative

$$\Delta\dot{\psi} = \dot{\psi} - \dot{\psi}_t = r - r_{st}$$

The term $r_{st}$ is the yaw rate of the path tangent, $r_{st} = v/R_{ref} = v\rho_{ref}$ in stationary circular cornering.

Hence,

$$\Delta\dot{\psi} = r - v \cdot \rho_{ref} \tag{2.12}$$

So,

$$\Delta\psi = \int (r - v \cdot \rho_{ref})dt$$

with the integration constant omitted.
With the aid of equations(2.8)...(2.12) , we are now able to put the equations of the model in the state space form,

$$\dot{\vec{x}} = A \cdot \vec{x} + B \cdot \vec{u} \tag{2.13}$$

$$\vec{y} = C \cdot \vec{x} + D \cdot \vec{u}$$

from (2.13) it follows,

$$\begin{bmatrix} \dot{\beta} \\ \dot{r} \\ \Delta\dot{\psi} \\ \dot{y}_f \\ \dot{y}_r \end{bmatrix} = \begin{bmatrix} a_{11} & a_{12} & 0 & 0 & 0 \\ a_{21} & a_{22} & 0 & 0 & 0 \\ 0 & 1 & 0 & 0 & 0 \\ v & l_s & v & 0 & 0 \\ v & -l_s & v & 0 & 0 \end{bmatrix} \begin{bmatrix} \beta \\ r \\ \Delta\psi \\ y_f \\ y_r \end{bmatrix} + \begin{bmatrix} b_{11} & b_{12} & 0 & \frac{1}{mv} \\ b_{21} & b_{22} & 0 & \frac{l_w}{J} \\ 0 & 0 & -v & 0 \\ 0 & 0 & -vl_s & 0 \\ 0 & 0 & vl_s & 0 \end{bmatrix} \begin{bmatrix} \delta_f \\ \delta_r \\ \rho_{ref} \\ f_w \end{bmatrix} \tag{2.14}$$

and for the output vector $\vec{y}$:

$$\begin{bmatrix} \beta \\ r \\ \Delta\psi \\ y_f \\ y_r \end{bmatrix} = \begin{bmatrix} 1 & 0 & 0 & 0 & 0 \\ 0 & 1 & 0 & 0 & 0 \\ 0 & 0 & 1 & 0 & 0 \\ 0 & 0 & 0 & 1 & 0 \\ 0 & 0 & 0 & 0 & 1 \end{bmatrix} \begin{bmatrix} \beta \\ r \\ \Delta\psi \\ y_f \\ y_r \end{bmatrix} + \begin{bmatrix} 0 & 0 & 0 & 0 \\ 0 & 0 & 0 & 0 \\ 0 & 0 & 0 & 0 \\ 0 & 0 & 0 & 0 \\ 0 & 0 & 0 & 0 \end{bmatrix} \begin{bmatrix} \delta_f \\ \delta_r \\ \rho_{ref} \\ f_w \end{bmatrix}$$

We assume, that we can measure all the states.

The vehicle mass is normalized by a road adhesion factor μ, i.e. $\bar{m}=m/\mu$ is a "virtual mass". Similarly, the moment of inertia J is normalized as $\bar{J}=J/\mu$.
The equation (2.14) will be reformulated in a form which is suitable for the controller design toolbox MHC [12] in the section "controller design".

## 2.3. Open loop characteristics of the process

The root locus analysis (for the SISO case) of the open loop process (for increasing velocity) is treated thoroughly by Chao[7]. The important outcome is, that the poles move to the Imaginary axis in the left half plane without pushing through to the right half plane. This is also true for the open loop zeros as they become complex for higher speeds (v >15 [m/s]). The open loop poles are real, and stay real, they are dependent on the adhesion coefficient $\mu$, which is a uncertain parameter. This parameter gives rise to robustness problems.

From the steady-state description of the process (bus), we can plot the characteristics. Because this is a MIMO- process with 4 inputs and 5 outputs, we have 20 possible transfers. We assume that we can measure all the outputs. The process is dependent on the parameters $\mu(t)$, the velocity v(t) and the mass of the bus. The variation of the mass is partially represented by the "virtual mass". We discuss the process which is linearized around v=20 [m/s], and $\mu$=0.5 (this choice will become clear later).
The mass is 10000 [kg], $l_w$= 0.565 [m], $c_f$= $c_r$ = 300 [kN/rad]
Figure 2.8 gives the plot of the open loop process:

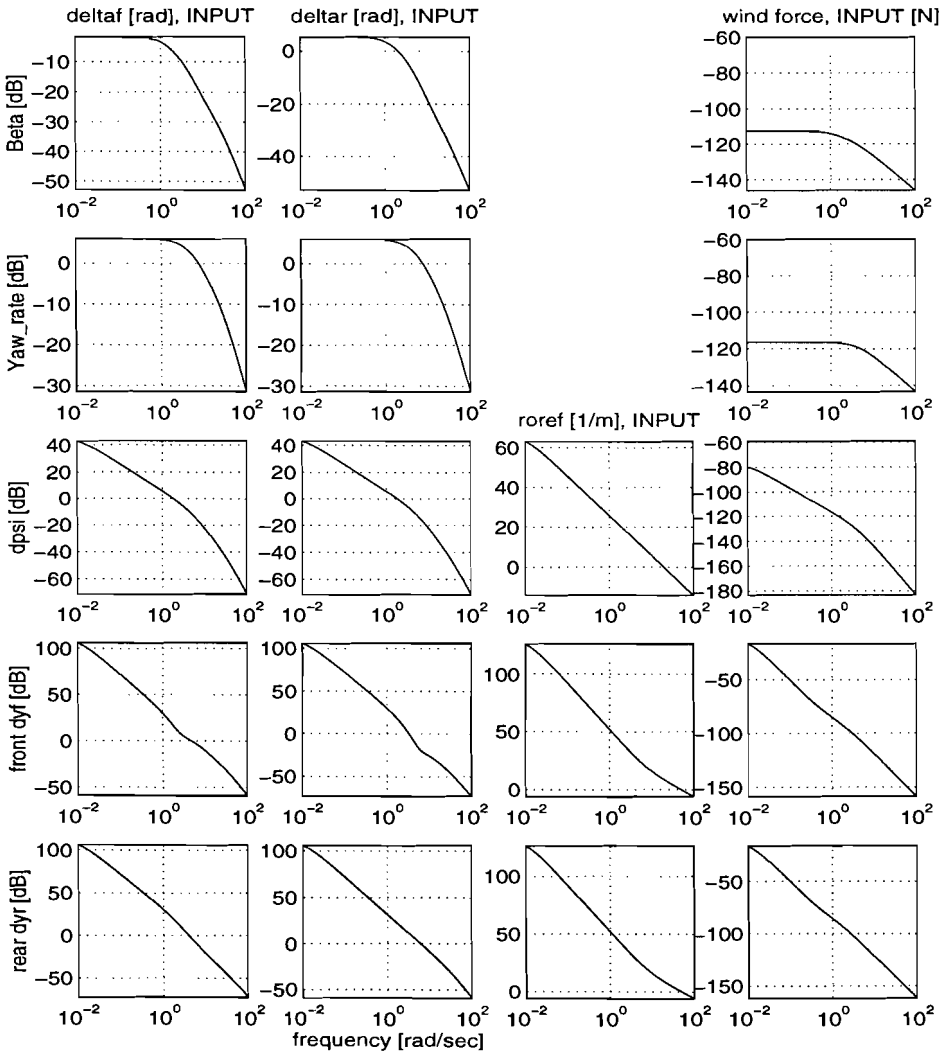


***Figure 2-8: Open loop transfer functions from the inputs (horizontal) to outputs (vertical)***

As can be seen in the figure the strongest magnification is between the inputs (the columns): control inputs deltaf, deltar, roref and the outputs ( the rows): dpsi, dy front and dy rear. The influence of the wind is on the outputs:
dy front and dy rear. There is no transfer between roref and the outputs Beta and Yaw-rate.

An other method to study the behavior of the process is the singular value decomposition. With this method we can see the maximum effect of each input to the output in the given direction of the vectors see Skogestad [10]. This singular value or 'principal gain' can be understood as follows (Skogestad [10]):
Suppose that we have a supermarket cart which we may want to move in three directions: forward, sideward and upward. The strongest direction, corresponding to the largest singular value, will clearly be the forward direction. The next direction, corresponding to the second singular value, will be sideways. Finally, the most "difficult" direction, corresponding with the smallest singular value, will be upwards. Now, suppose that we want to move the cart (supermarket trolley) sideward, then we have to apply a large force, since the singular value in this direction is small. But if we don't know about which direction the car is pointing, then some of our applied force will be directed forward (where the plant gain is large) and the car will suddenly move forward with an undesired large speed. So, this system is "ill-conditioned" since it depends on the "uncertain" direction (i.e. the steering angles, input to the system) of the wheels.

To make a singular value plot of the transfer function G of a open loop process, we have to find an expression for G which can be derived from the state space equations (2.13):

$$G = C(sI - A)^{-1}B$$

The singular value decomposition of this matrix G, is given by

$$G = U\Sigma V^T$$

Where $\Sigma$ is a diagonal matrix containing the singular values and $V^T$, U are unitary matrices for the input respectively, the output.
The open loop singular value plots are given in figure 2.9

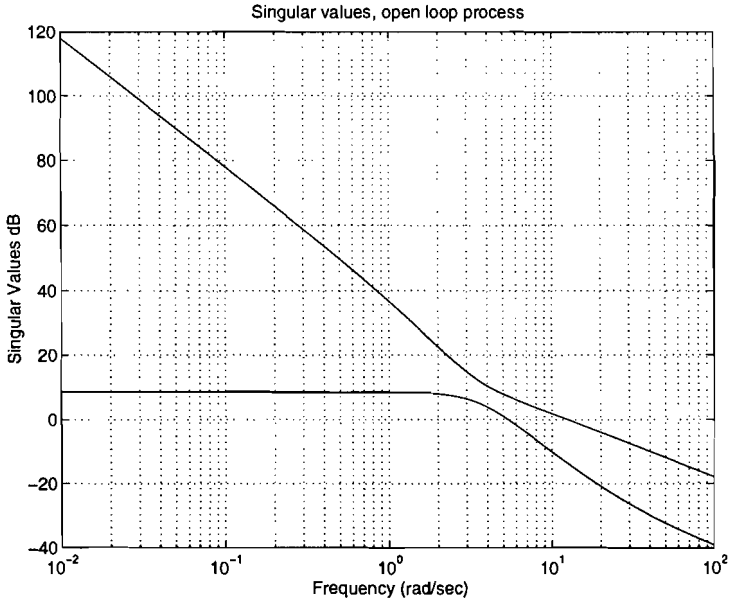


***Figure 2-9: Open loop singular value plots***

The singular values give better information about the gains and the bandwidth of the process; The bandwidth is about 4 [rad/sec] or 0.6366 [Hz], which is slow. The largest singular value is the transfer function for a combination (opposite steering directions) of the front and rear steering, such that maximal lateral deviation occurs. The determination of the steering directions can be found by examining the angles of the input vectors $V^T$

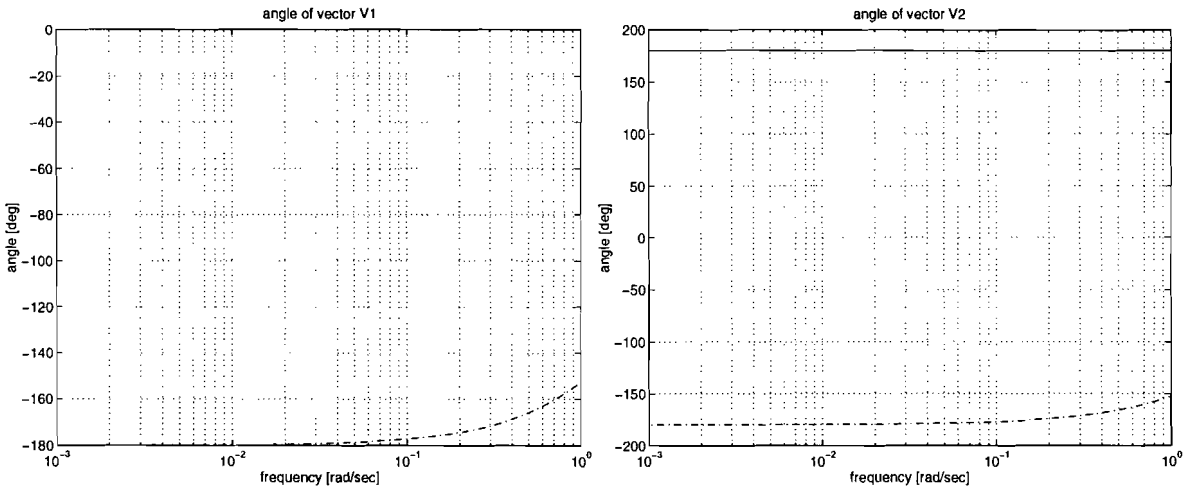


***Figure 2-9 a: Angles of the input vector V***

The left plot of figure 2-9a shows the opposite angle (striped, -180 [deg]) of the rear steering system for the largest singular value. There is also a line of the front steering system, which coincides with the zero axis. The right plot shows that the angles have the same direction (-180 and 180 [deg]) for the smallest singular value.

In the mode belonging to the largest singular value, the system acts like a double integrator (fig 2-9) For low frequencies, up to 4 [rad/sec]. Above, 4 [rad/sec] the system, has a lower roll off rate, -20 [dB/dec], which means that the system shall be less damped.

## 2.4. Design specifications

The data for the considered vehicle, the four wheel steered city bus, are
$l_f$=5 [m], $l_r$=5 [m], ls=2.5 [m], $c_f$=300000 [N/rad], $c_r$=300000 [N/rad], v ∈ [1;30] [m/s],
$\tilde{m}$ ∈ [9950; 32000] [kg] and $i^2$=10.85 [kgm$^2$]. J= $i^2$.m
The design specifications are for a symmetrical vehicle construction. They are primarily given in terms of maximal displacement from the guideline and maximal steering angle and steering angle rate.

In detail these values are:

- The steering angles are limited for the front wheels to $|\delta_f| < 40$ [deg], and for the rear wheels $|\delta_r| < 40$ [deg] ≈ 0.7 [rad].
- The steering angle rates are limited to $|\dot{\delta}_f|, |\dot{\delta}_r| <$ 23 [deg/sec] ≈ 0.4 [rad/sec].
- The displacement from the guideline must not exceed 0.15 [m] in transient state and 0.02 [m] in steady state.
- The lateral acceleration must not exceed 2 [m/sec$^2$].
- The natural frequency of the lateral motion must not exceed 1.3 [Hz].

The maximal displacement of 0.15 [m] is partially due to safety reasons, for example if the bus enters a bus stop bay where passengers are waiting to enter the bus, but also to sensor noise.

# 3. $H_\infty$- controller Design.

Why feedback ?
The main task of this controller would be good tracking performance, (the guideline has to be followed as accurate as possible) and disturbances (side-wind, road conditions, change of vehicle dynamics) reduction. In practice, the modeling of systems is not so ideal as we consider, there are always model uncertainties, which also have to be taken in consideration. If we use only a feedforward controller, then the controller can not compensate for the model uncertainties and disturbances (because there is no feedback control). So fundamental reasons for using feedback control are therefore the presence of:

1. Signal uncertainty - Unknown disturbance
2. Model uncertainty
3. An unstable plant (not in our case)

The third reason follows because unstable plants can only be stabilized by feedback.

From classical PID-controllers we know that the phase margin (PM) and gain margin (GM) are used to take robustness into account. So the stability of the PID- controller depends on two factors PM, GM. The allowable perturbations in dynamics are not quantised. If the dynamics of the controlled dynamics deviate somewhat from the nominal model, then the point -1 of the Nyquist diagram can be encircled resulting in an unstable system. Since we have a MIMO- process the parameter dependencies are stronger. So we have to choose/design a controller form which is suitable for MIMO- process handling. A thorough treatment of $H_\infty$- control design is given by the books of Zhou [9], Skogestad [10] and the college book of Damen [8]

## *3.1. Definition of $H_\infty$- controller problem*

To design a (sub)optimal MIMO $H_\infty$-controller the general problem has to be put in a special structure called the augmented plant. The problem is then well-defined and 'straight- forward' to obtain. Figure 3.1 shows a general problem structure of the $H_\infty$- controller structure.

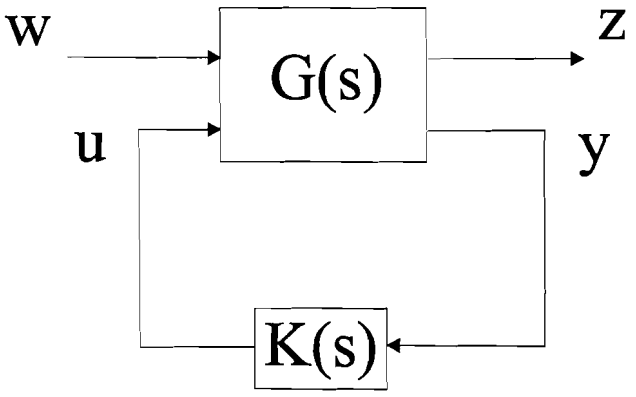


***Figure 3-1. Augmented plant, general structure***

This augmented plant contains, the process model and all the filters for characterizing the inputs and weighting the penalized outputs as well as the model error lines. In this figure the inputs (w, u) and outputs (z, y) denote,

- ***w:*** The exogenous inputs (These signals are entering the shaping filters that yield the actual inputs signals e.g. (reference, disturbance, sensor noise).
- ***u:*** The controller input, applied to the augmented plant with transfer function G(s).
- ***z:*** The (weighted) outputs (tracking errors, actuator inputs, model error block inputs). These signals are also called the "error" signals which are to be minimized in some sense (quadratic norm) to meet the control objectives.
- ***y:*** Contains actually measured signals that can be used as inputs to the controller.

We can describe the augmented plant by

$$\begin{bmatrix} z \\ y \end{bmatrix} = \begin{bmatrix} G_{11} & G_{12} \\ G_{21} & G_{22} \end{bmatrix} \begin{bmatrix} w \\ u \end{bmatrix} \tag{3.1}$$

while

$$u = K \cdot y \tag{3.2}$$

denotes the control law.

We would like to have an expression in the form z= M(K) w for the outputs z to be minimized. M(K) is called the linear fractional transformation and it maps w to z.
By eliminating u and y we find,

$$z = [G_{11} + G_{12}K(I - G_{22}K)^{-1}G_{21}]w = M(K)w \tag{3.3}$$

The control aim requires:

$$\min_{K\ stabilizing} \sup_{w \in L_2} \frac{\|z\|_2}{\|w\|_2} = \min_{K\ stabilizing} \sup_{\omega \in R} \bar{\sigma}(M(K)) = \min_{K\ stabilizing} \|M(K)\|_\infty \tag{3.4}$$

where $\|z(t)\|_2 = \sqrt{\int_0^\infty \sum_i |z_i(t)|^2 dt}$ is the 2-norm of the vector with $i^{th}$ the output to be minimized.
In general, this 2-norm expresses the power or energy of the signal s.
$L_2$ is the set of signals:

$$L_2 = \{s : T \rightarrow W \mid \|s\|_2 < \infty\}$$

When a signal s belongs to $L_2$ then its power or energy is bounded.

We can interpret the left side of the equation 3.4 as follows :
Above all we have to find a stabilizing controller K. "sup w$\in L_2$" indicates that w is worst case disturbance, which is however bounded. For this worst disturbance, we want to minimize the energy of z, containing the front lateral deviation $y_f$ , rear lateral deviation $y_r$ and control inputs. With

equation 3.3, the control aim can be written as in the right side of equation 3.4, where the $H_\infty$-norm, which maps $L_2$-signals to $L_2$-signals is used.
The $H_\infty$-norm of a SISO transfer function H, denoted by:

$$\|H\|_\infty := \max_{\omega \in R} |h(j\omega)|$$

which indicates the maximal peak in the Bode diagram of the frequency response of H.
The same can be done in the MIMO-case, but now we talk about the maximum singular values of each input to the outputs.

$$\|H(s)\|_\infty = \sup_{\omega \in R} \bar{\sigma}(H(j\omega)) = \sup_{\omega \in R} \|M(K)\|_\infty$$

The frequency dependent maximal singular value $\sigma(\omega)$, viewed as a function of $\omega$ gives information about the gain characteristics of the system. See for more detail Damen[8].

### 3.2. Tracking problem.

Figure 3.2 is used to illustrate the tracking problem (and disturbance rejection)

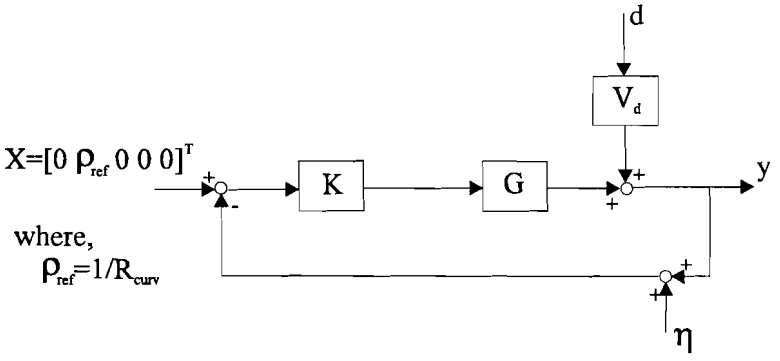


***Figure 3-2. Tracking problem.***

In this figure the reference vector is: $X = \begin{bmatrix} 0 & v \cdot \rho_{ref} & 0 & 0 & 0 \end{bmatrix}^T$, where $\rho_{ref} = \frac{1}{R_{curv}}$ is the curvature of the road, that has to be followed. The output vector y, contains the signals :

$y = \begin{bmatrix} \beta & r & \Delta\psi & y_f & y_r \end{bmatrix}^T$ and the vector $\eta$ (measurement noise) is:

$\eta = \begin{bmatrix} \eta_1 & \eta_2 & \eta_3 & \eta_4 & \eta_5 \end{bmatrix}^T$ and disturbance vector d: $d = \begin{bmatrix} d_1 & d_2 & d_3 & d_4 & d_5 \end{bmatrix}^T$

The inputs to the controller K(s) is $X-y_m$ where $y_m = y+\eta$ is the measured output. Thus, the input to the plant is

$$u = K(s)(vX - y - \eta) \tag{3.5}$$

The aim of control is to manipulate (design K) such that the error e remains small in spite of disturbances d. The control error is defined as

$$e = vX - y \tag{3.6}$$

where y is the actual value.

### 3.2.1. Derivation closed loop transfer functions

The plant model from Figure 3.2 is,

$$y = G(s)u + V_d(s)d \tag{3.7}$$

substitution of (3.5) into (3.7) yields

$$y = GK(vX - y - \eta) + V_d d \tag{3.8}$$

and hence the closed loop response is

$$y = (I + GK)^{-1} GKvX + (I + GK)^{-1} V_d d - (I + GK)^{-1} GK\eta \tag{3.9}$$

From (3.9) we can derive expressions for the following functions,

$GK = L$ the loop gain function

$(I + GK)^{-1} = S$ the sensitivity function (3.10)

$(I + GK)^{-1} GK = T$ the complementary sensitivity function (3.11)

The term complementary sensitivity comes from the identity,

$$S + T = I \tag{3.12}$$

The control error is

$$e = vX - y = -SvX + SV_d d - T\eta \tag{3.12}$$

with the corresponding plant input signal

$$u = KSvX - KSV_d d - KS\eta \tag{3.13}$$

with

$K(I + GK)^{-1} = KS = R$ the control sensitivity (3.14)

From the control error (3.12) we can conclude that, if we want to minimize the effect of the reference X, the disturbance signal d and the measurement noise η on the control error signal e, then the sensitivity functions: Sensitivity (for low frequency region), complementary sensitivity (for high frequency region) functions have to be small in the corresponding frequency region. Later, as we shall see in the following sections, this "smallness" can be achieved by using proper weighting functions. From (3.13) we can also conclude that the saturation of the actuator can be prevented by making the plant input signal, u small enough (keeping below the saturation value of the actuator) with the control sensitivity R, equation (3.13).We shall make use of this derived functions in the section "augmented plant".

### 3.3. Block scheme extended with weighting filters

In figure 3.3 the block scheme of figure 3.2 is extended with weighting filters, in this figure all the signals with their dimensions are also denoted. The use of weighting filters in $H_\infty$-controller design is of crucial importance in arriving at a controller which satisfies the design specifications. In this figure the outputs in the vector $\tilde{e} = -\bar{W}_e\{[\beta \quad v\rho_{ref} - r \quad \Delta\psi \quad y_f \quad y_r] + \vec{d}\}$, with the corresponding units: [-], [rad/s], [rad], [m], [m]. These output vectors are disturbed by the disturbance vector d. The lateral deviations are $y_f$ and $y_r$.

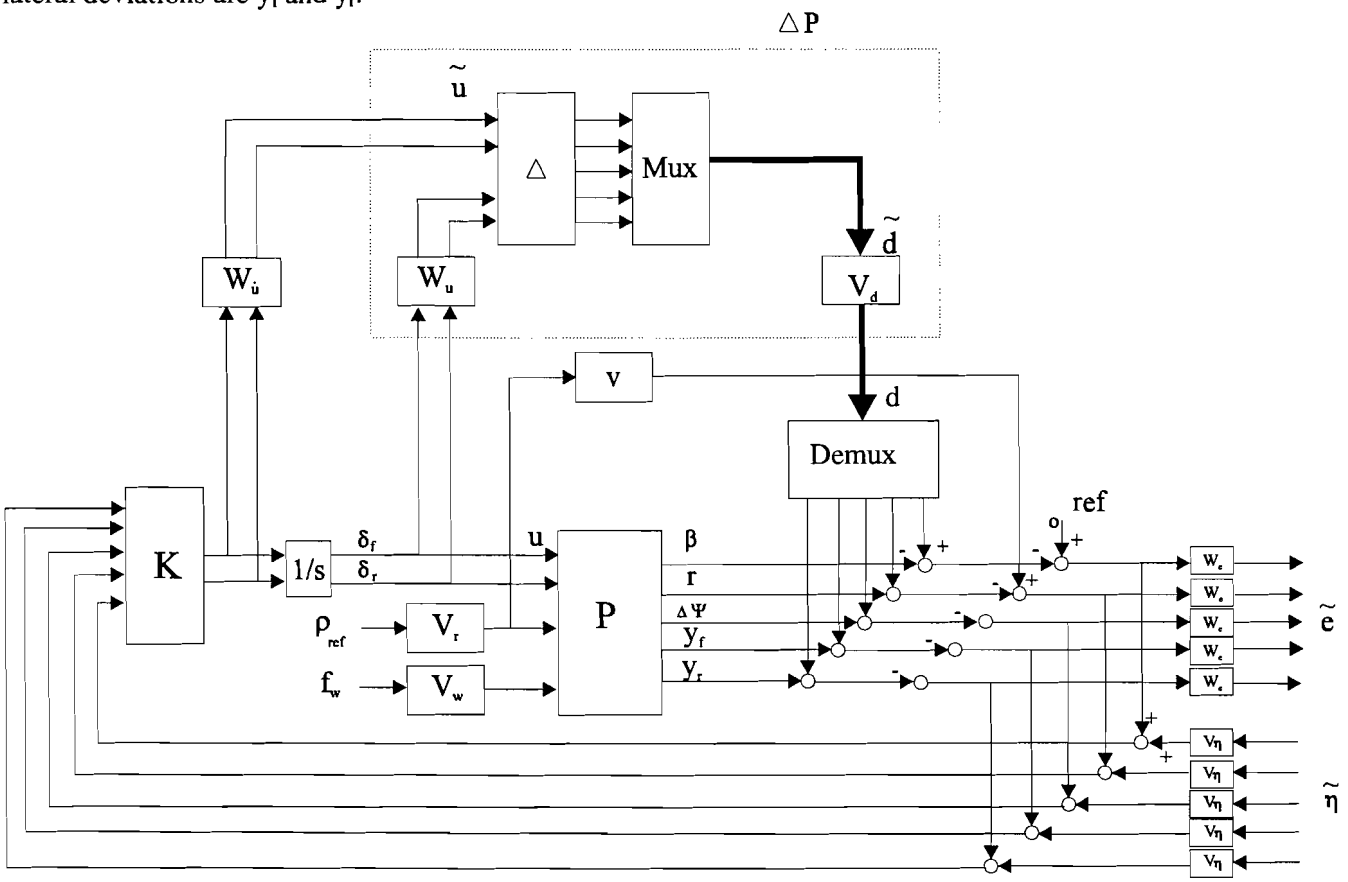


***Figure 3-3. Extended block scheme***

*Input- weighting* filters:

- $V_r$: This filter is used to characterize the reference curvature, the output of this filter is the actual reference signal curvature $\rho_{ref}$
- $V_d$: Filter used to characterize the disturbance signal, this disturbance is formed by the model perturbation $\Delta P$ (unmodelled dynamics). The output of $V_d$ is the actual disturbance signal d
- $V_\eta$: Weighting filter to characterize measurement noise.

*Output- weighting* filters:

- $W_e$: Used to put weight on the outputs to be minimized $e = vX - y$, where y is the actual measured value. The output vector e consists of the signals:

$$\tilde{e} = -\tilde{W}_e\{\begin{bmatrix}\beta & v\rho_{ref} - r & \Delta\psi & y_f & y_r\end{bmatrix} + \tilde{d}\}$$

with

$\beta$: side slip [-]

v $\rho_{ref}$-r: yaw- rate [rad/s]

$\Delta\psi$: angle between vehicle centerline and tangent to the road [rad]

$y_f$: lateral deviation, front of the vehicle [m]

$y_r$: lateral deviation rear of the vehicle [m]

- $W_u$: Used to put weight on the actuator input u in order to avoid saturation. The output vector consists of the signals:

$$\tilde{u} = \begin{bmatrix}\delta_f & \delta_r & \dot{\delta}_f & \dot{\delta}_r\end{bmatrix}$$

i.e. steering angles and its derivatives (steering rates) .

- Block $\Delta P$:

Block $\Delta P$ represents the additive model error. The effect of this perturbation on the robustness of stability and performance should be minimized. From the augmented plant we see that $\Delta P$ is an extra transfer between plant input u and input $d$. If we can keep the transfer from $d$ to $u$ small by a proper controller, the loop closed by $\Delta P$ will not have much effect. So robustness is increased by keeping $u$ small. In practice there is always this $\Delta P$ because there are:

-Unmodelled dynamics, varying loads.

### 3.4. Augmented plant

The augmented plant is given in figure 3.4 below.

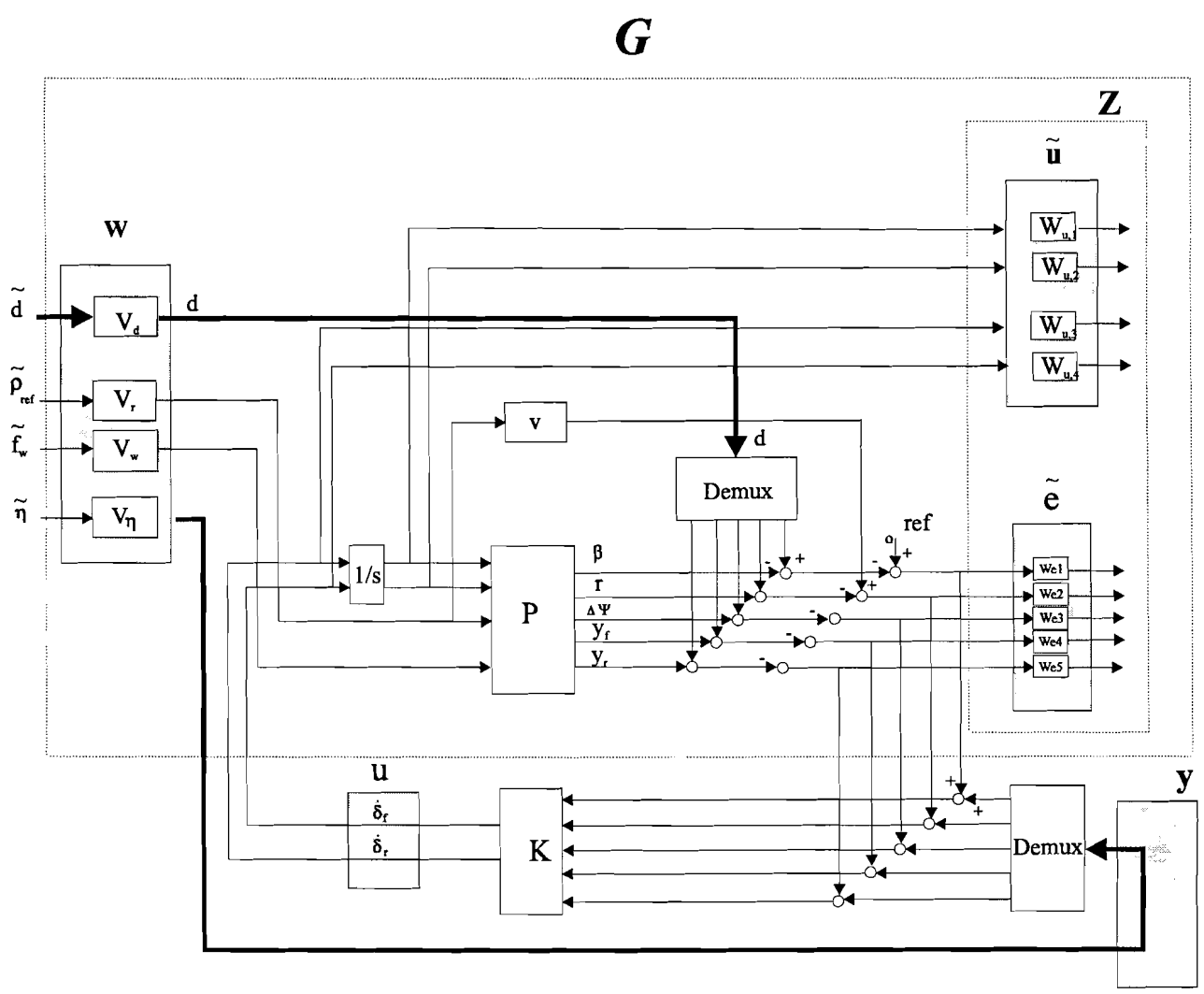


***Figure 3-4. The augmented plant.***

As we have seen earlier in section 3.1 the vectors ***w, z, y*** and ***u*** are vectors:

- ***w:*** Contains the exogenous inputs ***w*** = [***d***, $\rho_{ref}$, $f_w$, $\eta$]. Where the disturbance vector d is: $\mathbf{d} = \begin{bmatrix} d_1 & d_2 & d_3 & d_4 & d_5 \end{bmatrix}^T$ and $\eta = \begin{bmatrix} \eta_1 & \eta_2 & \eta_3 & \eta_4 & \eta_5 \end{bmatrix}^T$
- ***z:*** Contains the outputs signals that have to be minimized $\mathbf{z} = \begin{bmatrix} \beta + d_1 & v\rho_{ref} - r + d_2 & \Delta\psi + d_3 & y_f + d_4 & y_r + d_5 & \delta_f & \delta_r & \dot{\delta}_f & \dot{\delta}_r \end{bmatrix}^T$
- ***y:*** Contains the actually measured signal ***e*** = [β, Yaw, Δψ, $y_f$, , $y_r$].
- ***u:*** Contains the output of the controller $\tilde{u} = \begin{bmatrix} \dot{\delta}_f & \dot{\delta}_r \end{bmatrix}$ where [$\delta_f$, $\delta_r$] is applied to the augmented system with transfer function G(s).

From the expression ***z= M(K).w*** equation (3.3) we see that ***M(K)*** is the closed transfer function, which maps ***w*** to ***z***. We have three exogenous input vectors,

$$\vec{w} = \begin{bmatrix} \tilde{d} \\ \tilde{\rho}_{ref} \\ \tilde{\eta} \end{bmatrix} \tag{3.15}$$

and two output vectors

$$\vec{z} = \begin{bmatrix} \tilde{e} \\ \tilde{u} \end{bmatrix} \tag{3.16}$$

Since we have 3 inputs and 2 outputs, there are thus 6 closed loop transfer functions possible. The closed loop transfer function ***M(K)*** can be determined from the augmented plant:

***Table 3-1: Closed loop transfers.***

| input → output | $\tilde{e}$ dim[5] [error output] | $\tilde{u}$ dim[4] [control output] |
|---|---|---|
| $\tilde{d}$ | $W_e.S.V_r$ | $W_u.K.S.V_r$ |
| $\tilde{\rho}_{ref}$ | $W_e.S.V_d$ | $W_u.K.S.V_d$ |
| $\tilde{\eta}$ | $W_e.P.K.S.V_\eta$ | $W_u.K.S.V_\eta$ |

In this table P.K.S= T, the complementary sensitivity function, while KS= R, the control sensitivity function.
In matrix form these transfers are

$$M = \begin{bmatrix} \frac{\tilde{e}}{\tilde{\rho}_{ref}} & \frac{\tilde{u}}{\tilde{\rho}_{ref}} \\ \frac{\tilde{e}}{\tilde{d}} & \frac{\tilde{u}}{\tilde{d}} \\ \frac{\tilde{e}}{\tilde{\eta}} & \frac{\tilde{u}}{\tilde{\eta}} \end{bmatrix} = \begin{bmatrix} W_e S V_r & W_u R V_r \\ W_e S V_d & W_u R V_d \\ W_e T V_\eta & W_u R V_\eta \end{bmatrix} \tag{3.17}$$

Now, if we can manage to obtain:

$$\left\| M(K) \right\|_\infty \approx \gamma \leq 1 \tag{3.18}$$

then it can be guaranteed that

$$\forall \omega \in R: \begin{bmatrix} |S| < \frac{1}{|W_e V_r|} & |R| < \frac{1}{|W_u V_r|} \\ |S| < \frac{1}{|W_e V_d|} & |R| < \frac{1}{|W_u V_d|} \\ |T| < \frac{1}{|W_e V_\eta|} & |R| < \frac{1}{|W_u V_\eta|} \end{bmatrix} \tag{3.19}$$

## *3.5. Control objectives and constraints*

The control aim is to design a controller K such that, the lateral deviations (front, rear of the vehicle ) from the guideline must be kept zero. Also the side- slip (β), the reference $v\rho_{ref} - r$ and the deviation, $\Delta\psi$ of the centerline of the vehicle from the tangent to the road must also kept zero. We assume, that we can measure all the states (β, r, $\Delta\psi$, $y_f$, $y_r$) with the sensors (rate gyro, speed sensor, accelerometer, steering angle sensor).
To design such a controller, we have to find a compromise between control objectives and constraints. These are,

- Stability, The closed loop system has to be stable
- Disturbance reduction/ tracking, the influence of the disturbing noise d should be small.
- Sensor noise reduction, The sensor noise η must not affect the output vector (constraint)
- Actuator saturation, the actuator should not become saturated (constraint)
- Robustness, If the true dynamics of the process change from the nominal value, the system should not exceed the design specifications.

These points shall be discussed in the following subsections

### 3.5.1. Stability

The closed loop system must be stable. Nowhere in the closed loop system, some finite disturbance may cause other signals in the loop to grow to infinity, the system has to be BIBO- stable (Bounded input Bounded Output). Since we have a MIMO-process all the transfers from inputs to outputs have to be checked on possible unstable poles. To guarantee the existence of a stabilizing controller , the unstable modes ,if they exist (not in our case) of G(s) have to be reachable from $\boldsymbol{u}$ (controllability), while on the other hand all the unstable poles, must be observable from $\boldsymbol{y}$, so that the controller can deal with these unstable poles.
We use the Multivariable $H_\infty$ - Control design toolbox (MHC [12]) to calculate the controllers. This package checks if there exist an internally stabilizing controller. This is done by checking mathematical assumptions. See [12].

### 3.5.2. Disturbance reduction

The effect of the disturbance d on the output $\tilde{e}$ eq. (3.14) , can be decreased by designing a controller K such that the transfer $\tilde{e} / \tilde{d}$ (sensitivity S) is small in the frequency band, where d is most disturbing, at *low* frequencies, and where the outputs e has to be minimized. The disturbance reduction has to be large at *low* frequencies, because a small steady state error is desired. The transfer e/d will therefore be small for a *low* frequency band. For the tracking of the reference signal (the curvature), the complementary function T=1.

At high frequencies, the arguments stated above are also valid for the complementary sensitivity function, so the complementary sensitivity T has to be small at *high* frequencies (S=1). We must design a controller K which makes the sensitivity functions small in the frequency band of interest.

### 3.5.3. Sensor noise reduction

From equation (3.14) we see that if we want to decrease the influence of the sensor noise η on the output $\tilde{e}$ , we have to design a controller K such that the transfer $\tilde{e} / \tilde{\eta}$ (complementary sensitivity T)

will be small in the frequency band where η is most disturbing. In practice, sensor noise appears often at high frequencies and therefore e/η will be small for high frequencies. As we can see in the scheme the sensor noise must pass through the controller K and the process P before reaching the output $\tilde{e}$. So they can also acts as filters to remove noise.

### 3.5.4. Actuator saturation avoidance

In practice, every actuator has a limited input (physical restrictions of the actuator). In our case these restrictions for the steering angles are,

$$-40\,\text{deg} \le \delta_f, \delta_r \le 40\,\text{deg}$$

and for the steering angle rates,

$$-23\frac{\text{deg}}{s} \le \dot{\delta}_f, \dot{\delta}_r \le 23\frac{\text{deg}}{s}$$

In order to prevent the actuator from saturation we have to put a constraint on the control signal u:

- The transfer u/η(control sensitivity R) is small in the high frequency bands where the sensor noise η and the lateral deviations $y_f$ and $y_r$ are of interest.
- The transfer u/d (R) is small in the low frequency bands where the process disturbance d and the lateral deviations are of interest.

As we have seen earlier, the control signal u was dependent on the control-sensitivity R=KS (3.14) and see also equation (3.19) so, we have to make R small in the band of X, η, d (remembering that u= KS(X-η- $V_d$ d)). So by proper choice of the weighting filters in the augmented plant (fig 3.4) $W_u$, $V_v$, $V_\eta$ we can prevent actuator saturation. The filters $V_d$ and $V_\eta$ are the characterization filters for process disturbance and noise. We can check by time- domain simulations if the actuator does not saturate. If it does then the filter $W_u$ has to be adjusted.

### 3.5.5. Robustness

In practice many plants are perturbed due to: unmodelled dynamics, varying loads (the mass of the bus), limited identification etc. In these situations we can represent the true system with

$$P_{true} = P + \Delta P \qquad (3.20)$$

where P represents the nominal model while ΔP represents the additive model perturbation.
The effect of the robustness is illustrated in figure 3.5.
In this figure the line with the large peak illustrates a very good performance for the nominal process. If the model error ΔP becomes larger, then the performance detoriates fast. The other line shows more robustness, but the performance for the nominal model P has become worse.

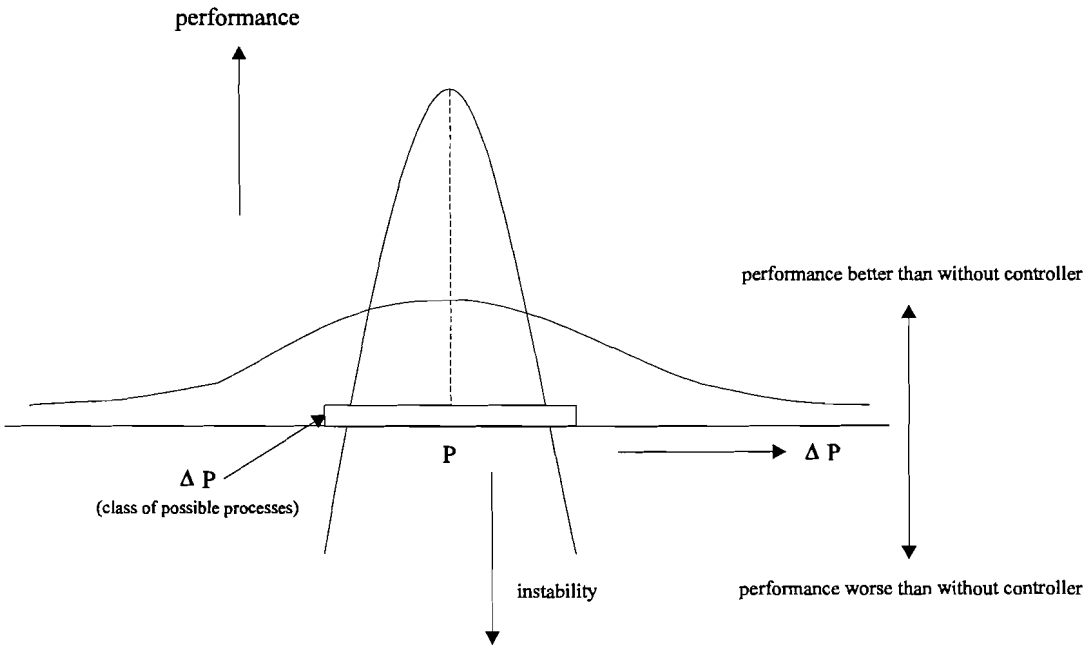


*Figure 3-5. Performance/ robustness tradeoff.*

The small gain configuration is given in Figure 3-6. The uncertainty block ΔP is an additive perturbation which, as it were "pulled out" from the rest of the configuration. For additive perturbations:

*M= R (under additive perturbations see figure 3-3)*

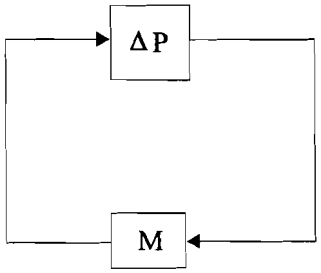


*Figure 3-6: Small gain configuration*

According to the "small gain theorem" the system of figure 3.6 is stable if:

$$\| M \cdot \Delta P \|_\infty = \| R \cdot \Delta P \|_\infty < 1 \tag{3.21}$$

Equation (3.21) can be refined by considering for each frequency the maximal allowable perturbation ΔP which makes the system unstable. If we assume that K stabilizes the nominal plant P then the closed-loop system is stable for all stable additive stable perturbations ΔP if :

$$\forall \omega \in R: |\Delta P(j\omega)| < \frac{1}{|R(j\omega)|} \tag{3.22}$$

With this equation and a Bode plot of |R(jω)| we can determine for each frequency ω the maximal allowable model error |ΔP(jω)|. If we can manage to make |R(jω)| smaller, ΔP may become larger and

so the robustness is increased. From (3.19) we see that R is determined by the filters $W_u$ ,$V_d$ and $V_\eta$ . So by choosing these weighting filters, we can combine the control objectives for actuator saturation and robust stability.

### 3.6. The criterion (mixed sensitivity problem) and selection weighting functions

Our requirements on the controller design can be stacked up: The so called mixed-sensitivity (S/KS) problem. We can put these requirements in the form:

$$M = \begin{bmatrix} \frac{\tilde{e}}{\tilde{\rho}_{ref}} & \frac{\tilde{u}}{\tilde{\rho}_{ref}} \\ \frac{\tilde{e}}{\tilde{d}} & \frac{\tilde{u}}{\tilde{d}} \\ \frac{\tilde{e}}{\tilde{\eta}} & \frac{\tilde{u}}{\tilde{\eta}} \end{bmatrix} = \begin{bmatrix} W_e S V_r & W_u R V_r \\ W_e S V_d & W_u R V_d \\ W_e T V_\eta & W_u R V_\eta \end{bmatrix}$$

where,

$$\|M\|_\infty = \max_\omega \bar{\sigma}(M(j\omega)) < 1$$

So, the maximum singular value of M must be smaller then 1.
After selecting the form of N and the weights, the $H_\infty$ - (sub) optimal controller is obtained by minimizing

$$\min_K \|M(K)\|_\infty$$

where K is a stabilizing controller.
Before outlining the selection of the weighting functions we first discuss the functions S, T. There is a compromise between these functions : S+T= I. So if we demand a small S, then T is necessarily large. This is also true if T is small then S is large. A typical plot of such a compromise is given in figure 3.7

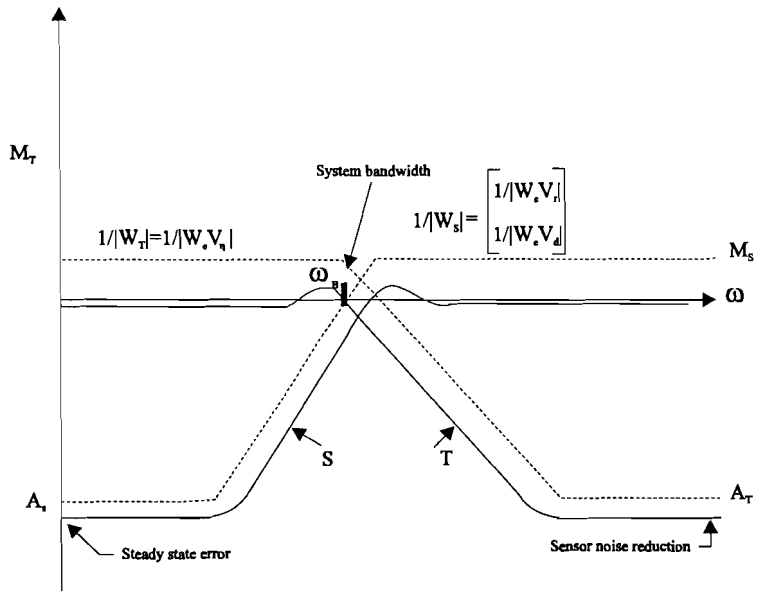


*Figure 3-7. Typical plots for S and T.*

From this figure we see that the sensitivity S is shaped by a weighting function $1/|W_S|$ , and the complementary sensitivity T is shaped by a function $1/|W_T|$ . The filter $W_S$ is a combination of the filters $W_e$ and $V_d$, and the filter $W_T$ is a combination of the filters $W_e$ and $V_\eta$.
In order to investigate the role of the functions S and T in the input- output relations these equations are given once more below

$$y(s) = T(s)X(s) + S(s)d(s) - T(s)n(s) \tag{3.9}$$
$$u(s) = K(s)S(s)[X(s) - n(s) - d(s)] \tag{3.13}$$

The equations (3.9) and (3.13) derived earlier determine several closed- loop control objectives, in addition to the requirement that K stabilizes G, namely:

- For *disturbance rejection* make S small (low frequencies).
- For *noise attenuation* make T small (high frequencies).
- For *reference tracking* make $T \approx 1$ (low frequencies).
- For *control energy reduction* make R=KS small (if possible for all frequency range).

We represent the unstructured uncertainty in the plant P(s) by an additive perturbation $P_{true} = P+\Delta P$, then a further closed-loop objective is

- For robust stability in the presence of an additive perturbation make R=KS small.

In this figure (3.7) we further assume that the steady-state error is determined by the choice of $A_s$, which is the magnitude of S at $\omega = 0$. The bandwidth $\omega_B$, is determined by the choice of the crossover frequency of S. The sensor noise reduction is determined by the choice of $A_T$ , the magnitude of T at high frequencies. The disturbance reduction at low frequencies is determined by the value of S at low frequencies. To obtain controllers with desirable performance the weighting filters has to be chosen carefully. We start with the discussion of the filters at the input see augmented plant figure 3.4.

The weighting filters V at the input of the augmented plant are:

$$V = \begin{bmatrix} V_r & & & 0 \\ & V_w & & \\ & & V_d & \\ 0 & & & V_\eta \end{bmatrix}$$

where $V_d$= diag($V_{d1}$, $V_{d2}$, $V_{d3}$, $V_{d4}$, $V_{d5}$) and $V_\eta$= diag($V_{\eta 1}$ ,$V_{\eta 2}$ ,$V_{\eta 3}$ ,$V_{\eta 4}$ ,$V_{\eta 5}$)
The inputs of the filters are normalized to 1.
We shall now discuss in brief these filters:

- The *reference* filter:

This filter characterizes the dynamics of the curvature $\rho_{ref}(t)$. The bandwidth of this filter is found by analysis of the Fourier - transform of the signal , (see figure 3.9), which represents the curvature:

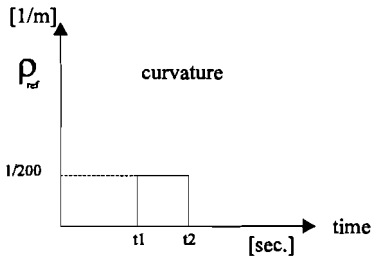


***Figure 3-8 Signal representing the curvature***

We assume that the vehicle needs 5 seconds to make the sharpest curvature. So the time difference $\Delta t = t_2 - t_1 = 5$ [sec]. These moments $t_1, t_2$ are chosen arbitrarily, its important for how long the curve lasts, this is determined by $\Delta t$.
To determine the amplitude of the curvature, $\rho_{ref}$ we make use of the relationship:

$$\rho_{ref} \cdot v^2 \leq a$$

In this relationship, v is the vehicle's velocity and a= 2 [m/sec$^2$], the lateral acceleration of the vehicle. This is the limit value of the acceleration, where human susceptibility begins for lateral motions of the vehicle. With v=20 [m/s] this curvature is $\rho_{ref}$=1/200 [m$^{-1}$]. The maximum radius of the curvature is also determined by the physical limitations of the steering angles of the four wheels: 40 [deg]

The Fourier -transform is given by

$$F(\omega) = \int f(t) \cdot e^{-j\omega t} dt = \frac{1}{200} \frac{\sin 5\pi\omega}{5\pi\omega}$$

The spectral plot of this figure 3.10 is:

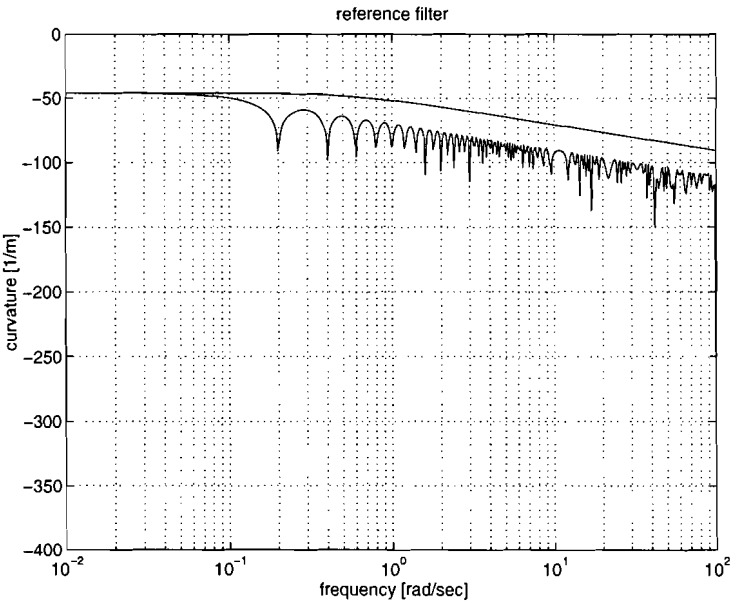


***Figure 3-9: spectral plot of the curvature.***

From this figure, we can fit a filter which forms an upper bound to the spectral plot. We choose for the bandwidth ω=0.6 [rad/sec] and for the amplitude 0.003 so,

$V_{ref} = 0.003 \cdot \frac{1}{s+0.6}$. In steady state $V_{ref} = 0.005$ [$m^{-1}$] $\Rightarrow$ The gain is 1/200=0.003/0.6= $5.10^{-3}$ and $R_{ref} = 1/\rho_{ref} \approx 200$ m.

- The *wind- disturbance* filter:

The disturbance of the force can be very large, $f_w$=10000 N. So we have to put large weight on this disturbance force.
This disturbance force can be calculated as follows:

Disturbances like the wind -disturbance acting on the system have to be reduced by the controller. Therefore, it's important to find out what the magnitude of the disturbance can be.
To say something about the forces due to wind acting on the bus, we have to know about the "dynamical pressure" acting on the vehicle. The dynamical pressure occurs when air in motion acts on the vehicle. This pressure can be calculated with Bernoulli's law, which holds for non-compressible liquids. According to Chao [7] this law is also valid for gasses, provided that the velocity of the gas is below 66 [m/s]. Below this value of the velocity, the specific mass of the gas can be seen as constant. With these assumptions, it holds for the dynamical pressure,

$$P = \frac{1}{2} \cdot \rho \cdot C_{ws} \cdot v^2$$

where,

P: The dynamical pressure [$N/m^2$].
ρ: Specific mass of the air ≈ 1.225 [$kg/m^3$].
v: Velocity of the air relative far from the vehicle.
$C_{ws}$: Side wind coefficient 1.25 [-]

We assume that the wind disturbance acts perpendicular on the side area of the bus, the area is a rectangle. Suppose there is a wind force 7 (stormy wind, storm ), v=20 m/s. Then we can calculate the force as:

$P= ½*\rho* C_{ws}*v^2$

$P= ½*1.225*1.25*20^2= 306.25$ N/m$^2$; Forces acting effective on the side area ($A \approx H*(l_f+l_r)$), where H= 3 [m] height bus, $l_f+l_r$ = 10 [m] total length of the bus. So the force becomes,

$F= P*H* (l_f+l_r )= 306.25*3*10= 9187.5$ [N].

To determine the bandwidth of the filter, which characterizes the wind disturbance we use again the Fourier - transform, of the function:

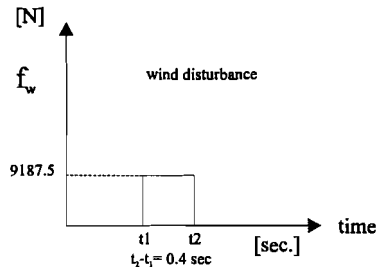


***Figure 3-10: Wind force***

$$F(\omega) = \int f(t) \cdot e^{-j\omega t} dt = 9187.5 \cdot \frac{\sin 0.4\pi\omega}{0.4\pi\omega}$$

with the spectral plot,

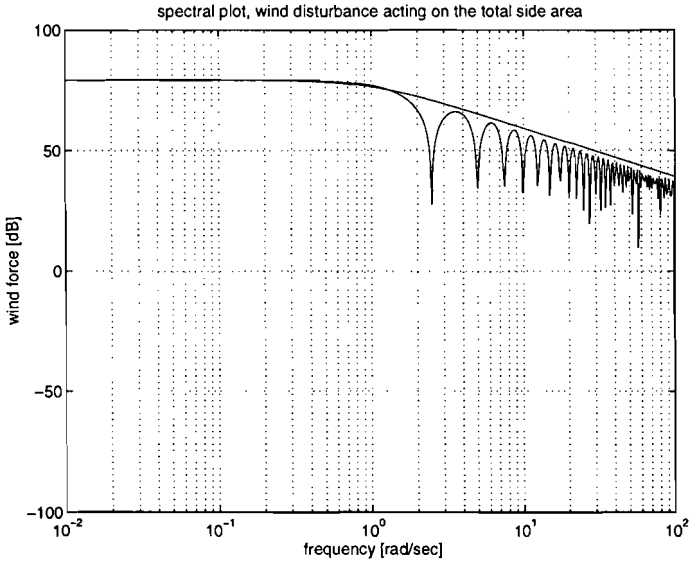


***Figure 3-11: Spectral plot of the wind disturbance***

We can fit a filter, which forms an upper bound to the spectral plot. This filter has the form

$V_w = 9187.5 \cdot \frac{1}{s+1}$; the bandwidth is about 1 [rad/sec] or 0.16 [Hz].

- The *model- uncertainty* filter:

$V_d$= diag($V_{d1}$, $V_{d2}$, $V_{d3}$, $V_{d4}$, $V_{d5}$), to be added at the outputs. In control design toolbox MHC these filters are: V=diag($V_{33}$..$V_{77}$)

These are chosen constant, and they represent disturbances at the output of the process. In these filters, model uncertainties due to parameter variations of v(t) and μ(t) are defined. We use these filters for the robustness problem in section 3.8.2 "closed-loop transfers; control sensitivity functions"

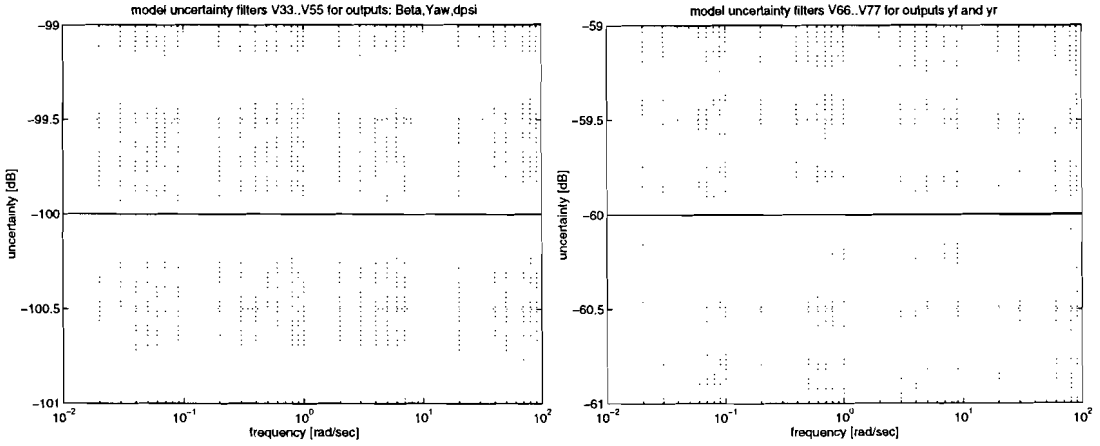


***Figure 3-12: Model uncertainty filters***

- The *measurement* filter:

$V_\eta$=diag($V_{\eta 1}$ ,$V_{\eta 2}$ ,$V_{\eta 3}$ ,$V_{\eta 4}$ ,$V_{\eta 5}$)
These are chosen constant and they represent the measurement noise.
$V_{\eta 1}$ is chosen the same as $V_{77}=10^{-3}$. ,$V_{\eta 2}$ .. $V_{\eta 5}$ are chosen as:

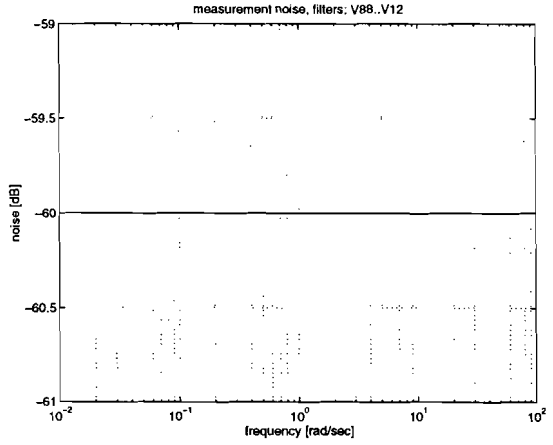


**Figure 3-13: Measurement noise filters**

Here, we have no specific information about the sensors that are going to be used; We choose here also a constant values. This constraint is a bottleneck at low frequencies as we shall see later in section 3.8

- The *output-error* filter

The filters at the output of the augmented plant can be categorized in the filter W:

$$W = \begin{bmatrix} W_e \\ W_u \end{bmatrix}$$

These are the filters which characterizes the outputs to be minimized. The output filters are given in figure 3.14

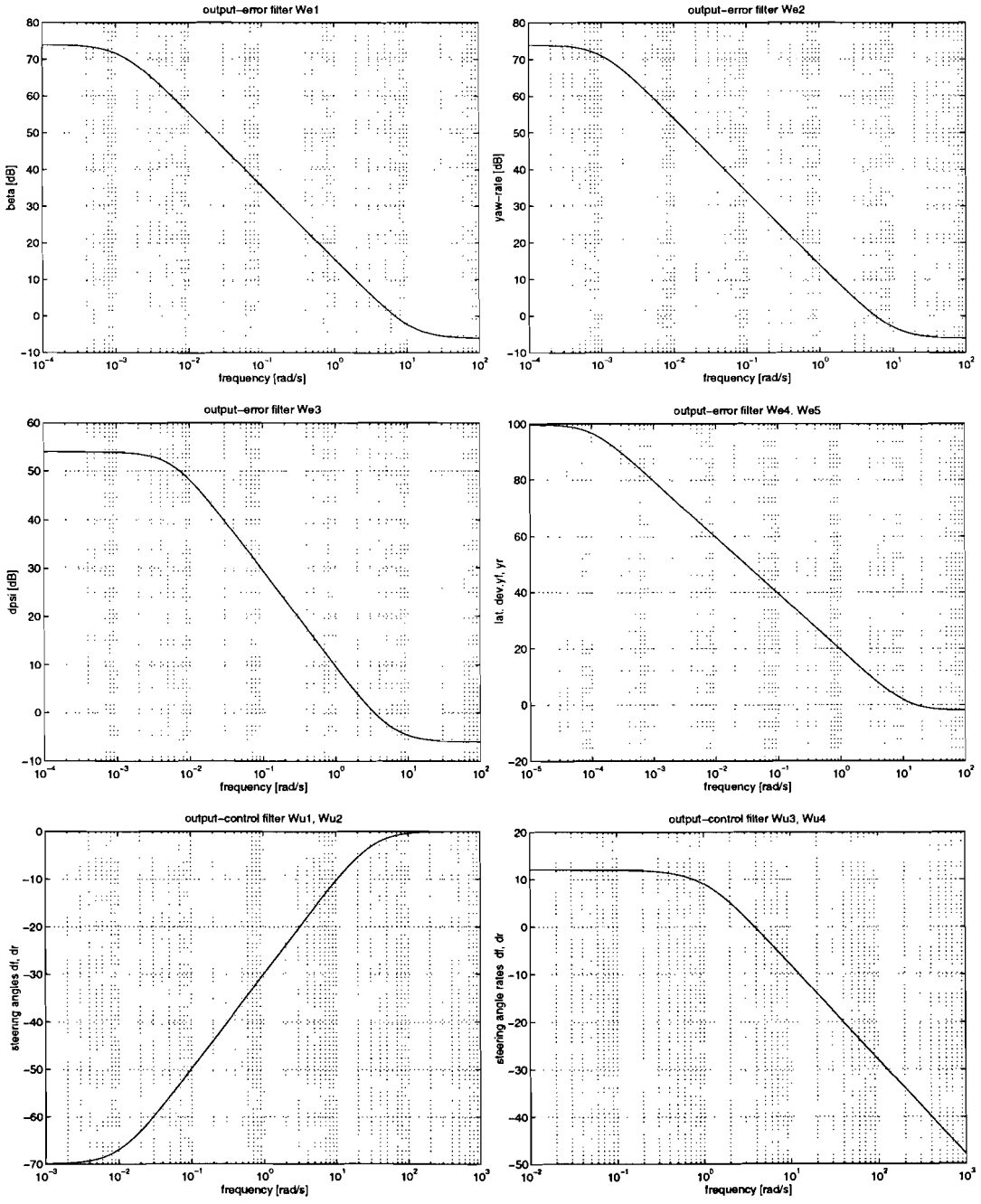


***Figure 3-14: The filters used for the minimization of the outputs.***

These filters shall be discussed below.
$W_e$= diag [$W_{e1}$ $W_{e2}$ $W_{e3}$ $W_{e4}$ $W_{e5}$]$^T$ which are the weights for the corresponding outputs $\tilde{e} = \left[\beta \quad v\rho_{ref} - r \quad \Delta\psi \quad y_f \quad y_r\right]^T$. $W_u$=[ $W_{u1}$ $W_{u2}$ $W_{u3}$ $W_{u4}$] the weights for the corresponding outputs: $\tilde{u} = \left[\delta_f \quad \delta_r \quad \dot{\delta}_f \quad \dot{\delta}_r\right]$.

$$W_{e1} = 0.5 \cdot \frac{s+12}{s+0.0012}; W_{e2} = 0.5 \cdot \frac{s+10}{s+0.001}; W_{e3} = 0.5 \cdot \frac{s+6}{s+0.006}; W_{e4} = W_{e5} = 0.8 \cdot \frac{s+12}{s+0.0001};$$

$$W_{u1} = W_{u2} = \frac{s+0.01}{s+10\pi}; W_{u3} = W_{u4} = \frac{4}{s+1}$$

For good tracking accuracy in each of the controlled outputs the sensitivity function is required to be small. This asks for a forcing integrator action into the controller by selecting $s^{-1}$ shape in the weights associated with the control outputs.
As can bee seen all these filters $W_e1$ ..$W_{e5}$ have an $s^{-1}$ shape for low frequencies, and can be seen as pure integrators. But these integrators are shifted away from the origin with a small value say $\varepsilon << 1$, this is done because the controller-design algorithm (MHC) can not deal with pure integrators, with this shift the equations for the algorithm is "well- posed" and can be solved. These integrators are also responsible for the small steady- state error of the outputs.
The filters used to put constraints on the control signal u are given once more below :

$W_u$= diag[$W_{\delta f}$, $W_{\delta r}$ ,$W_{\delta f\text{-}dot}$ ,$W_{\delta r\text{-}dot}$]

$W_{\delta_f} = W_{\delta_r} = \frac{s+0.01}{s+10\cdot\pi}$; where the bandwidth of the actuator is $f_b$= 5 Hz.
To limit the input magnitudes at high frequencies a first order high pass filter is used. The high frequency gain of this filter can be used to limit fast actuator movement. The low frequency gain is set to -70 dB to ensure that the cost function is dominated by $W_e$ at low frequencies .

And for the steering angle rates,

$$W_{\dot{\delta}_f} = W_{\dot{\delta}_r} = 4 \cdot \frac{1}{s+1}$$

The actuators can be controlled with a maximum allowable steering angle rate. This is the reason why we have to put a constraints on them. This constraint seems to be a bottleneck at high frequencies as we shall see, in the section "closed loop transfers"

### 3.7. Controller system design

Now that we have defined all the necessary conditions, theorems and augmented plant , we can start with the controller design. The basic idea is to design 6 controllers (this number is a choice, for each velocity range of 5 [m/s], one controller is designed to make the control range small ) for the total velocity range of v [0;30] m/s, we may use less number of controllers but the controllers are then less robust because the interval for each of the controllers becomes bigger . We shall discuss one of these controllers, the controller designed for v= 20 m/s for its behavior. The same investigations can be done for the other controllers. The model perturbation due to variation of the velocity v(t) and the road adhesion coefficient μ(t) is incorporated (via uncertainty filter, $V_d$ and the weighting filter for the control signals, $W_u$ ) in the controller design, see section 3.8.3 "closed loop transfers; 'robustness problem' also 'control sensitivity functions' ". As will be discussed later this can be done by determining the maximal model perturbation $\Delta P$ due to maximal variations of v(t) and μ(t) . The state-space model equation (2.14) shall be made dependent on the parameters v(t), μ(t). So the perturbed plant looks like:

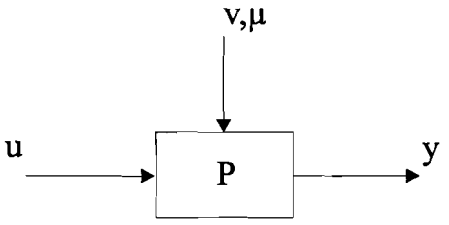


***Figure 3-14: Perturbed plant***

This can be written as

$$P_{true}(s,v,\mu) = P(s) + \Delta P(s,v,\mu) \tag{3.23}$$

The state space model has the following form:

$$\dot{\vec{x}} = A_m\vec{x} + B_m\vec{u}\,;\ \vec{x} = \begin{bmatrix}\beta & r & \Delta\psi & y_f & y_r & \delta_f & \delta_r\end{bmatrix}^T;\vec{u} = \begin{bmatrix}u_f & u_r & \rho_{ref} & f_w\end{bmatrix}^T$$

$$\vec{y} = C_m\vec{x} + D_m\vec{u}\,;\ \vec{y} = \begin{bmatrix}\beta & r & \Delta\psi & y_f & y_r\end{bmatrix}$$

In this state-space model description, actuator dynamics are also included so there are two more states $\delta_f, \delta_r$ then in (2.8).
and where,

$$A_m = \begin{bmatrix} -\mu\cdot\frac{c_r+c_f}{mv} & -1+\mu\cdot\frac{c_r l_r - c_f l_f}{mv^2} & 0 & 0 & 0 & \frac{\mu\cdot c_f}{m\cdot v} & \frac{\mu\cdot c_r}{m\cdot v} \\ \mu\cdot\frac{c_r l_r - c_f l_f}{J} & -\mu\cdot\cdot\frac{c_r l_r^2 - c_f l_r^2}{Jv} & 0 & 0 & 0 & \mu\frac{c_f\cdot l_f}{J} & -\mu\frac{c_r\cdot l_r}{J} \\ 0 & 1 & 0 & 0 & 0 & 0 & 0 \\ v & l_s & v & 0 & 0 & 0 & 0 \\ v & -l_s & v & 0 & 0 & 0 & 0 \\ 0 & 0 & 0 & 0 & 0 & -10\pi & 0 \\ 0 & 0 & 0 & 0 & 0 & 0 & -10\pi \end{bmatrix};$$

$$B_m = \begin{bmatrix} 0 & 0 & 0 & \frac{1}{mv} \\ 0 & 0 & 0 & \frac{l_w}{J} \\ 0 & 0 & -v & 0 \\ 0 & 0 & -vl_s & 0 \\ 0 & 0 & vl_s & 0 \\ 10\pi & 0 & 0 & 0 \\ 0 & 10\pi & 0 & 0 \end{bmatrix}; C_m = C_0 = \begin{bmatrix} 1 & 0 & 0 & 0 & 0 & 0 & 0 \\ 0 & 1 & 0 & 0 & 0 & 0 & 0 \\ 0 & 0 & 1 & 0 & 0 & 0 & 0 \\ 0 & 0 & 0 & 1 & 0 & 0 & 0 \\ 0 & 0 & 0 & 0 & 1 & 0 & 0 \end{bmatrix}; \; D_m = D_0 = zeros(5,4)$$

To describe the model behavior on the time dependent parameters v(t), μ(t) the model ($A_m$, $B_m$, $C_m$, $D_m$) has to be put in the following form:

$A_m(v,\mu) = A_0 + \Sigma A(v)$ which is

$$A_m(v,\mu) = A_0 + v\cdot A_1 + \frac{1}{v}\cdot A_2 + (\frac{1}{v^2})\cdot A_3 \tag{3.24}$$

$B_m(v,\mu) = B_0 + \Sigma B(v)$ which is

$$B_m(v,\mu) = B_0 + v\cdot B_1 + \frac{1}{v}\cdot B_2 \tag{3.25}$$

$$C_m = C_0 \tag{3.26}$$

$$D_m = D_0 \tag{3.27}$$

where $A_0$, $B_0$, $C_0$, $D_0$ are constant values.
From (3.24) follows,

$$A_0 = \begin{bmatrix} 0 & -1 & 0 & 0 & 0 & 0 & 0 \\ \mu\cdot\frac{c_r l_r - c_f l_f}{J} & 0 & 0 & 0 & 0 & \mu\cdot\frac{c_f l_f}{J} & -\mu\cdot\frac{c_r l_r}{J} \\ 0 & 1 & 0 & 0 & 0 & 0 & 0 \\ 0 & l_s & 0 & 0 & 0 & 0 & 0 \\ 0 & -l_s & 0 & 0 & 0 & 0 & 0 \\ 0 & 0 & 0 & 0 & 0 & -10\pi & 0 \\ 0 & 0 & 0 & 0 & 0 & 0 & -10\pi \end{bmatrix}; A_1 = \begin{bmatrix} 0 & 0 & 0 & 0 & 0 & 0 & 0 \\ 0 & 0 & 0 & 0 & 0 & 0 & 0 \\ 0 & 0 & 0 & 0 & 0 & 0 & 0 \\ 1 & 0 & 1 & 0 & 0 & 0 & 0 \\ 1 & 0 & 1 & 0 & 0 & 0 & 0 \\ 0 & 0 & 0 & 0 & 0 & 0 & 0 \\ 0 & 0 & 0 & 0 & 0 & 0 & 0 \end{bmatrix}$$

$$A_2 = \begin{bmatrix} -\mu\cdot\frac{c_r + c_f}{m} & 0 & 0 & 0 & 0 & \frac{\mu\cdot c_f}{m} & \frac{\mu\cdot c_r}{m} \\ 0 & -\mu\cdot\cdot\frac{c_r l_r^{\,2} - c_f l_r^{\,2}}{J} & 0 & 0 & 0 & 0 & 0 \\ 0 & 0 & 0 & 0 & 0 & 0 & 0 \\ 0 & 0 & 0 & 0 & 0 & 0 & 0 \\ 0 & 0 & 0 & 0 & 0 & 0 & 0 \\ 0 & 0 & 0 & 0 & 0 & 0 & 0 \\ 0 & 0 & 0 & 0 & 0 & 0 & 0 \end{bmatrix};$$

$$A_3 = \begin{bmatrix} 0 & \mu\cdot\frac{c_r l_r - c_f l_f}{m} & 0 & 0 & 0 & 0 & 0 \\ 0 & 0 & 0 & 0 & 0 & 0 & 0 \\ 0 & 0 & 0 & 0 & 0 & 0 & 0 \\ 0 & 0 & 0 & 0 & 0 & 0 & 0 \\ 0 & 0 & 0 & 0 & 0 & 0 & 0 \\ 0 & 0 & 0 & 0 & 0 & 0 & 0 \\ 0 & 0 & 0 & 0 & 0 & 0 & 0 \end{bmatrix};$$

From (3.25) follows,

$$B_0 = \begin{bmatrix} 0 & 0 & 0 & 0 \\ 0 & 0 & 0 & \frac{l_w}{J} \\ 0 & 0 & 0 & 0 \\ 0 & 0 & 0 & 0 \\ 0 & 0 & 0 & 0 \\ 10\pi & 0 & 0 & 0 \\ 0 & 10\pi & 0 & 0 \end{bmatrix};\ B_1 = \begin{bmatrix} 0 & 0 & 0 & 0 \\ 0 & 0 & 0 & 0 \\ 0 & 0 & -1 & 0 \\ 0 & 0 & -l_s & 0 \\ 0 & 0 & l_s & 0 \\ 0 & 0 & 0 & 0 \\ 0 & 0 & 0 & 0 \end{bmatrix};\ B_2 = \begin{bmatrix} 0 & 0 & 0 & \frac{1}{m} \\ 0 & 0 & 0 & 0 \\ 0 & 0 & 0 & 0 \\ 0 & 0 & 0 & 0 \\ 0 & 0 & 0 & 0 \\ 0 & 0 & 0 & 0 \\ 0 & 0 & 0 & 0 \end{bmatrix}$$

Now, for each range of the controllers, for example the controller 4 (v= 20 m/s) we must find a controller which is robust against model uncertainties μ, v:

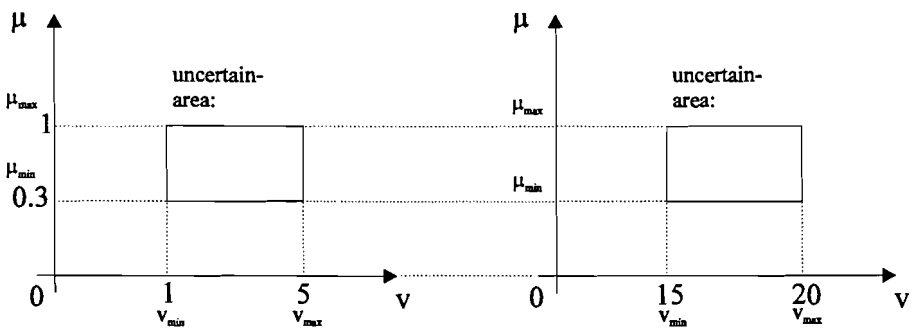


***Figure 3-15: Model uncertainty area.***

Now for $\mu$= 0.5 and $\mu$=1, 6 controllers for each have been designed. Results (performance) of the controllers designed for $\mu$=1 (dry road surface) subjected to process with operation point $\mu$=0.5 gives a damped oscillatory response, this was expected because it takes more effort to control the vehicle on wet road, then on dry road. While on the other hand controller designed for $\mu$= 0.5 subjected to process with operation point $\mu$=1, give a more stable response, the steering angles have been little distorted. This can be explained by the fact that driving on the dry road is more controllable then on wet road. So the controllers designed for $\mu$= 0.5 do well for process with $\mu$ = 1. To design a robust controller we take as starting point the "worst case" situation that is designing controllers for $\mu_{nom}$= 0.5, $v_{nom}$= $v_{max}$.
With the proper choice of the weighting filters and with the aid of the control-design toolbox MHC [12] a controller has been designed, after a "few" iterations. The best $\gamma$ -value of 0.9661 has been found. The classification of the other controllers shall be given in section 3.9

## 3.8. Controller validation/ closed loop transfers

For the controller validation we use the controller for v=20 [m/s] which is derived in the previous section. Since the controller has 5-inputs and two outputs, we have 10 possible transfer functions. We discuss now the relevant transfers.

### 3.8.1. controller validation

The plots of the controller transfer are given in figure (3-16)

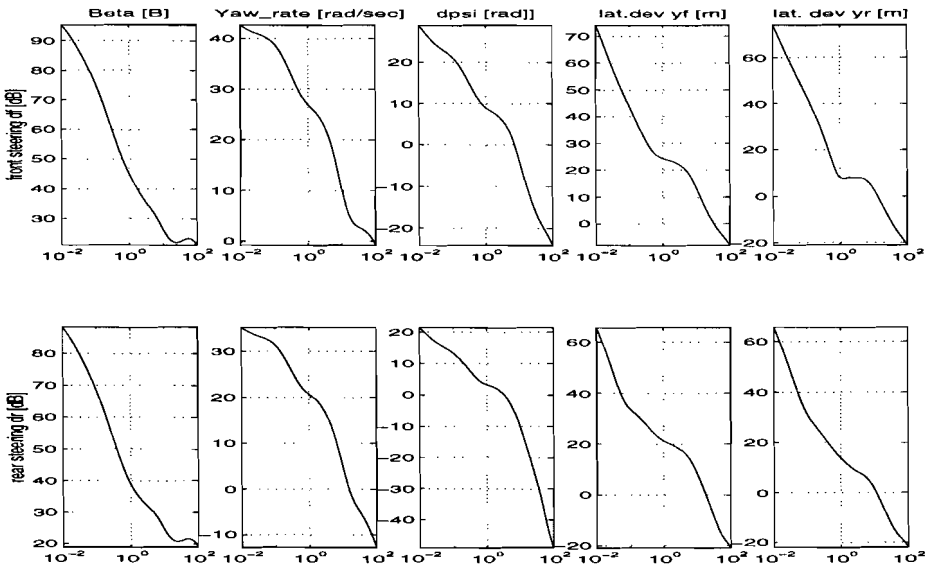


*Figure 3-16: Transfers functions of the controller 5_inputs → 2_outputs*

Since we have a process which has a low frequent behavior (bandwidth is about 10 [rad/sec] or 1.59 [Hz]), we discuss frequencies up to 30 [rad/sec]. Especially the interval 0 up to 10 [rad/sec] is of interest.

The transfers functions : $\begin{matrix} y_f \rightarrow \delta_f & y_f \rightarrow \delta_r \\ y_r \rightarrow \delta_f & y_r \rightarrow \delta_r \end{matrix}$ and shall be discussed.

These functions are given in figure(3-17) below,

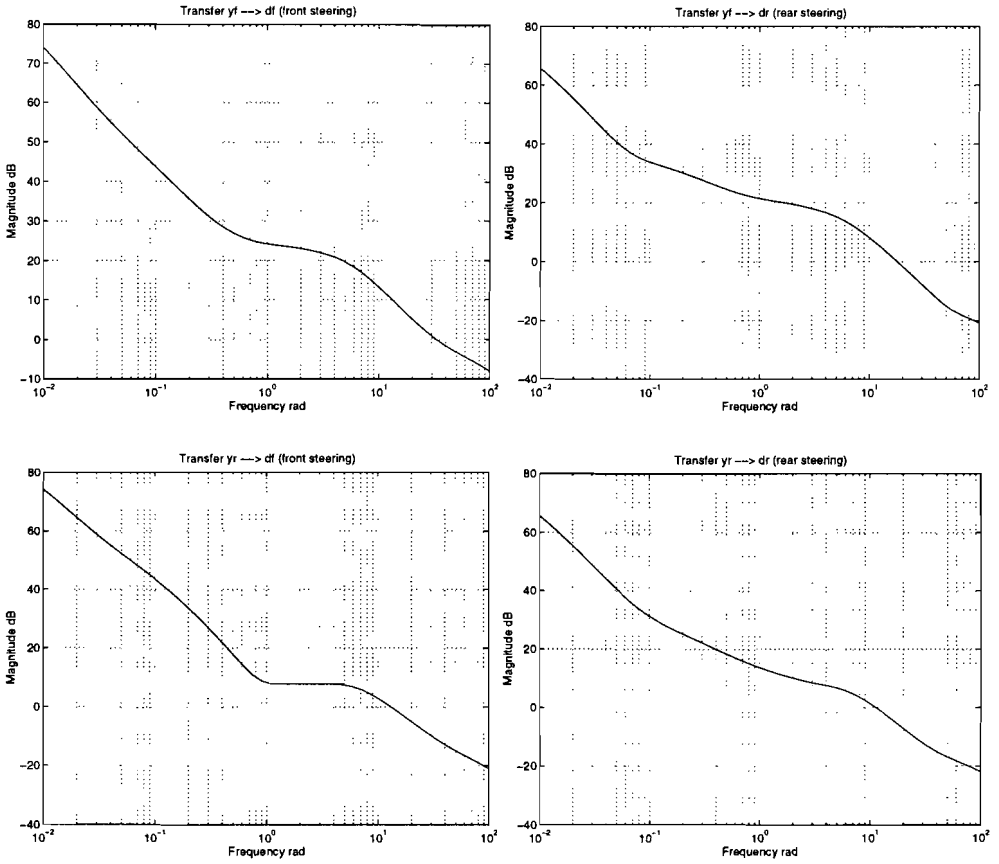


***Figure 3-17: Transfer functions of the controller***

From the first transfer yf→df , we see that the controller starts with integrating action up to 0.5 [rad/sec]. Between 0.1 and 6 [rad/sec] we see that the function has a low roll-off rate. This implicates a D-Action. So in this interval the controller behaves like a phase-lead controller. The phase margin of the system is increased, the system becomes more stable in this interval. In the interval 6 to 30 [rad/sec], the controller again acts as an integrator.
The same comments can be done on the second transfer yf→dr, however the intervals are different, the D-action is in the interval 0.7 to 6 [rad/sec]. From the third transfer yr→ df we see that the controller keeps integrating up to 1 [rad/sec]. In the interval 1 to 6 [rad/s], the controller behaves like a Proportional controller, with magnification about 7.5 [dB]. Thus, the coupling (yr→df) is small in this interval . In the interval 6 to 30 [rad/sec], the controller remains integrating action. The fourth transfer shows us that the D-action takes place within the interval 0.8 to 6 [rad/sec]. If we compare the first transfer, the coupling yf→ df and the last diagonal transfer, the coupling yr→ dr then we see that the coupling in the first transfer is stronger. This is because, the rear steering system is strongly dependent (rigid mechanical coupling) on the front steering system. The order of the controller is 17 states.

### 3.8.2. Closed loop transfers

We have in the augmented plant 12 inputs (input vector $w$) and 9 outputs (output vector $z$ ), in total 108 possible transfers. Also here, we discuss the important transfer functions. The transfer functions to lateral deviations and steering angles and steering angle rates. The closed loop transfers are shown in figure 3.18

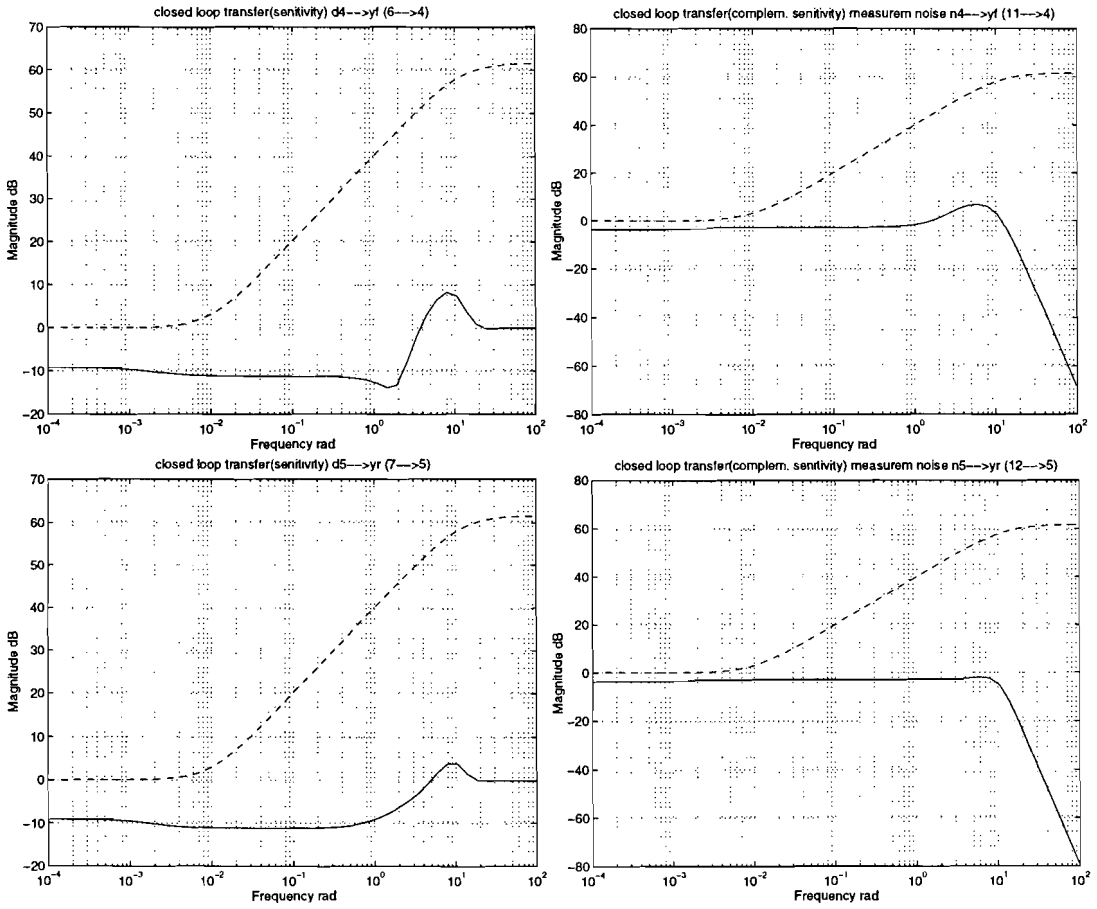


**Figure 3-18: closed loop transfer sensitivity and complementary functions**

In this figure, d4 and d5 are disturbances at the output and n4, n5 are the measurement noises.

- The sensitivity functions:

In this figure (3-18) striped lines denote the constraints (upper bounds) determined by the choice of the weighting filters. The solid lines are the transfer of the closed loop system *without* weighting filters. These lines have to lie below the striped lines, according to the equation (3.19). When the striped lines are hit by the solid lines in a certain frequency band, this indicates a bottleneck. From this figure we see that the transfer functions 6→4 (d4→yf) and 7→5 (d5→yr) have no bottlenecks. This is however tricky, because in practice the upper bound of the filters (striped lines) for frequencies below $10^{-2}$ rad/sec must have a constant slope as in the interval $10^{-2}$ → 10 . This occurs, because the controller design programs (MHC) cannot not deal with pure integrators. In our case we have used a filter ($W_e$) where the integrator term, s in 1/s form is shifted with a small value s+0.01. This shifting however should not effect the simulations. This shifting operation can be corrected in the simulation scheme (SIMULINK) by adding a function (s+0.001/s) before the process or after (since this is the closed loop situation). For low frequencies this function acts like 0.001/s (integration) and for higher frequencies with a transfer 1. This limitation of the weighting filters (no pure integrator characteristic) puts constraint for the sensitivity function S, at low frequencies < 0.01 rad/sec. The disturbance rejection is for frequencies up to 4 rad/sec. (bandwidth) about -12 [dB] which is not a ultimate high value (for example -40 dB). We see that the transfer rises above 0 dB around 8 rad/sec. This implies that there shall be an overshoot in the step response, this overshoot is however, tolerable (see simulations). This peak is smaller for transfer 7→5 (d5→yr) which means a lower overshoot. The sensitivity function had to be made small at low frequencies in order to make the steady state error of the outputs small (not necessarily zero). Another constraint to the sensitivity

function is the maximum allowable model uncertainty added to the output and represented by the function $V_d$ : $S = \frac{\gamma}{W_e V_d}$. So if we want to make S small, then we have to make $V_d$ large. However, this can be done up to a certain maximum value of $V_d$ if we should further increase this value, then the $\gamma$ -value of the of the controller increases rapidly $\gamma >> 1$ (see formula above) . And so, the disturbance rejection property is lost and also tracking property $T = \frac{\gamma}{W_e V_\eta}$ , because S, T are related with S+T=I. Since there is room left for low frequencies, we may be improve the performance (S) for low frequencies by increasing the gain of $W_e$ however, this is not sot possible because the bottleneck of transfer 11→4 (complementary function) does not allow this. Because increasing $W_e$ would lower $T = \frac{\gamma}{W_e V_\eta}$ .

The sensitivity functions from reference curvature $\rho_{ref} \rightarrow y_f$ and $\rho_{ref} \rightarrow y_r$ is given below,

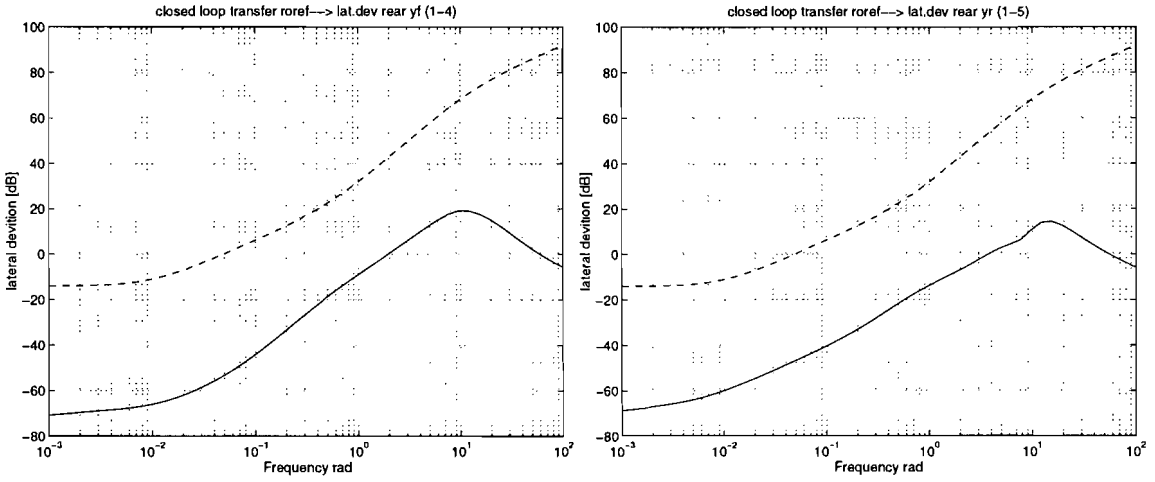


***Figure 3-19: The sensitivity functions from the reference curv. to lateral deviations ($y_f$ and $y_r$)***

As can be seen in this figure, there are no bottlenecks. The reference signal is attenuated (left figure) for frequencies up to 2 [rad/sec]. The steady state attenuation is about -70 [dB]. We see a peak (19 dB]) around 10 [rad/sec] which implicates that there shall be overshoot in time responses. The steady state attenuation is almost the same in the right figure. But here the reference is attenuated for frequencies up to 4 [rad/sec]. And the peak is lower (16 [dB]) and also shifted to a higher frequency 16 [rad/sec]. So we can conclude that the latter one (rear lateral deviation) is less sensitive to the curvature then the front lateral deviation, as expected.

- The complementary sensitivity functions

If we look at the transfer functions 11→4 (measurement noise4→ yf) in figure (3-18) then we see here are no bottlenecks. However, this can be a bottleneck in the practice, since we do not information about the specifications of the sensors. If we compare the peak in transfer (11→4) with the peak in transfer 12→5, the latter one is smaller. The rear lateral deviation is less susceptible then the front lateral deviation, because the rear lateral deviation is dependent on the front lateral deviation.

- The control sensitivity functions

The control sensitivities (R) are

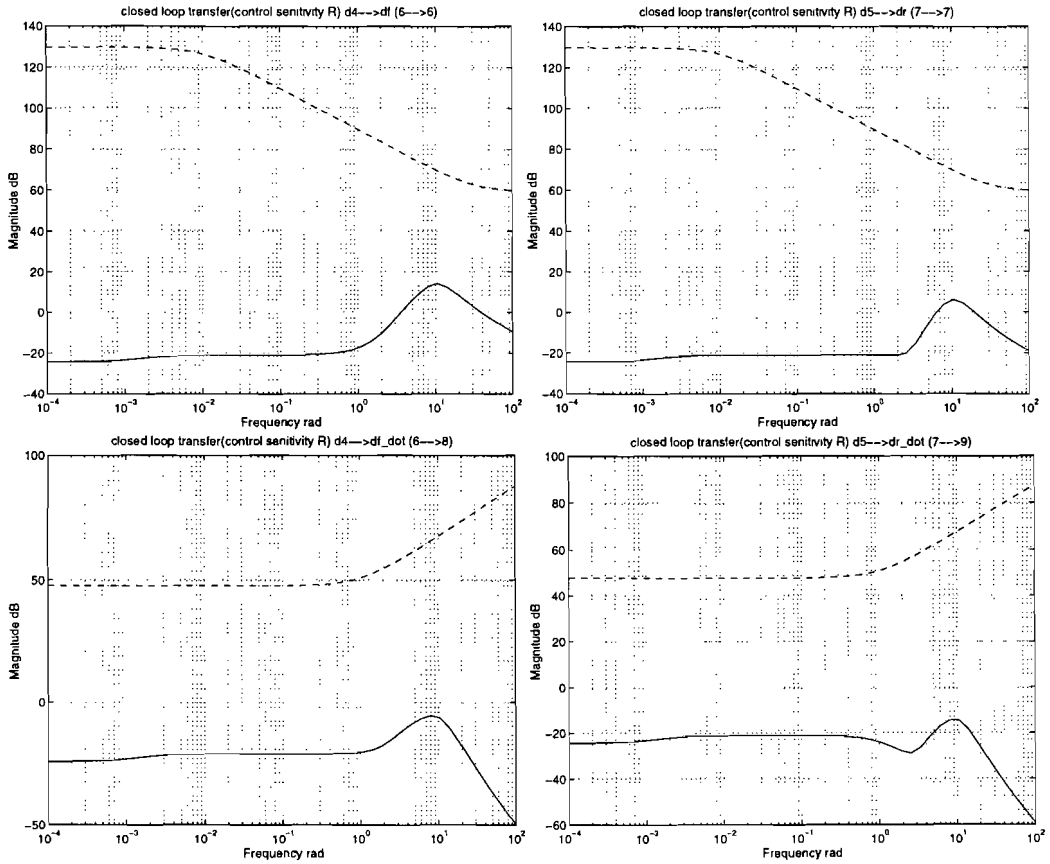


***Figure 3-20: The control sensitivities***

From these transfers we can see there are no bottlenecks, and therefore the actuators will not saturate. The weighting filters $V_d$ (which represents model uncertainty) together with the filters $W_u$ forms an upper bound (striped lines) of the control sensitivity (solid line): $|R| \leq \frac{\gamma}{|W_u V_v|}$

For the robustness we have to look (transfer 6→8) at the inverse of the function (3-22):

$|\Delta P| \leq \frac{1}{|R|} = \frac{|W_u V_d|}{\gamma}$, we see, roughly $|\Delta P| \leq +20$, up to 1 rad/sec and ≤-18 dB (peak value) at 10 rad/sec. Thus, the system is robust to frequencies up to 1 [rad/sec.] and less robust above this frequency (peak value -18 dB at 10 rad/sec). The same can be done for the other functions.

The closed loop transfer functions (control sensitivity) $\rho_{ref} \rightarrow \dot{\delta}_f$ and $\rho_{ref} \rightarrow \dot{\delta}_r$ are given below,

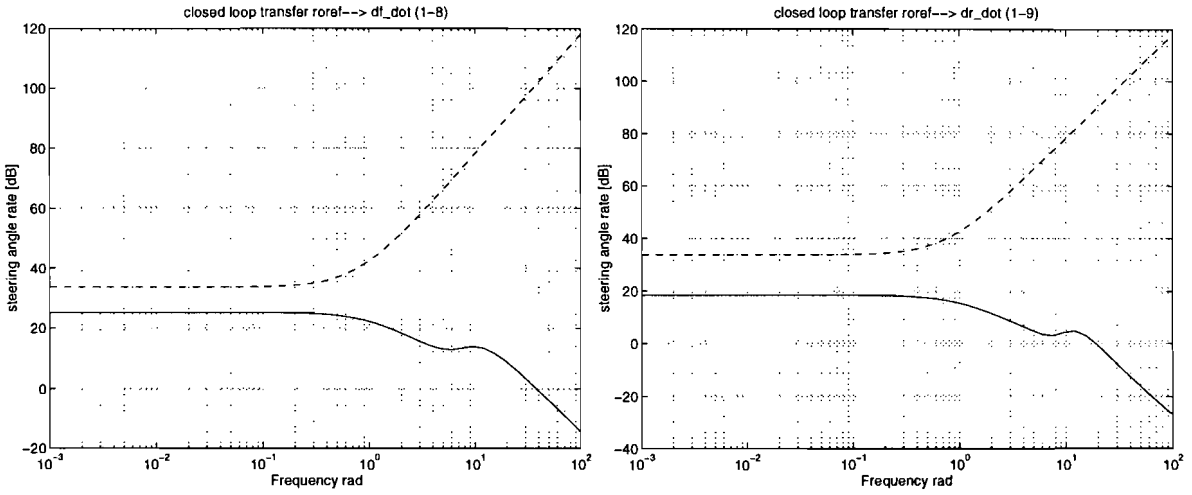


***Figure 3-21: The closed loop transfers*** $\rho_{ref} \rightarrow \dot{\delta}_f$ ***and*** $\rho_{ref} \rightarrow \dot{\delta}_r$

In this figure there are no bottlenecks, but if we should increase the weighting on the steering angle rates, then there shall be a bottleneck. So, the steering angle rates are sensitive for the reference signal. We shall see this with time simulations also. We see that the system shows (both cases) less robustness up to 1 [rad/sec]. Above this frequency the robustness increases. But the overall robustness of the rear steering angle rate is bigger. We see further, that there is a peak around 10 [rad/sec] implicating overshoot for the steering angle rates.

The transfer functions from the wind disturbance to the steering angle rates are also worth to mention these are,

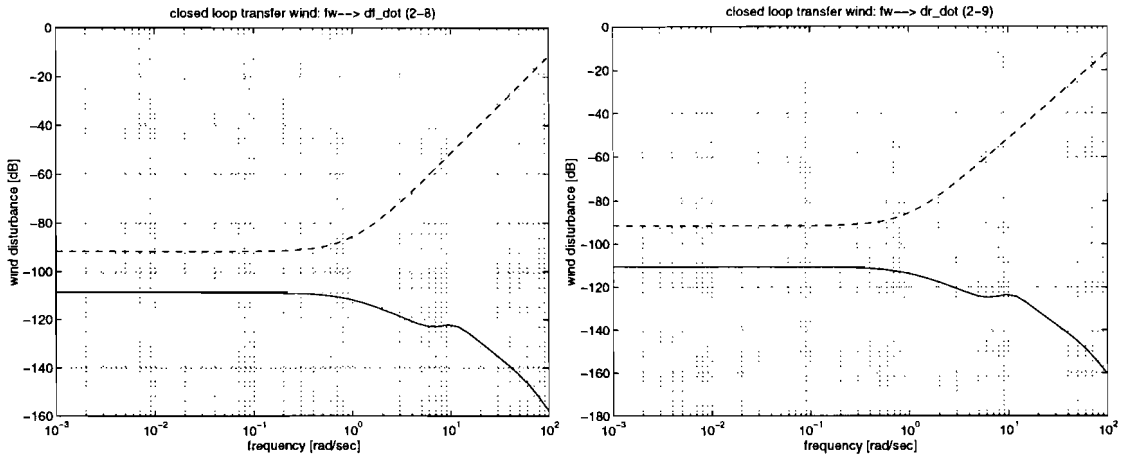


***Figure 3-22: closed loop transfer wind disturbance →*** $f_w \rightarrow \dot{\delta}_f$ ***and*** $f_w \rightarrow \dot{\delta}_r$

The wind disturbance attenuation is large for the whole frequency spectrum of interest due to the large weighting of this disturbing signal at the input of the augmented plant.
The wind disturbance has most of its influence on these steering angle rates. This is also expected because, if there is a disturbance, then the important factor to compensate for this disturbance are the steering angle rates, which is the reaction time of the steering actuator. The robustness to this disturbance is large +100 [dB] for frequencies up to 1 [rad/sec] and even increases above this frequency. The other outputs do also not suffer from this disturbance.

We can draw some conclusions from the closed loop transfer functions:

# We have seen that the measurement noise can be a potential bottleneck at low frequencies.

# Also the reference signal (curvature) to the steering angle rates can be a bottleneck, in practice when driving a car, one can feel that steering becomes a tough (and dangerous) job when a tight (sharp) curvature, $R<R_{max}$ at high speed has to be taken. So there is link to the reality of everyday car driving. See later with time simulations on the maximal curvature.

# The wind disturbance to the steering angle rates can be a bottleneck. Because the steering angle rates puts a limit on how fast the system can react to lateral disturbances.

- The robustness problem

We shall discuss these robustness problem now more in detail:
We know that the true process is represented by the equation:

$$P_{true} = P_{nom} + \Delta P$$

$\Delta P$ (process error) occurs because the true process has parameter uncertainties, in our case these are: $\mu(t)$ and v(t) . With

$$|\Delta P| = |P_{true} - P_{nom}|$$

we can determine the maximal process errors by plotting the maximal transfer functions for parameter uncertainties $\mu(t)$=[0.1:1] while $\mu_{nom}(t) = 0.5$ and v(t)= [15..22] m/s and $v_{nom}$=20 m/s. We assume that the mass is constant. However, also a plot can be made where the mass can vary between [9950..16000] [kg.] with $m_{nom}$=12000 [kg]. The plot of nominal and maximal transfer functions (only the transfer functions, steering angles→ outputs, are discussed) with varying mass looks like,

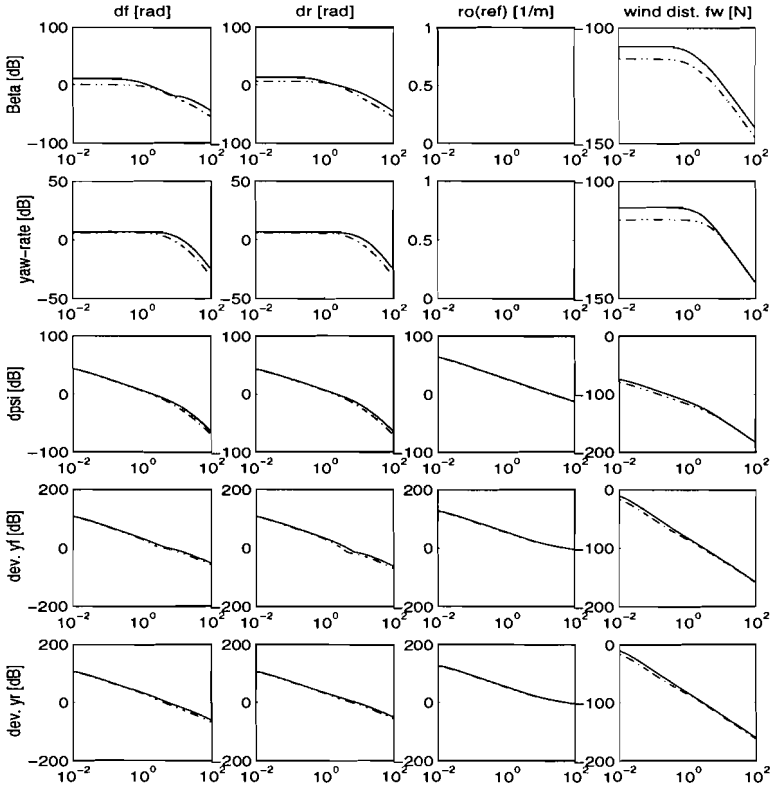


***Figure 3-23: Plot of maximal transfers and nominal transfers due to parameter variations***

In this plot the striped-dotted lines are the nominal process and the solid lines the maximal transfer of the process due to parameter variations. We consider this plot as a matrix where, the inputs are the $i^{th}$ column, i=1..4 and the outputs are the $j^{th}$ row, j=1..5. So we look for the transfers with indices: i=1,2 (first two columns) and j=1..5. We see that there is a large $\Delta P$ for the transfers to Beta . Also the $\Delta P$ for the transfers to yf and yr is large but, here the transfer functions are integrators, so parameter uncertainties at low frequencies can cause large $\Delta P$ . We can now plot the maximal $\Delta P$ which is the difference of the above functions.

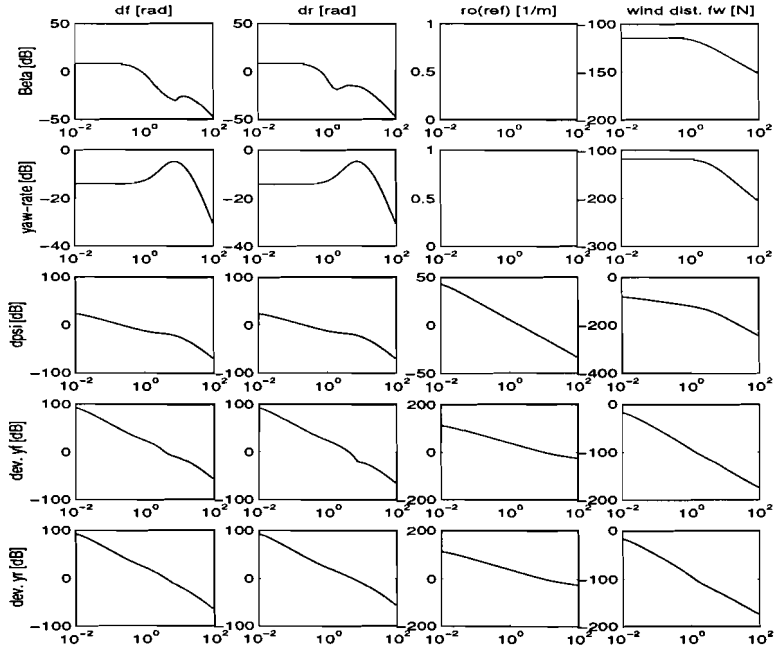


***Figure 3-24: Plot of $\Delta P$ , the maximal perturbation due to parameter variations.***

Here, the input→output relations are the same as in the previous figure (3-23): The inputs are $i^{th}$ columns and the outputs the $j^{th}$ rows. Only the first two columns are considered.

We see that there are peaks for the transfer to the yaw-rate; These peaks, which occurs due to parameter( $\mu(t)$, v(t)) changes, can be suppressed with proper choice of the filters in the equation $|R| \le \frac{\gamma}{|W_u V_d|}$ or $\boxed{|\Delta P| \le \frac{1}{|R|} \le \frac{|W_u V_d|}{\gamma}}$ which is the robustness criterion. So, the upper bound of these filters, and also the inverse plot of $|R|$ (figure 3-26) must lie above $\Delta P$ - plot (3-24) to guarantee robustness. This is so for all the transfers (robustness guaranteed ) except for the transfers to yf and yr which have a pure integrator form. A plot of the overall control sensitivity function R and inverse $R^{-1}$ is given in figure (3-25). We should look at the inverse of these functions (figure 3-26) and think if it were placed on figure (3-24), and check if it lies above the functions in (3-24), the plot of this is shown in figure 3-27

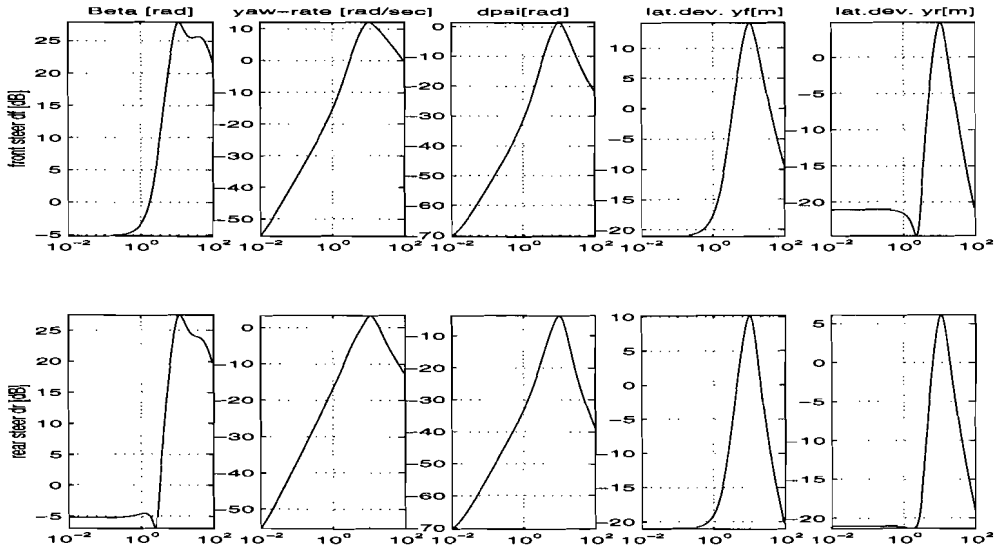


***Figure 3-25:The overall transfer plot of the control sensitivity***

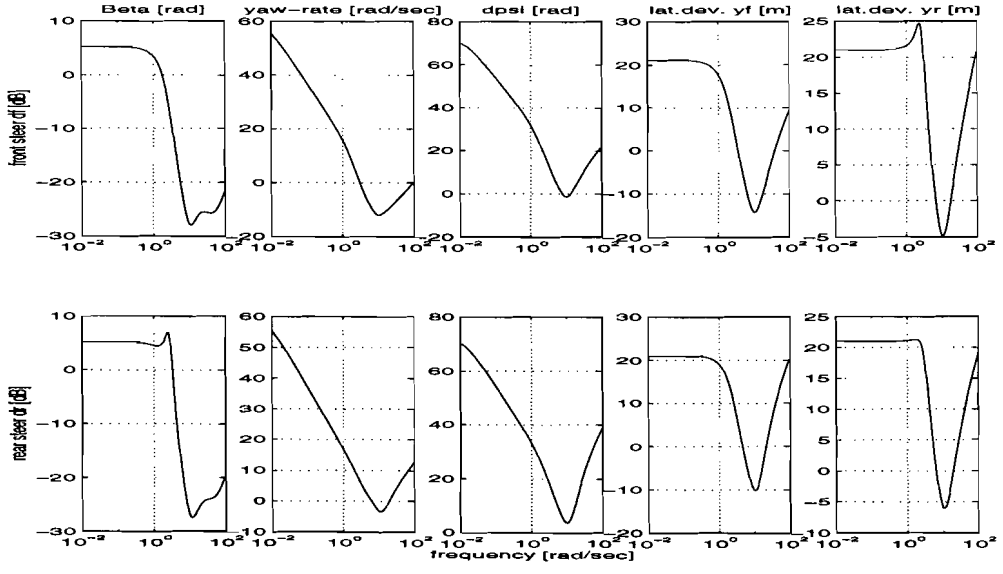


***Figure 3-26: The overall transfer plot of the inverse control sensitivity, $R^{-1}$***

In this plot the inputs are the $i^{th}$ -rows, i=1..5 (i=1→ Beta) and the outputs the $j^{th}$-columns, j=1,2 (j=1→ deltaf). We consider all the transfers i→j.

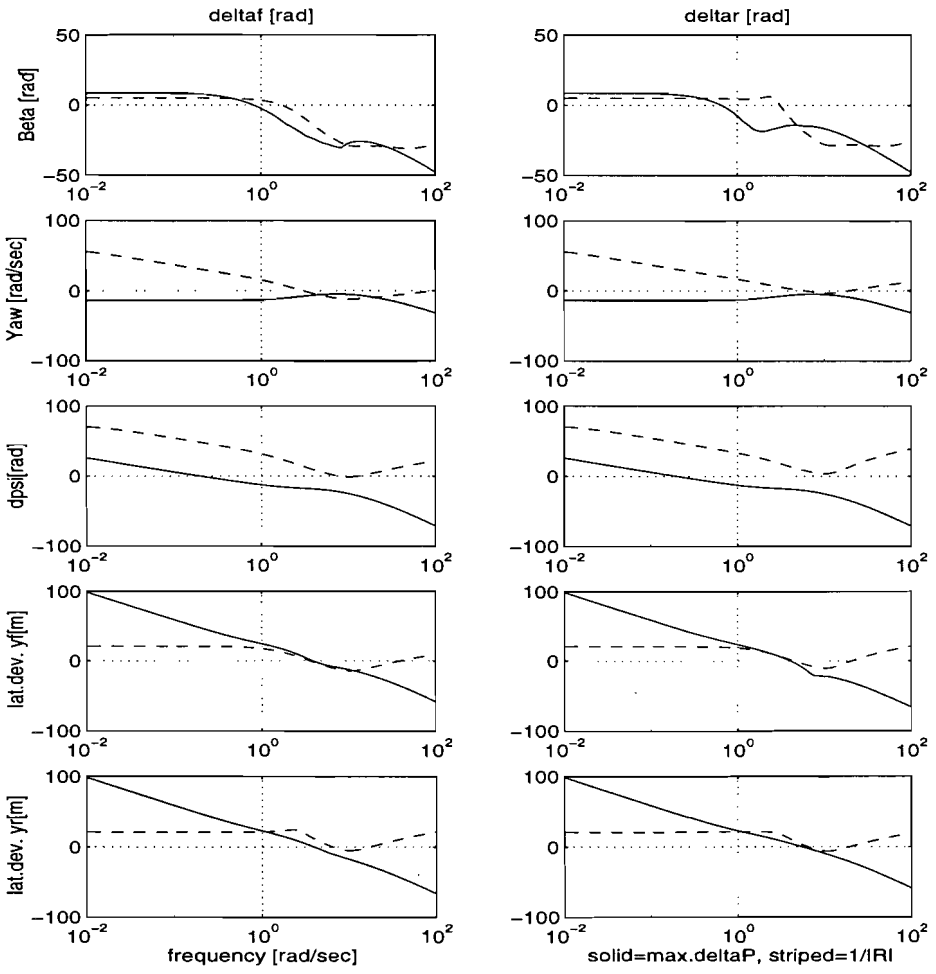


***Figure 3-27: Plot of max. ΔP and 1/lRl, (ΔP ≤ 1/lRl)***

In this figure the solid line is the max. ΔP and the striped line is the inverse control sensitivity. From this figure, we see that robustness to uncertainties for the input Beta to the outputs (deltaf, deltar) is acceptable for frequencies < 10 [rad/sec]. But if we look at frequencies around 10 [rad/sec] the striped line is under the solid line, which means that robustness here, may be improved by putting a large weight on the model uncertainty characterization-filter, $V_{d3}$ (around this frequency). It is clear from this figure, that the input Beta is most susceptible for parameter uncertainties. This is also verified with simulations later.

The maximal allowable model error (robustness) is for the inputs 'Yaw rate' and 'dpsi 'acceptable, especially for low frequencies (< 4 [rad/sec) and frequencies above 10 [rad/sec].

It is also clear from this figure, that the robustness to lateral deviations (front, rear) for low frequencies (< 1 [rad/sec]) robustness is not guaranteed, due to pure integrator form of these transfer functions (small variations, give large ΔP at low frequencies). The results may be improved by more precise modeling of ΔP (μ analysis/ synthesis).

### 3.9. Classification of the controllers

We have discussed the controller designed for v=20 [m/s] in the previous sections. Now, with this notion we can elaborate the other controllers.
The design steps for all the controllers is the same. Thus all the weighting -filters are tuned the same way, except the reference filter $V_{11}$ of the controllers where the maximum tightness of the curvature $\rho_{ref}$ is dependent on the speed of the vehicle as mentioned before,

$\rho_{ref} \cdot v^2 \leq a$ , with a =2 [m/s$^2$]

The properties of the filters are given in Table 2. In this table, the $\gamma$ -value, $V_{11}$ and velocity range are elaborated .

***Table 3-2: Properties of the total controllers***

| Controllers | velocity range [m/s] | $\gamma$ , controllers [-] | Ref. Filter $V_{11}$ |
|---|---|---|---|
| $K_1$ | 0..5 | 2.03031 | $\frac{0.048}{s+0.6}$ |
| $K_2$ | 5..10 | 0.96606 | $\frac{0.012}{s+0.6}$ |
| $K_3$ | 10..15 | 0.96606 | $\frac{0.00533}{s+0.6}$ |
| $K_4$ | 15..20 | 0.9661 | $\frac{0.003}{s+0.6}$ |
| $K_5$ | 20.25 | 0.95 | $\frac{0.00192}{s+0.6}$ |
| $K_6$ | 25..30 | 0.9961 | $\frac{0.00133}{s+0.6}$ |

The denominator of the reference filter is the same for all the filters. We assume that the bandwidth of the curvature for all the controllers is the same as for the controller $K_4$ . This is certainly true at low velocities of the vehicle. The $\gamma$ -values of the controllers $K_2$....$K_6$ are nearly one. The $\gamma$ -value of $K_1$ is a little higher , indicating that the robustness is small compared with the other controllers.

# 4. Bumpless transfer

In practice many plants cannot be controlled by a single linear controller because their dynamics vary too greatly over the operating range. The dynamics of the vehicle depend on v, which may very between 0 and 30 [m/s.
So gaining speed or decay of the speed, depending on the operation point, there is a need to switch between different controllers. In the next section a method is discussed to switch between the controllers.

## *4.1. Switching between controllers*

For the operating range v=[0;30] [m/s] mentioned above we have designed 6 controllers:

| controllers | nominal velocity [m/s] | range [m/s] | relays on |
|---|---|---|---|
| $K_1$ | 5 | 0..5 | Relay1 |
| $K_2$ | 10 | 5..10 | Relay2-Relay1 |
| $K_3$ | 15 | 10..15 | Relay3-Relay2 |
| $K_4$ | 20 | 15..20 | Relay4-Relay3 |
| $K_5$ | 25 | 20..25 | Relay5-Relay4 |
| $K_6$ | 30 | 25..30 | 1- Relay5 |

***Table 4-1: Controller intervals***

Intervals mentioned above can be chosen different. We could have chosen fewer controllers (may be 3 or 4) but this would decay the performance of each controller, since we then require each controller to be robust for a larger velocity range.
From the reasons mentioned above, we can conclude that we need a controller scheme . The switching of the controllers is depicted in the figure below.

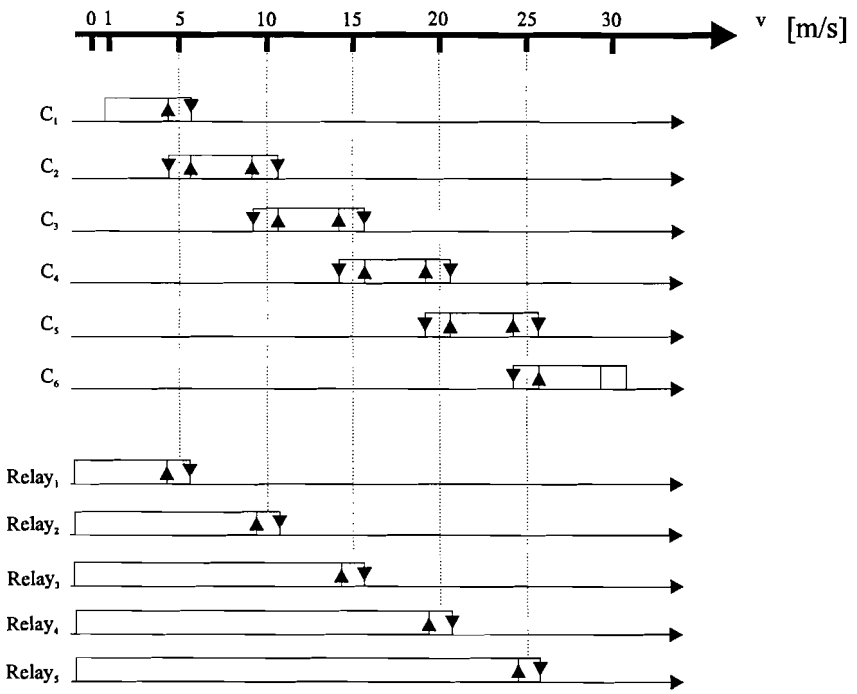


***Figure 4-1: Switching of the controllers.***

During the switching from one controller to the other however, oscillations can occur between two controllers across a switching line. This can be prevented by building hysteresis (+/- 1 [m/s]) into the switching levels. A switching element which has this property is a relay block.

From this figure (4.1) we can see that relay blocks are being used for switching. Table 1 gives the switching moments for each controller. The total range of velocity v is divided into sub intervals each of 5 m/s . Further, the switching points between the controllers are depicted during gaining or decay of the speed. For each operating range of the controllers, we have to investigate which relay is on or off. The switching moments given in table 1 can be put in a matrix form and then implemented in Simulink.

So the switching matrix is then

$$\begin{bmatrix} K_1 \\ K_2 \\ K_3 \\ K_4 \\ K_5 \\ K_6 \end{bmatrix} = \begin{bmatrix} 1 & & & & & \\ -1 & 1 & & & 0 & \\ & -1 & 1 & & & \\ & & -1 & 1 & & \\ & 0 & & -1 & 1 & \\ & & & & -1 & 1 \end{bmatrix} \begin{bmatrix} \mathrm{Re}lay_1 \\ \mathrm{Re}lay_2 \\ \mathrm{Re}lay_3 \\ \mathrm{Re}lay_4 \\ \mathrm{Re}lay_5 \\ 1 \end{bmatrix} \tag{5.1}$$

$K_1$ works if Relay1 is on, $K_2$ works if Relay2 on and so on.

### 4.2. Bumpless transfer

Hanus [12] has done some research in the field of 'anti windup' precautions of integrators. This method can also be used for bumpless transfer with some adjustments of the scheme. This technique achieves smooth transition between controllers by ensuring that the states of the next controller to be switched are always the same with current controller states.
We consider the case of two controllers $K_1$ and $K_2$ which meet the performance requirements while working at their operating points. Figure 4.2 shows the bumpless transfer scheme in which $K_1(s)$ is switched on, works in the usual mode while the $K_i(s)$ 's (for i$\in$ {2..6}) operate in open loop. The $F_i$'s are used to stabilize the $K_i(s)$'s and inhibit the growth of the $u_i$'s. From the figure 4.2 we can now derive an expression for $u_2$

$$u_2 = K_2\{e - F_2(u_2 - u)\}$$

which can be rewritten as

$$u_2 = (I + K_2F_2)^{-1}\{K_2e + K_2F_2u\} \tag{5.2}$$

and for the error

$$\hat{e}_2 = K_2(e - F_2\hat{e}_2) - u$$

which can be rewritten as

$$\hat{e}_2 = (1 + K_2F_2)^{-1}\{K_2e - u\} \tag{5.3}$$

If we choose a constant $F_2$ such that $||F||_2 >> 1$, we see that $\hat{e} \approx 0$. This means that $u \approx u_2$ and a bumpless transfer is possible. Once the switch is toggled $K_1(s)$ and $K_2(s)$ interchanges roles, $K_1(s)$ now operate in open loop and the feedback loop around $K_1(s)$ is activated while that around $K_2(s)$ is disabled. The large gain of $F_1$ acts rapidly to take $\hat{e}_1$ to zero so that $u_1 \approx u$. This scheme may be generalized to include more then two controllers. Furthermore in this setup the constant $F_i$'s serve a dual purpose firstly, they provide a rapid decay on the transients in the $u_i$'s following switches between controllers and secondly, they act as "anti- windup" compensation whenever the $u_i$'s saturate.

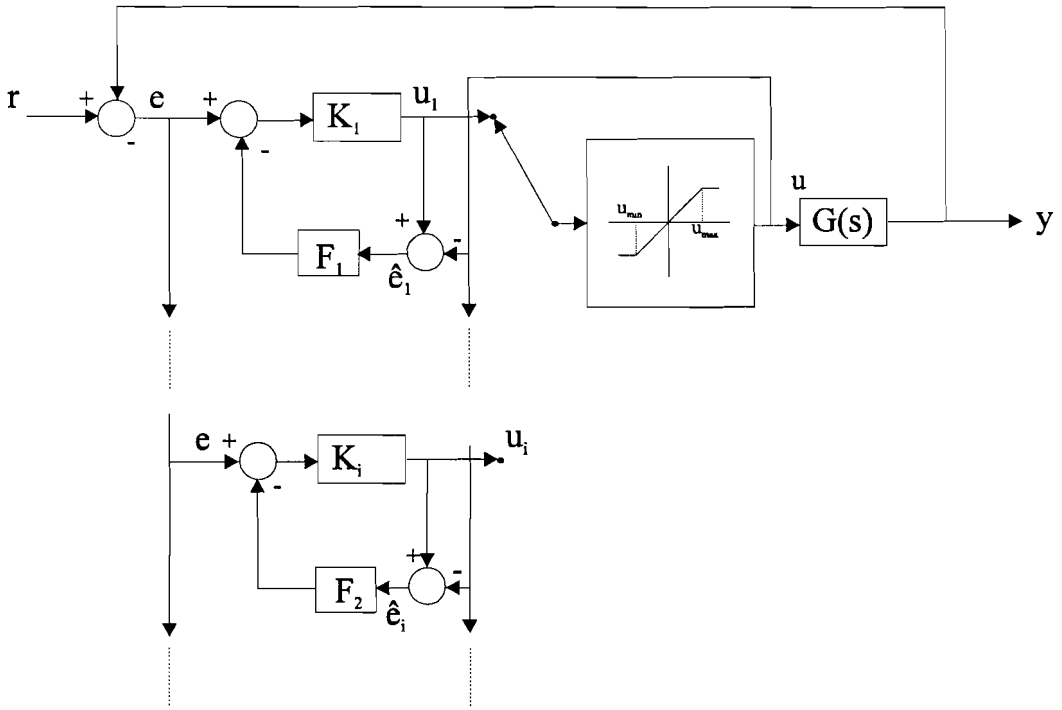


*Figure 4-2: Controller bumpless transfer scheme with anti windup protection*

We shall see by the simulations section 5 , that the use of this scheme is crucial of importance
In the next section we will discuss the anti wind up phenomenon more extensively.

## 4.3. Windup and anti-windup precautions

In the context of electrical driven vehicles, the electrical motors (the actuator) can have a maximum and a minimum voltage say $U_{min}$ , $U_{max}$ . If integral control is combined with such actuators, a phenomenon known as *integrator windup* may occur when the actuator saturates. For example, in the event of persistent large commands, the integrator build up a large output, causing the actuator to saturate resulting in a large overshoot and control effort.
In this section, we consider the scheme in figure 4.3 which inhibits the unlimited growth of the signal $u_c$. This anti-windup scheme consists of a feedback loop around the controller which is activated as soon as $u=u_{max}$ (or $u_{min}$) and acts rapidly to take e to zero. In the event that $u= u_c$, everything works normal. If u saturates at $u_{max}$ (or $u_{min}$), we see that

$$u_c = K(e - F(u_c - u_{max}))$$

which can be rewritten as

$$u_c = (I + KF)^{-1}(Ke + KFu_{max})$$

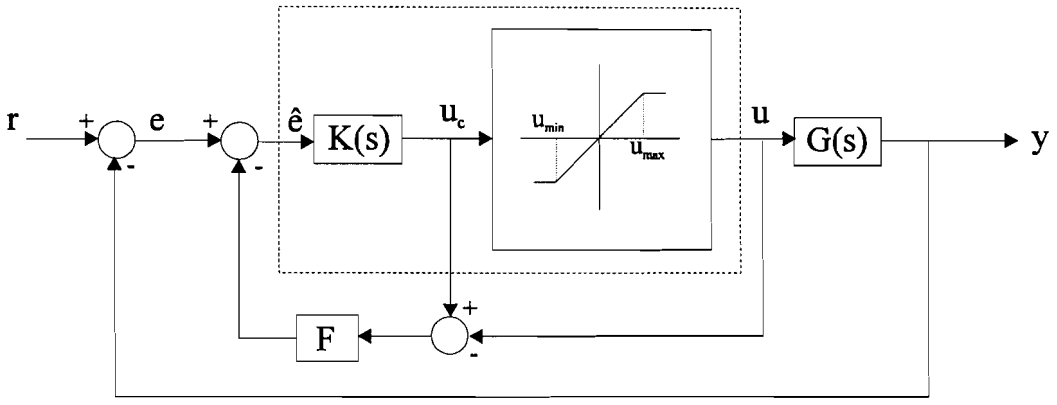


***Figure 4-3: Anti-windup scheme for plant input saturation.***

By choosing a constant or an active low pass filter $||F||_2 >> ||K(s)||_\infty$ such that $||FK(s)||_\infty >> 1$ we get

$$u_c = (KF)^{-1}(Ke + KFu_{max})$$
$$\approx u_{max}$$

Thus during saturation, $u_c$ is clamped at $u_{max}$ and windup is prevented, consequently, the controller may come out of saturation rapidly with a moderate control effort and the system resumes normal operation. Otherwise, the presence of integrators in the controller will cause windup eventually resulting in instability if the system remains in saturation for a long period.
All this results in a calmer actuator activity, and the actuator can not easily be damaged.

# 5. Simulations process with controllers

In this section simulations shall be done for the derived controllers. First the simulation schemes shall be discussed. Then simulations are done for environmental conditions like:

- The influence of strong wind- gusts.
- Radius of the curvature.
- Road adhesion factor
- Simulation with limited steering angle rates

And simulations due to the influence of varying mechanical parameters of the vehicle:

- Cornering stiffness of the tires.
- The placement of the sensor. This parameter shall be varied to show the importance of the sensors places .
- Center of gravity of the vehicle, distance of the CG to the front ($l_f$ )and rear ($l_r$) axles.

Furthermore, the importance of the bumpless- transfer method shall be outlined.

Before discussing the simulation results, we first outline the simulation schemes.

## *5.1. Simulation schemes.*

The simulations are done with Simulink- program. The process parameters are calculated with matlab m- files. These programs are given in the section software.

The simulation scheme of the vehicle with controller is given in figure,

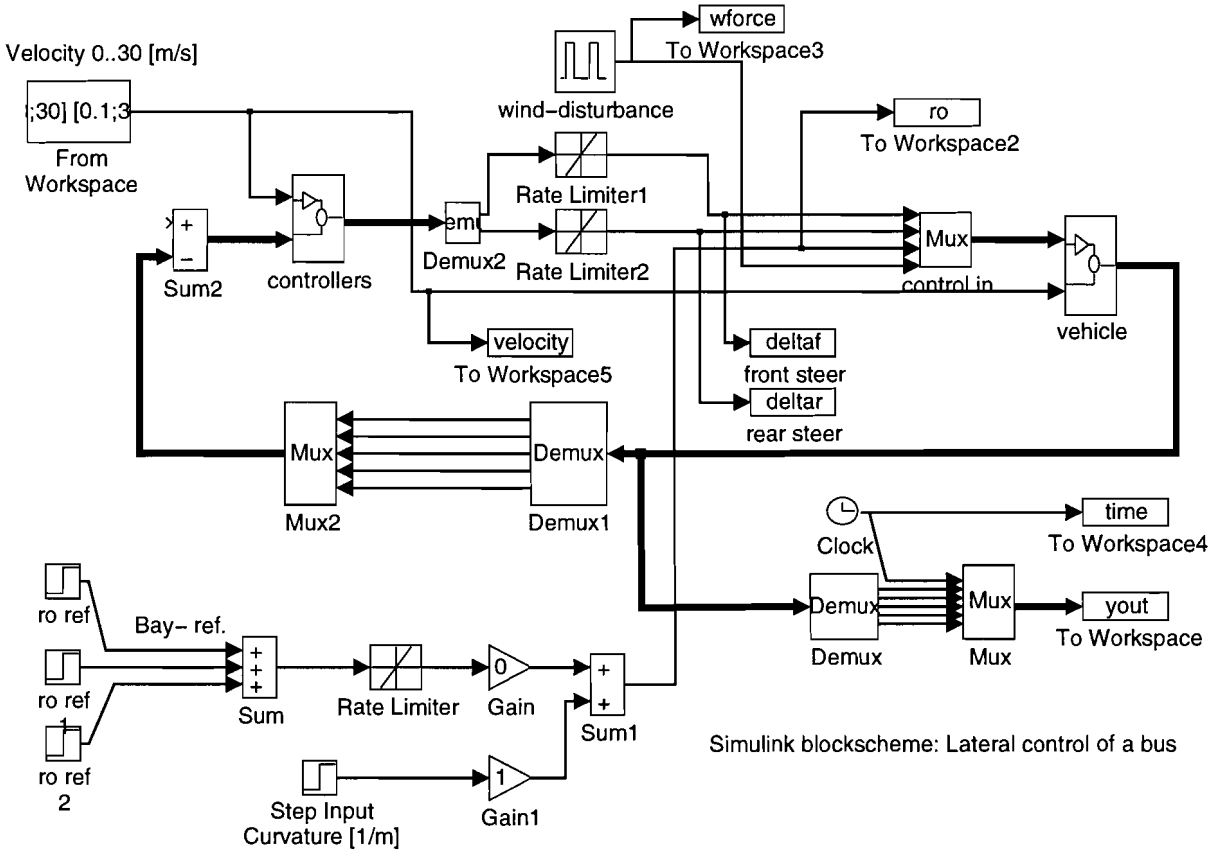


***Figure 5-1:Simulink- Block scheme***

In this scheme the following signals are saved to workspace: $y_{out}$, contains the output signals and $w_{force}$ = wind force, ro= reference (curvature). In this the rate- limiters 1,2 are used to determine the maximal steering angle rates.

The block controllers looks like,

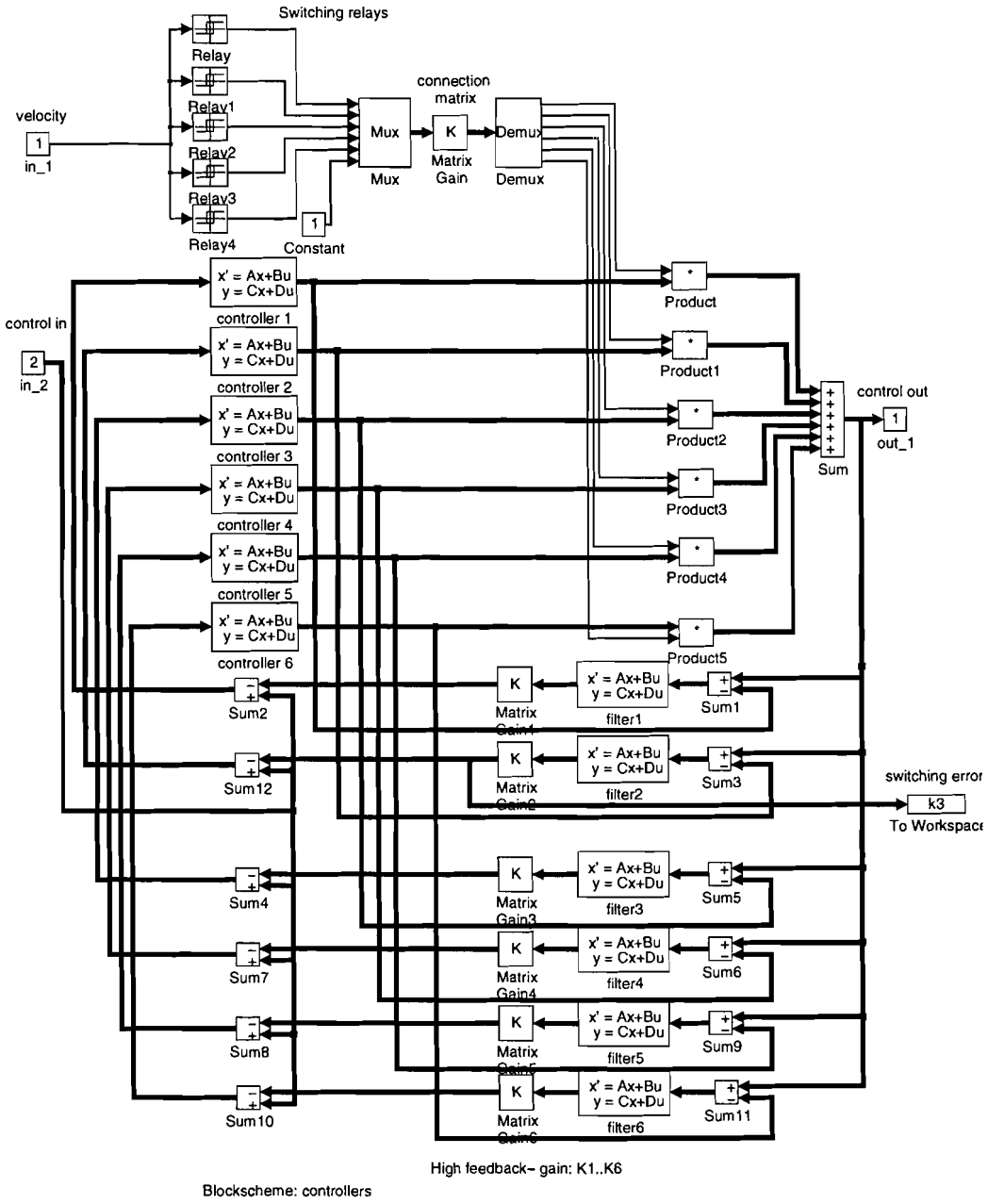


***Figure 5-2: Block scheme of the controllers with bumpless transfer***

The high- gain feedback $K_{HG}1..K_{HG}6$ is a constant matrix gain:

$$K_{HG_i} = 10^8 \begin{bmatrix} 1 & 0 \\ 0 & 1 \\ 0 & 0 \\ 1 & 0 \\ 0 & 1 \end{bmatrix}, \text{i= 1..6}$$

The two controller output signals $\delta_f$ *and* $\delta_r$ are fed back to the controller input (via the Bumpless transfer scheme). However, there is no feedback to the third input, see matrix gain $K_{HGi}$ since this input is already in the fourth and respectively on the fifth input. A high gain of $10^8$ is used to make bumpless transfer possible (smooth switching of the controller states).
First order lag smoothing filters: Filter1..Filter6 are used for each channel (=2 control channels) in order to suppress noise. The transfer function of the filter for each channel is

$$V_{smooth,ch1,ch2} = \frac{10}{s+5}$$

the Bode- plot of this transfer function is,

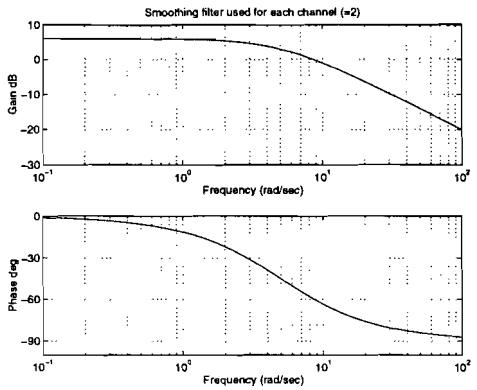


***Figure 5-3: Smoothing filters***

The bandwidth of the filter is about 10 [rad/sec] or 1.59 [Hz]. Amplitudes above this frequency are attenuated. The implementation is in state space form,

$$\dot{\vec{x}} = A\vec{x} + B\vec{u}$$
$$\vec{y} = C\vec{x} + D\vec{u}$$

which is

$$\dot{\vec{x}} = \begin{bmatrix} -5 & 0 \\ 0 & -5 \end{bmatrix}\begin{bmatrix} \delta_f \\ \delta_r \end{bmatrix} + \begin{bmatrix} 10 & 0 \\ 0 & 10 \end{bmatrix}\begin{bmatrix} u_1 \\ u_2 \end{bmatrix}$$

$$\dot{\vec{y}} = \begin{bmatrix} 1 & 0 \\ 0 & 1 \end{bmatrix}\begin{bmatrix} \delta_f \\ \delta_r \end{bmatrix} + \begin{bmatrix} 0 & 0 \\ 0 & 0 \end{bmatrix}\begin{bmatrix} u_1 \\ u_2 \end{bmatrix}$$

The block "vehicle" which represents the velocity dependent state-space description of the process and looks like,

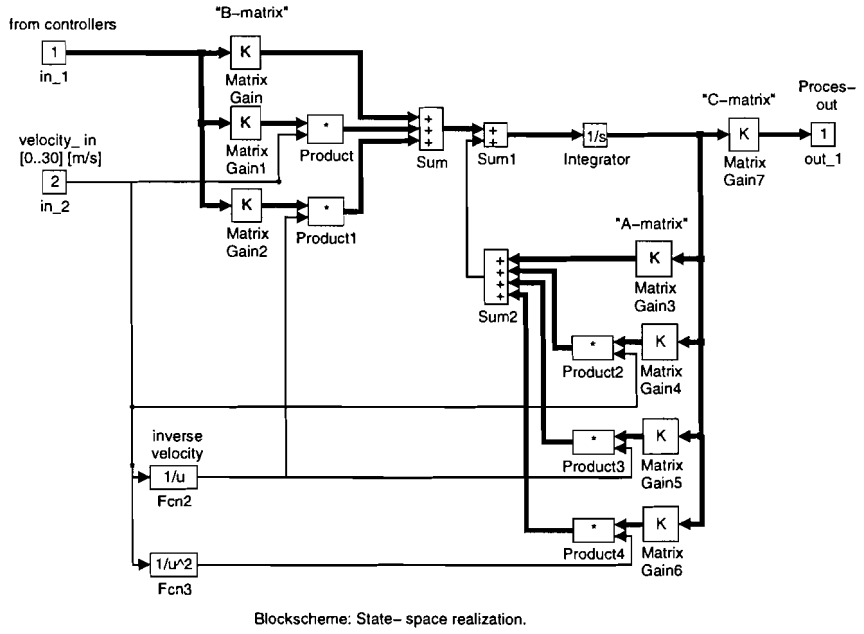


***Figure 5-4: Block scheme state- space realization of the process***

## 5.2. Simulations environmental conditions and parameter uncertainties

In this section, we discuss the simulations mentioned at the beginning of this section and also mentioned by the sub-section 'Design- specifications'. We start with the nominal values of the vehicle parameters:

Environmental parameters:
ro (ref)=1/200 [1/m], fw=10000 [N] ,

Vehicle parameters (nominal):
mu=0.5 [-], $c_f=c_r=300$ [kN/rad], $l_s=2.5$ [m], $l_f=l_r=5$ [m], m=10000 [kg],

Then simulations are done with parameter uncertainties of the vehicle parameters:

mu=[0.3..1], $c_f=198$ [kN/rad], $c_r=470$ [kN/rad], $l_s=[0.5, 1.5, 6.5]$ [m], and shifting the CG: $l_f=3$ and $l_r=7$ [m], to front and vice- versa: $l_f=7$ and $l_r=3$ [m] to rear.

- Nominal environmental simulations are done for the curvature and the wind disturbance. Figure 5.5a shows the nominal simulation. Figure on the right shows the simulation of maximal acceleration.

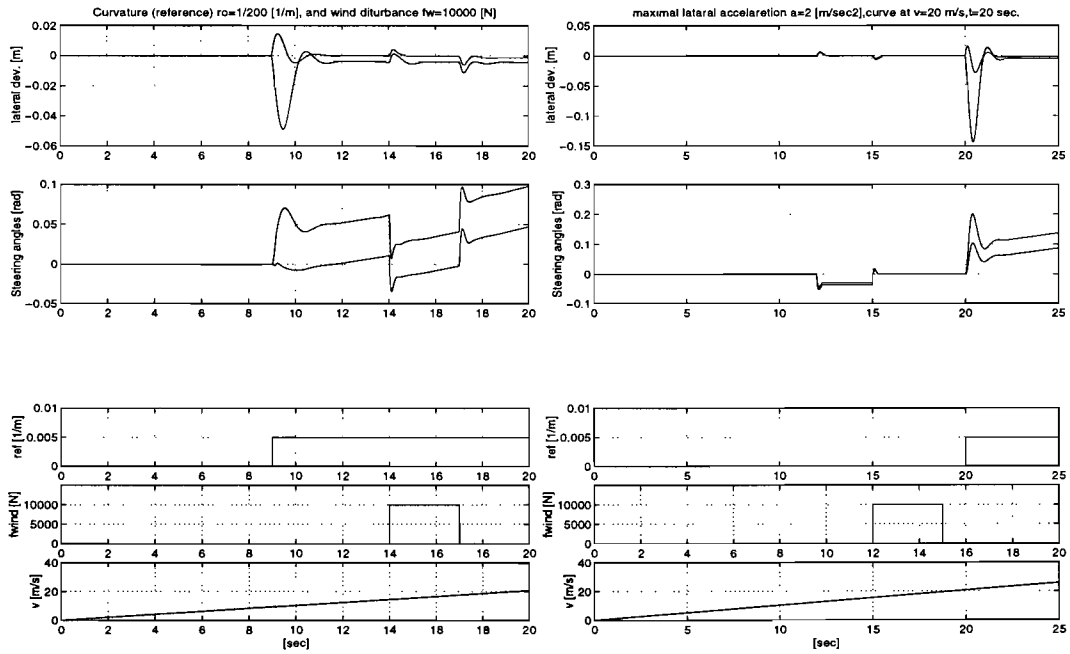


***Figure 5-5a: Nominal plot for environmental test***

In this (left) figure we see that the lateral maximal deviation at the front: -4.8 [cm] and for the rear deviation:1.5 [cm]. The latter one is small because the rear steering system is dependent (rigid coupling) on the front steering system. The simulation inputs are the signals denoted at the bottom of the figure. There is a small steady-state error 0.5 [cm]. This occurs due to the steady state performance of the sensitivity function which, can be improved. But, the limited integrator action of the weighting filter: $W_e$ does not allow this improvement. We see also in this figure that the steering angles have a constant difference during steady state cornering which starts at 9 sec. and holds on.

There is a constant difference in steering angles during a wind gust which starts at 14 [sec]. This can be explained by the fact the wind force acts on the aerodynamical center of the vehicle which lies at a distance $l_w$ from the CG (see also figure (2-7)). This causes a disturbing moment $m_z=f_w . l_w$ , which is compensated by the vehicle (moment balance), by applying a opposite moment which arises due to a constant difference between the front and rear steering angles. See also equation (2.7). The lateral deviations due to this disturbance moment is small: 1 [cm] maximum. One interesting observation is also that the steering angles have opposite signs at low speeds (left figure). This is also logical, since if we consider a truck with multiple axles, then it can take a curve easily if the rear wheels have a opposite steering angle. So there is also less friction of the tires with the road, since the rear tires are moving with an steering angle to the good direction (they are not forced ) . At higher speeds ($v_{critical}$>15 [m/s]) the steering angles have the same direction; The rear wheels give an opposite lateral force, in order not to slip out of the curve during cornering.
An other example where the steering wheels can have the same direction is when a car a with four wheel steering starts a line change maneuver to pass by some other vehicle. Then this maneuver can done fast, if the rear wheels have the same direction as the front wheels.

- The "slalom"- test

To study the behavior of the steering angles for increasing speed, the following simulation is done in figure below,

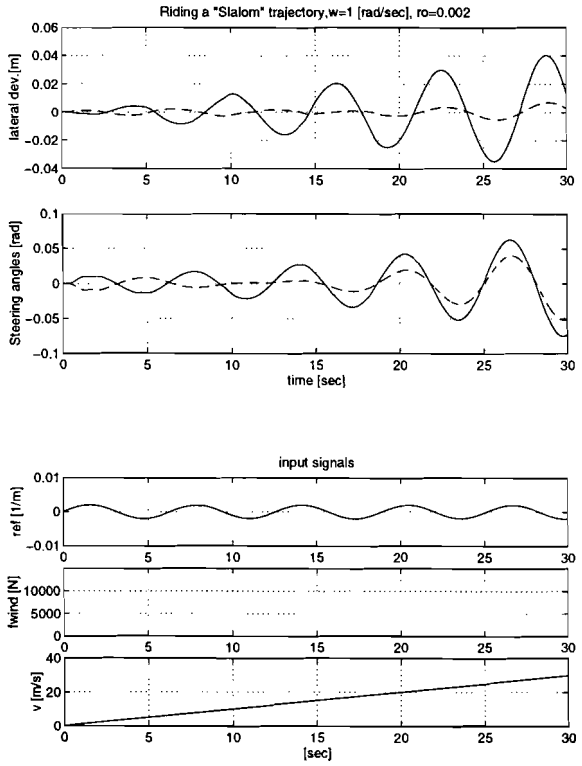


***Figure 5.5.b: The slalom test***

In this simulation we take for the reference curvature, a sinusoid function to simulate a "slalom" test. This function is $\rho(t) = 0.001 \cdot \sin(\omega t), \omega = 1[rad\ /\ s]$. The speed is increasing from 0..30 [m/s]. As we can see from the figure, the steering angles are in the opposite direction, this is so up to the so called, critical speed (15 [m/s]). Above this speed, the steering angles are in the same direction. We see, that the front steering (solid) is more active then rear steering (dashed) with increasing speed. For this maneuver, the deviations are acceptable. The system is under control.

Maximal acceleration at velocity v= 20 [m/sec]

The lateral deviations however, are becoming large (peak -14.5 [cm]) for the situation of the maximal (right figure of 5-5) lateral acceleration; $\rho_{ref} \cdot v^2 \leq a$ where, a=2 [m/s$^2$] and the velocity starts at: v=[20 m/sec]. Also the steering angles are larger (front steering angle, peak value: 0.2 [rad]). The system becomes less damped.

Besides the lateral deviations $y_f$ and $y_r$, we have the outputs: $\beta, r, \Delta\psi$ who also need to be considered on their behavior.
The plot of the time responses, for these outputs is given below,

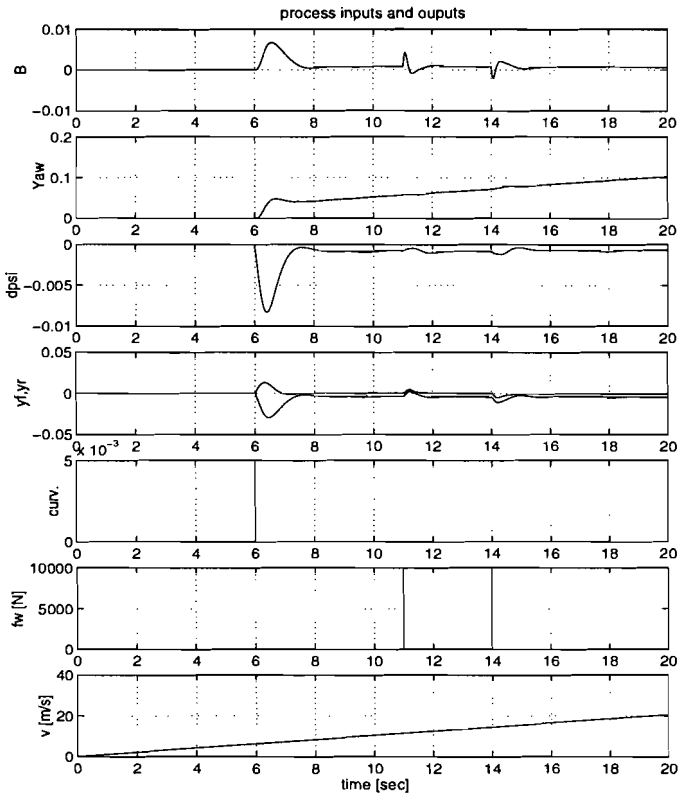


***Figure 5-6: Input and output signals of the process***

All the outputs show acceptable levels. We see that the side slip shows some overshoot for the wind disturbance, which is corrected by the controller. The deviation $\Delta\psi$ ,the deviation between centerline vehicle and the tangent to the road shows a small steady state error. The Yaw increases, due to v, to equalize the reference term $\rho_{ref} \cdot v$ , so that the r- $\rho_{ref} \cdot v$ =0 or r= $\rho_{ref} \cdot v$ ; The reference trajectory.

- In reality the condition of the road surface can be icy, wet or dry, this condition is represented by the road adhesion coefficient $\mu$ . To see what influence it has to the system the following simulations has been done:

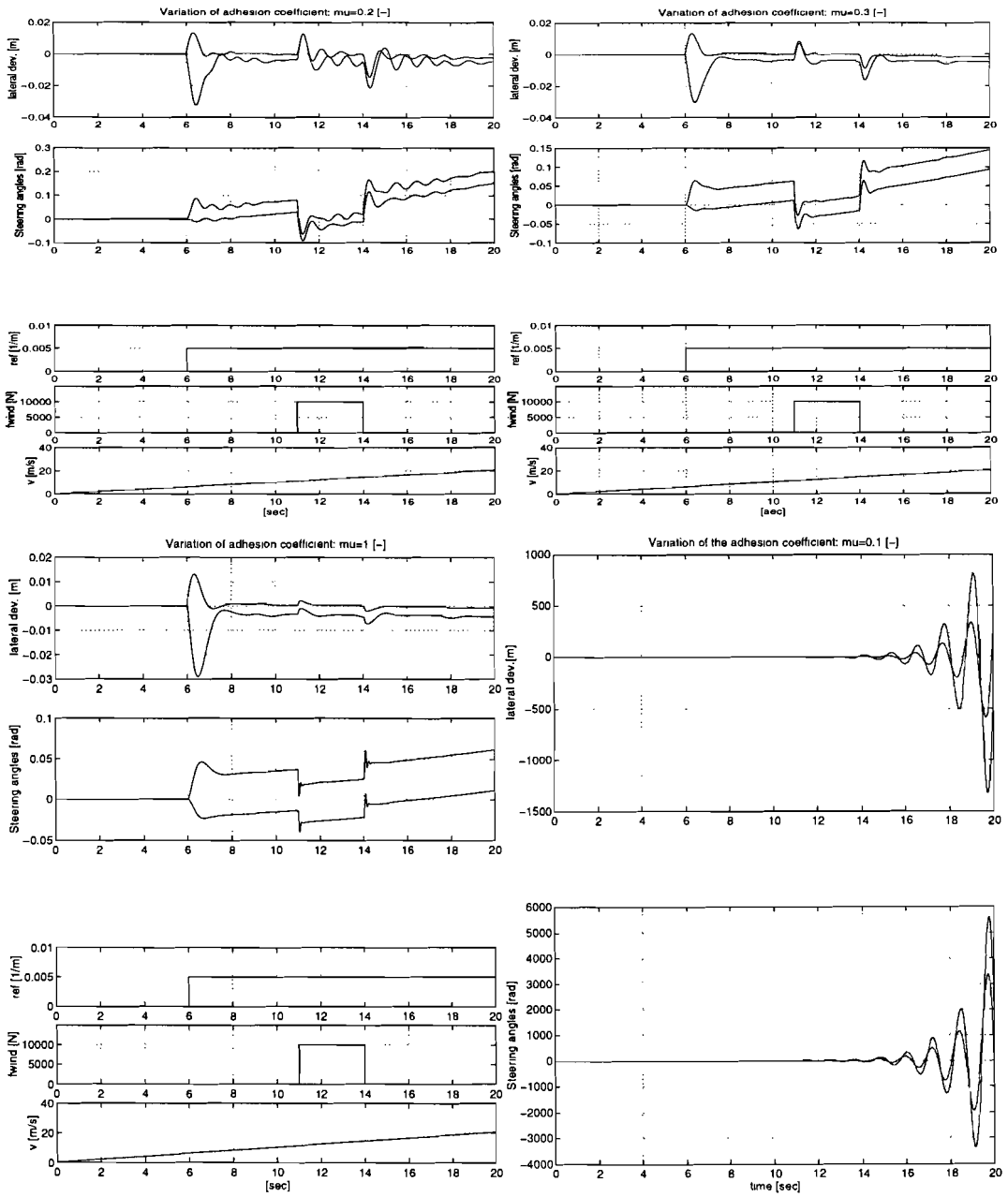


***Figure 5-7: Simulations different road conditions: icy, wet, dry***

Upper left figure shows us nearly icy condition ( $\mu = 0.2$), we see that the controllers are still stabilizing the system. However, there are some oscillations , the system tends to instability. For $\mu = 0.1$ the system gets unstable. The upper right figure shows us that for $\mu = 0.3$ the system is stable. There are no oscillations (indication, wet road condition: $\mu = 0.5$). The steering angles are smaller from the previous case and so are the lateral deviations. So if the value of $\mu$ gets bigger, the deviations are getting smaller. The figure beneath shows the dry road condition, the system is stable. If we look at the steering angles in this figure, then it becomes clear that steering is fast (small settling time of the steering angles), and accurate on dry road condition, in comparison with the icy or wet condition. The steering angles are smaller as in the previous cases. This is because the tires have better grip on the dry road condition. Consequently, the lateral deviations are small for the dry road condition. Thus, the vehicle is more controllable.

From the simulations, it seems that the vehicle is very susceptible for this parameter uncertainty $\mu$ .

This is because the 'normalized mass' $\tilde{m} = \frac{m}{\mu}$ is dependent on this parameter. So a little change of this parameter causes the system characteristics vary drastically, because of the large mass m=[10000..16000] [kg] and so the normalized mass varies in a large range for example for $\mu$ =0.5 between [20000..32000] [kg] . The system zeros move to the imaginary axis and the system becomes less damped, which can result in a large overshoot

- Simulation with limited steering angle rate

In reality the steering angles, and also the steering angle rates are clamped to a certain maximal value. This maximal value can be determined by simulations.
For this Simulation a Rate-limiter block must be placed in the Simulink-scheme.

We discuss four situations:

**Table 5-1: Determination, maximal steering angle rate.**

| $\dot{\delta}_f, \dot{\delta}_r$ [*rad* / sec] | State [controllable or not] |
|---|---|
| 0.6 (34.3 deg/sec) | not |
| 0.717 (41.08 deg/sec) | not |
| 0.7175 (41.11 deg/sec) | just/yes |
| 1 (57.3 deg/sec) | yes |

The four time responses are given below,

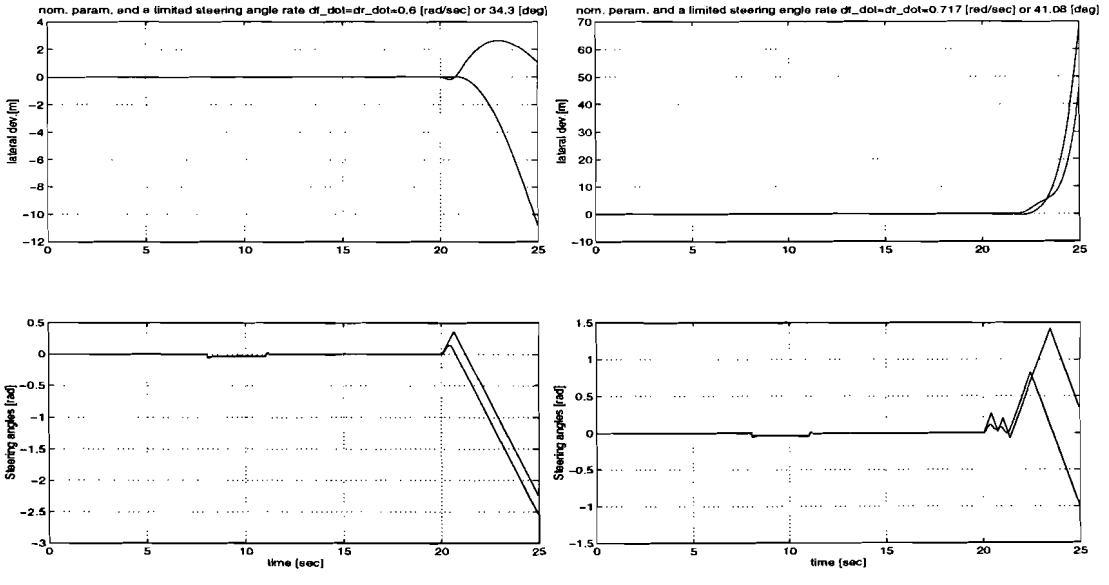

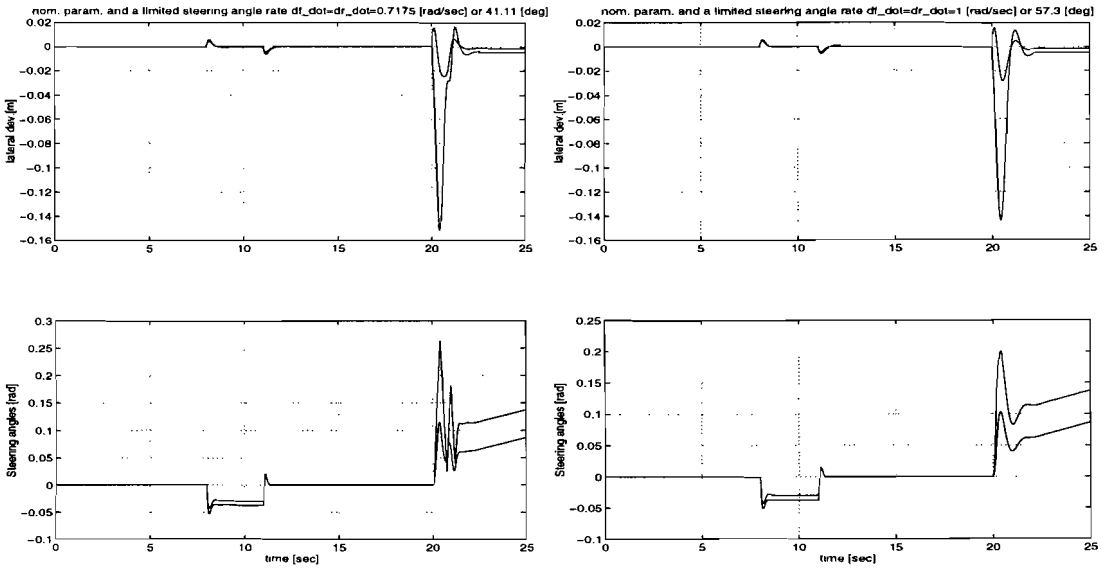


***Figure 5-8: Determination of the maximal steering angle rates at high speeds.***

From the first two figures of figure 5-8 we see that the controller tries to stabilize the system, but due to limited steering angle rate, this is not possible. From the last two figures it is clear that the controller can stabilize the system, since we allow a smaller constraint (larger steering angle rate). So, the maximum steering angle rate is:0.7175 [rad/sec] or 41.11 [deg]. The last figure there is no problem at all. It is also to interesting, to see that the other outputs show a large overshoot in case for limited steering angle rate ;

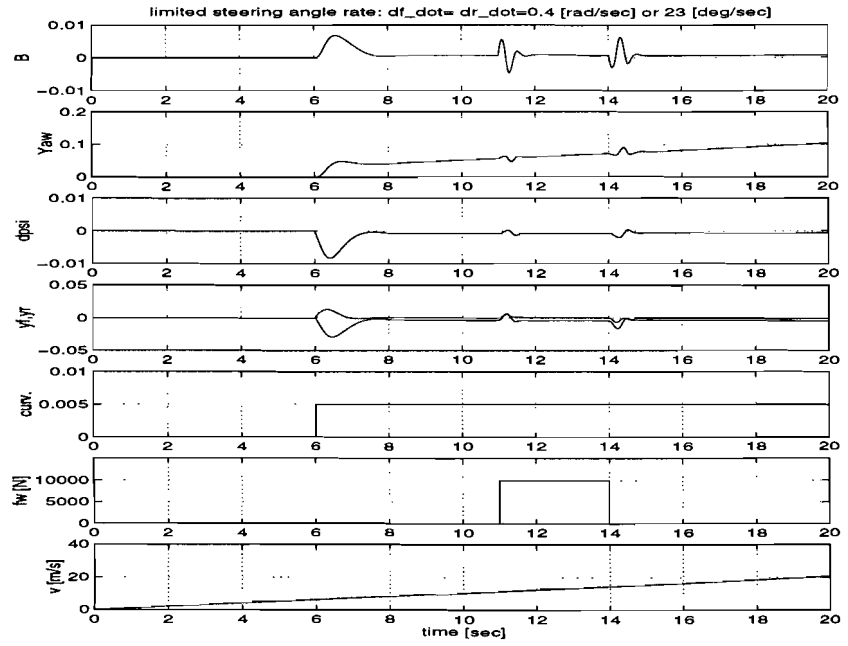


***Figure 5-9: Influence wind force on the outputs for a limited angle rate.***

The influence of the wind disturbance on the slip angle (B) can be clearly seen in this figure; If we look at the first output, the side slip, shows a large deviation both for the curvature which starts at t=6 sec and a wind disturbance at t=11 sec. So the order of magnitude of the wind disturbance is large, if there is a limited steering angle rate. This confirms the remark in the section closed loop transfers: the transfer function from the wind disturbance to the steering angle rates forms a bottleneck.

- Variations of the cornering stiffness

The variation in the cornering stiffness of the tire is also represented by the road adhesion coefficient because the lateral forces are dependent on this parameter by $f_i = \mu \cdot c \cdot \alpha_i$, with i=f, r. But suppose that the cornering stiffness is also different by itself $c_f$=198 [kN/rad] and $c_r$=470 [kN/rad]; for example, the rear tires have larger value (broader road patch) is used. Then the following simulation let us see what happens:

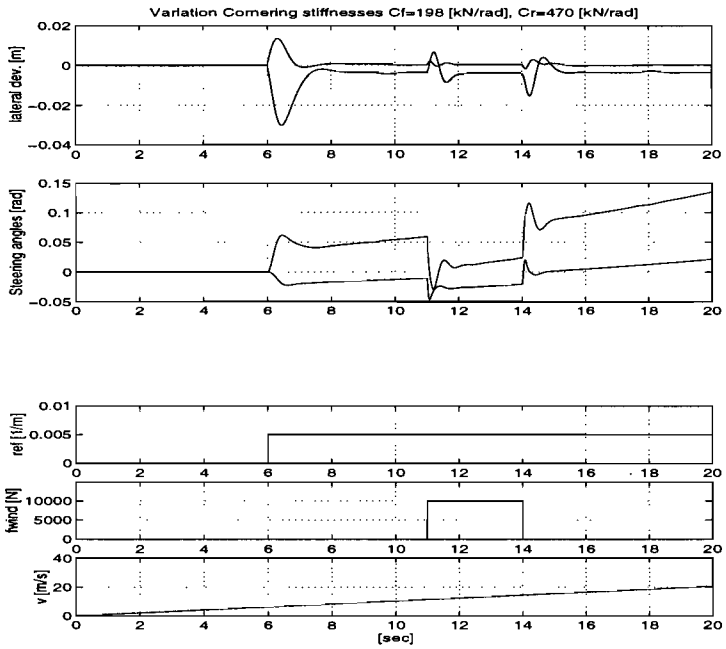


***Figure 5-10: Different types of tires is used.***

If we look at the steering angles in this figure, then we see that the front steering angle increases more then the rear steering angle. The rear steering acts slow, because of the larger value of the cornering stiffness.

- Shifted center of gravity (CG)

The center of gravity shall be shifted to rear, if all the people in the bus are sitting at the rear. And vice-versa. This can be simulated by changing the distance between the CG and the axles: rear($l_r$) and front ($l_f$). Figure (5-8) shows this.

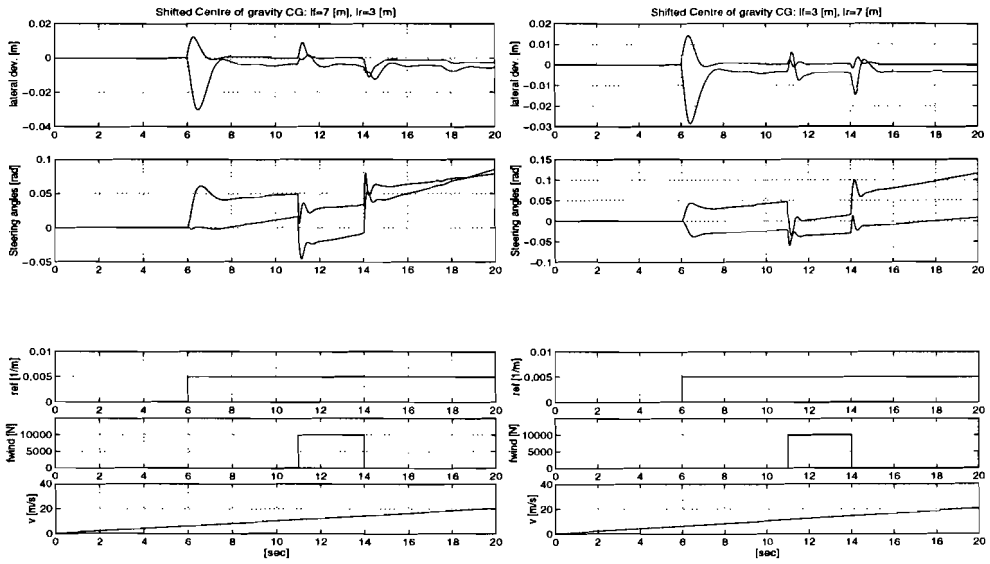


*Figure 5-11: Shifting the center of gravity CG*

If we shift the CG to the rear, left figure, the rear steering system responds more, the rear steering angle increases more and gets even bigger then the front angle, to maintain the same lateral deviation (keeping track). The figure on the right shows that moving the CG to front causes the front steering to be more active. This situation can be compared with the previous figure.

## 5.3. Shifting the sensors place

If we should shift the sensor place towards the CG or from it, then we can see how the controller which was designed for $l_s$=2.5 [m] reacts. Figure (5-9) shows some simulations for various distances.

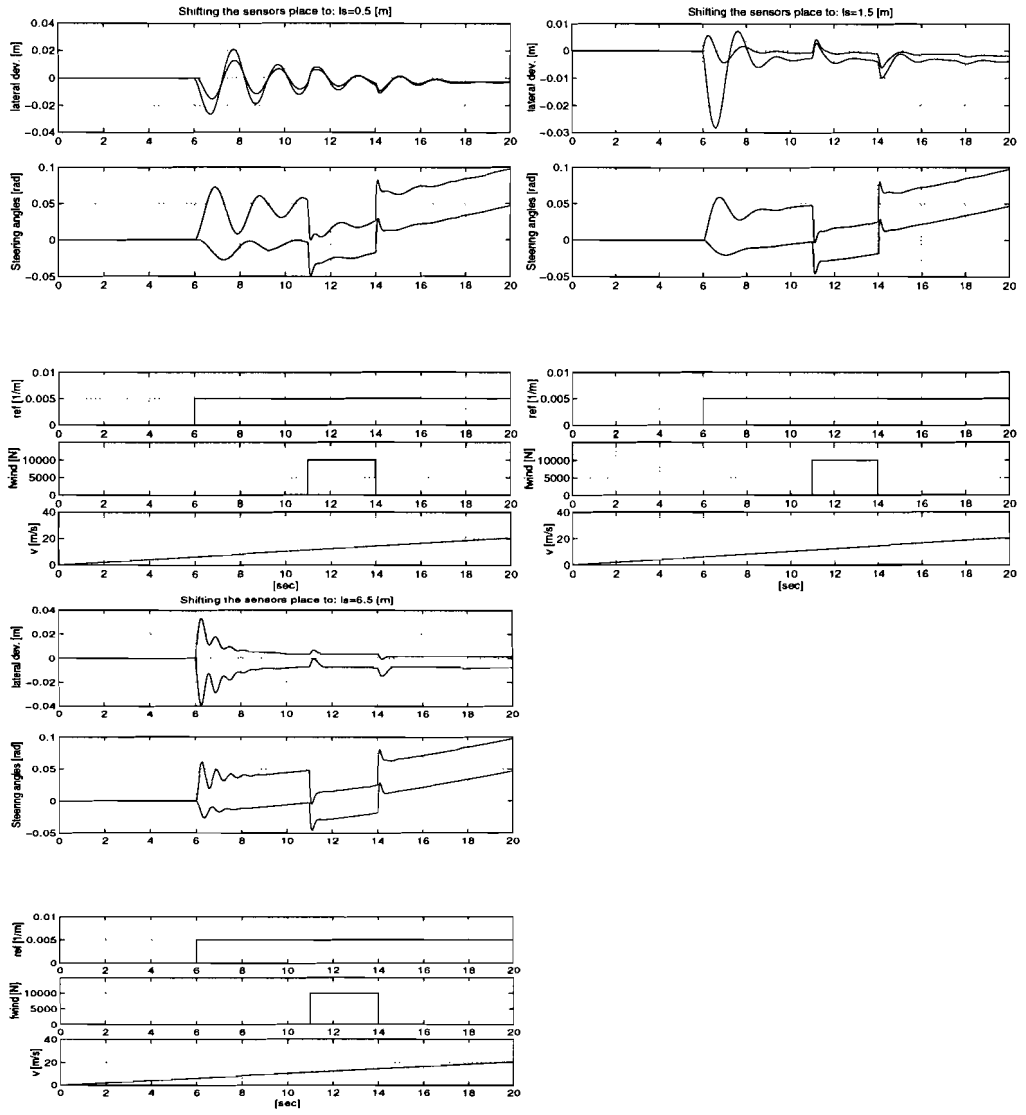


***Figure 5-12: Shifting the sensors place***

If we shift the sensor towards the CG the simulations show oscillations, upper left figure. Moving it from the CG (upper right figure) gives a stable result. If we should move it further, the system reacts slow, it takes long to make the lateral deviation small. Also, there is some oscillation.

- We simulate the situation when entering a bus "stop"-bay, where the velocity starts to decay from v=3 [m/sec.] to zero. Figure 5-13 illustrates this,

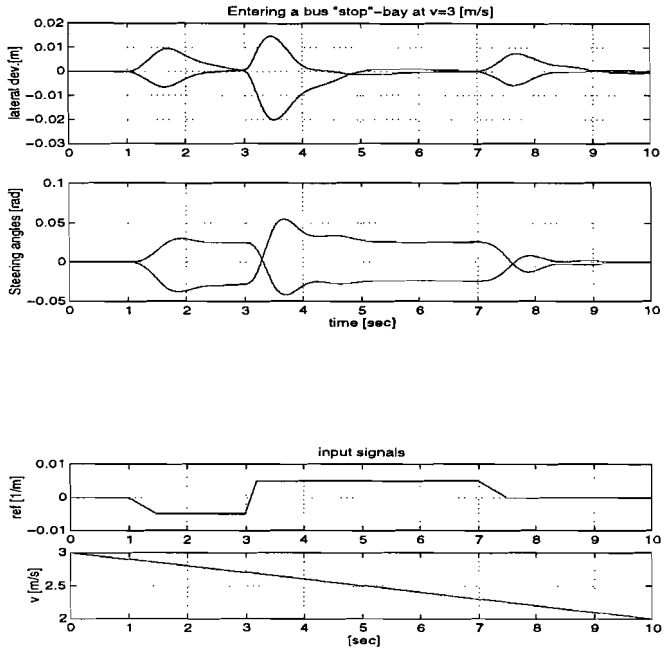


***Figure 5-13: Entering a bus "stop"-bay v decays from 3 [m/sec] to zero.***

At t=1 [sec], the bus enters the bay and leaves the bay at t=3 [sec] (with a opposite curvature direction). At 7.5 [sec.], the bus is "back on track". Actually, the bus makes not a real bus- stop somewhere between 1.5 and 3 [sec] , since the velocity must be zero during a real stop and this is outside control range; the controller can not stabilize the bus. But, for the understanding, it's sufficient to assume that the velocity decays in this interval. We see further, that the steering angles and the lateral deviations, have a acceptable levels.

The results presented in this section are done for gaining velocity, but this can of course also be done for the decay of the speed.

- To illustrate the vehicle's behavior for "driving a trajectory" the following simulation is done,

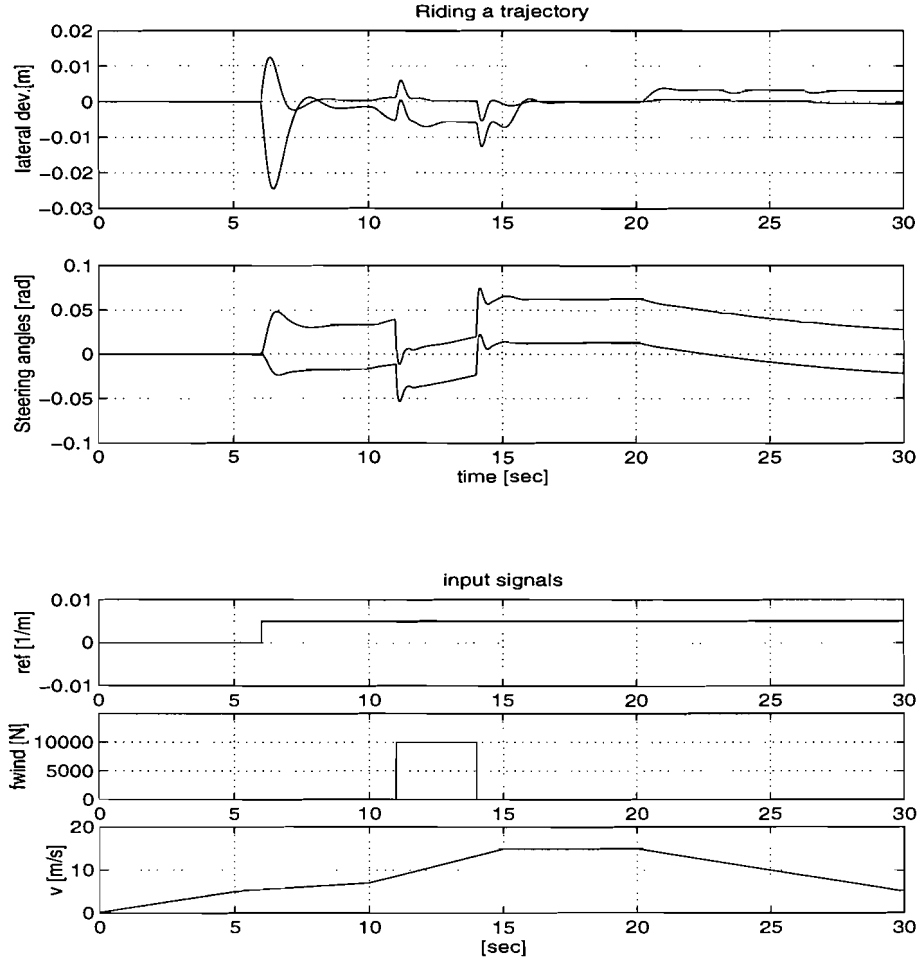


***Figure 5-14: Driving a trajectory***

From this figure, we see that the steady state error, of the lateral deviations becomes larger in the time interval 11..14 [sec] (in comparison with the interval 6..10 [sec]), because the acceleration of the vehicle is larger. Between 15..18 [sec.] we see that the steering angles are constant (acceleration zero), because we have a constant velocity in this interval. In the interval 18..30 [m/sec] there is a decay of the speed (negative acceleration). The direction of the steering angles are gradually heading towards the steady state cornering.

## 5.4. Simulations Bumpless- transfer behavior

In this sub-section we shall discuss with the aid of simulations, the Bumpless- Transfer mechanism. This will be done in the following steps;

1. Simulations without Bumpless- Transfer, from now on abbreviated as (BT).
2. The simulations with (BT) but without the use of the active filters used for smoothing (Filter1..Filter6 in controller scheme).
3. Simulations with (BT) and the use of the smoothing filters (Filter1..Filter6).

We shall elaborate these steps below,

1. The simulation resulted from this configuration is given in figure 5-10,

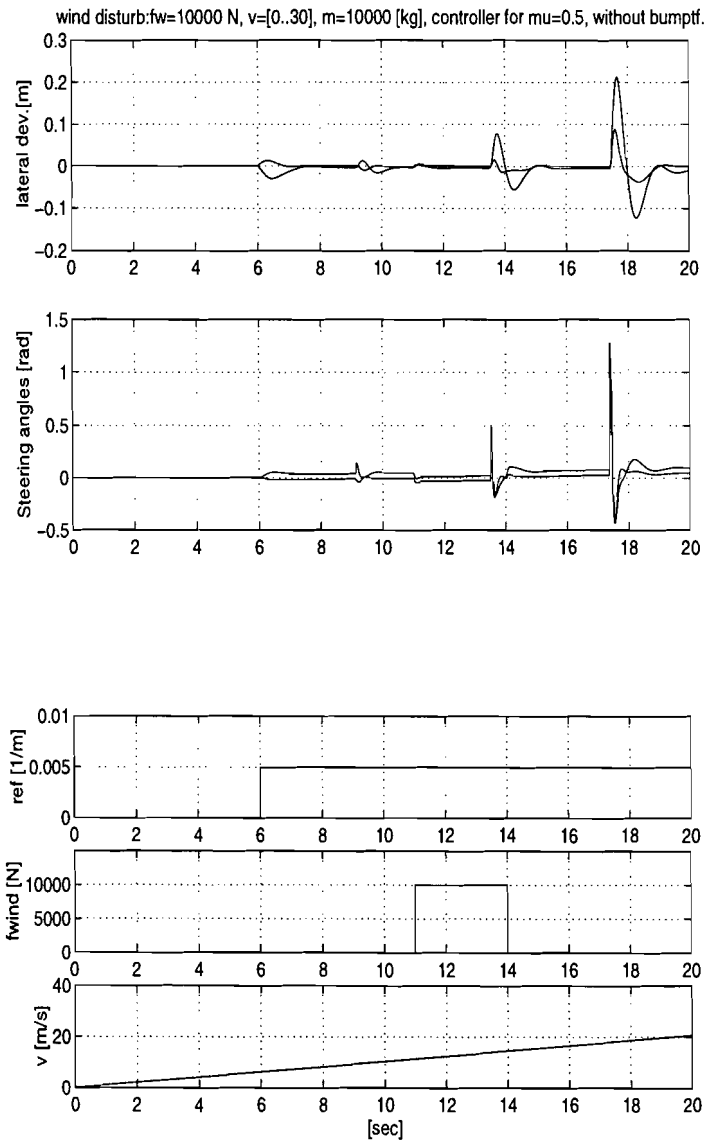


*Figure 5-15: Simulation without Bumpless Transfer*

In figure 5-15, the switching events are on the time instants: $t_{sw1}$=9, $t_{sw2}$=13.5, $t_{sw3}$=17.5 [sec.]. The velocities at the switching moments are given in Table 5-1.

In Table 5.1 the maximum values of the steering angles and the maximum lateral deviations at these time instants are given.

**Table 5-1: The maximum values of the steering angles and lateral deviations.**

| Time [sec.] | $v_{switch}$ [m/sec] | $\delta_f$ [rad.] | $\delta_r$ [rad.] | lat. dev $y_f$ [m] | lat.dev $y_r$ [m] |
|---|---|---|---|---|---|
| $t_{nom,cur}$=6 | - | 0.08 | -0.04 | -0.025 | 0.01 |
| $t_{s1}$=9 | 9.5 | 0.15 | -0.05 | -0.02 | -0.015 |
| $t_{nom,wind}$ | - | -0.01 | 0.005 | 0.005 | 0.005 |
| $t_{s2}$=13.5 | 14 | 0.5 | 0.2(!) | 0.075(!) | 0.02(!) |
| $t_{s3}$=17.5 | 18 | 1.25(!) | 0.75(!) | 0.21(!) | 0.1(!) |

From this table we can conclude that the values denoted by (!) at these switching moments are larger then the nominal values, where at t=6 sec. a curvature starts and at time t=11 sec. a wind gust occurs.

The velocity v is a ramp function v= a.t, where a is the acceleration [m/s$^2$] of the vehicle. Also in this figure we see, that switching at higher speeds at instant ($t_{s2}$, $t_{s3}$ ) the deviations are getting larger; at higher speeds the system has lower damping. Despite this, the switching between the controllers must be smooth.
The switching error (k3 in the controller scheme) and the simulation in figure(5-11) below is of course zero, because there is no feedback of the Bumpless- transfer.

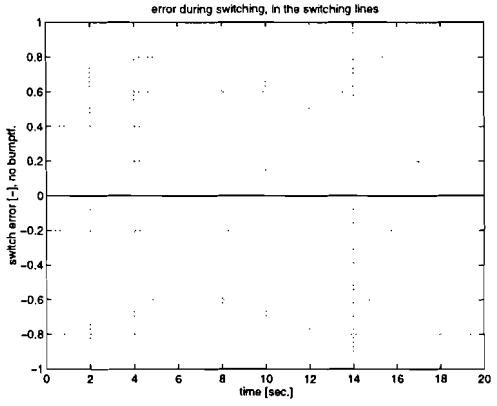


***Figure 5-16: The switching error***

2. Simulations with (BT) and without smoothing filters

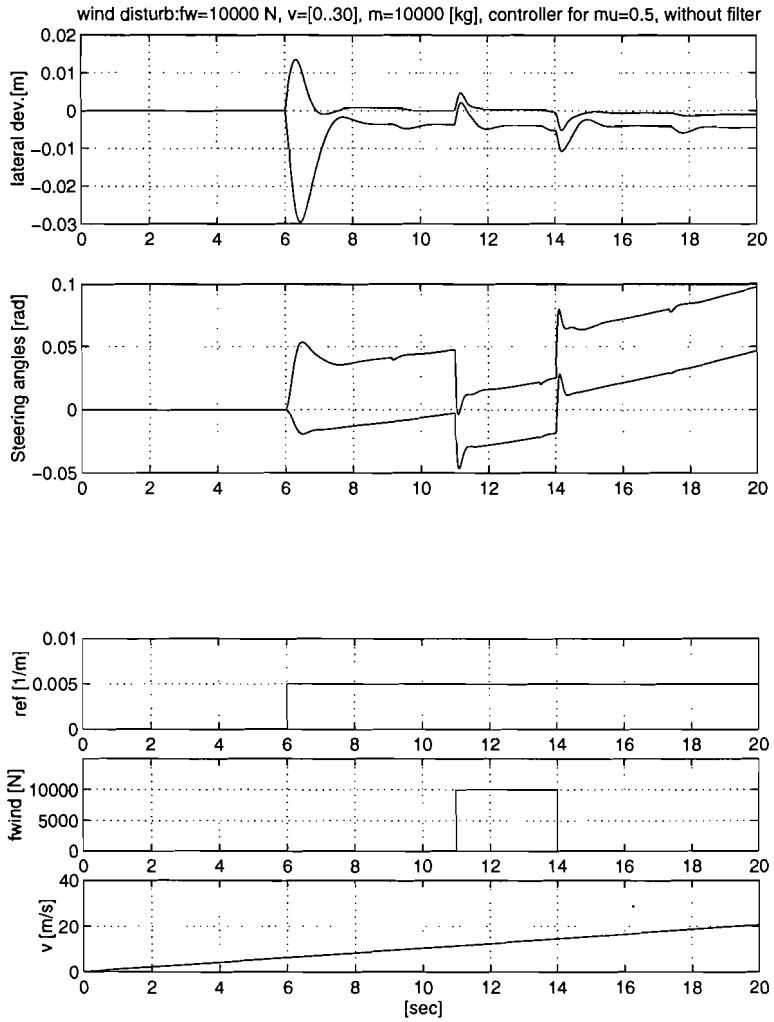


***Figure 5-17: Simulation (BT) without smoothing filters***

From the figure we can see the effect of the Bumpless transfer method; The deviations (bumps) at the switching moments at (6, 13.5, 17.5 [sec]) are very small. It seems that the methods works well. But we must be careful, since the error which is induced during switching, can be very large (large spikes, max. magnitude 60) and this error signal contains high frequent noise. Figure 5-17 illustrates this.

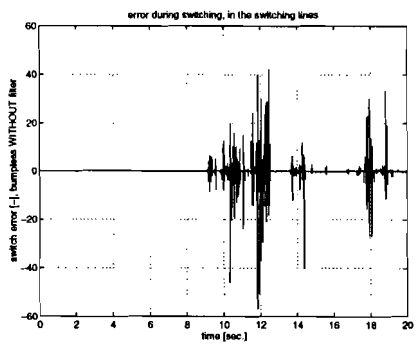


***Figure 5-18:The switching error without smoothing filters.***

3. Last step is the use of complete configuration (BT) and smoothing filters.

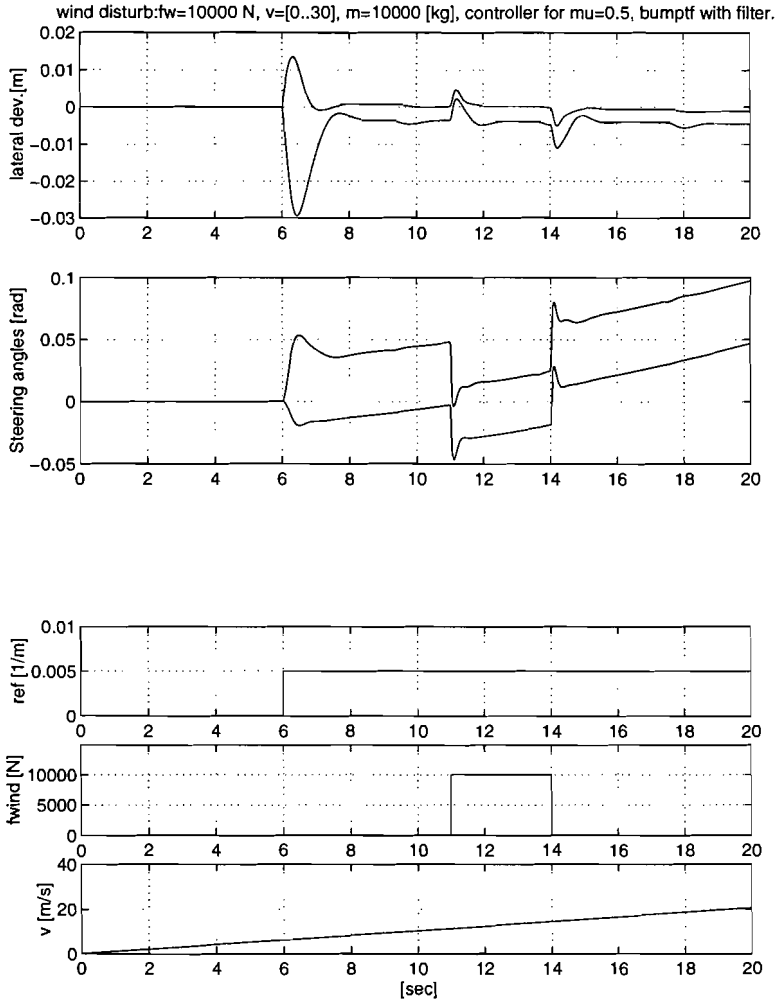


***Figure 5-19: Simulations with (BT) and smoothing filters***

By adding the smoothing filters, we can suppress the noise and the results are much better (the bumps at the switching moments are almost vanished). Figure 5-18 and figure 5-19 show this. The amplitude of the noise is small ($4.10^{-3}$) and the high frequent noise is suppressed, see figure 5-19.

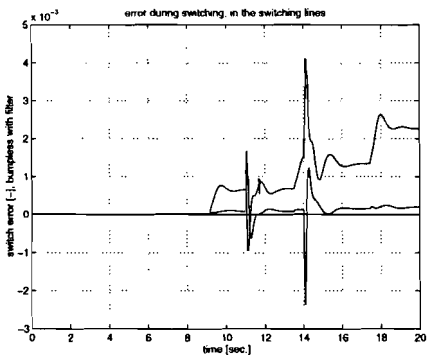


***Figure 5-20: The switching error, with high frequent noise suppressed***

If we compare the results from the three previous simulations, then the implementation of a Bumpless- transfer becomes inevitable.

# 6. Conclusions and recommendations.

Conclusions:

A model to describe the lateral deviation of the front and the rear of the vehicle has been described. This model is augmented with the model of the circular path, that has to be followed. In this model also the actuator dynamics are incorporated, to better describe the vehicle's behavior. We assume that the actuators have a bandwidth of 31.4 [rad/sec] or 5 [Hz], which is enough for this purpose since the process has a low frequent behavior. The model is tested with simulations and gives acceptable results. The bandwidth of the system is about 4 [rad/sec] or 0.64 [Hz]. So, the controller action shall be at low frequencies up to 10 [rad/sec].

Since we have a velocity range of v=[0..30] [m/sec], we have to use more than one controller. We have divided this interval into 6 sub intervals. For each interval, a controller is designed. This number of controllers is a choice, which is determined by the performance requirements. We could have also chosen less controllers but, this will be at the cost of the performance.

For controller design, a mixed sensitivity, $H_\infty$-control design approach is used. Because with this method, we can define our design specifications; control objectives and control constraints with proper sensitivity functions which are determined by the proper choice of the weighting functions. Unmodelled process disturbances occur due to parameter uncertainties like, the adhesion coefficient $\mu$ (t) and v(t). The controller has to be robust against these uncertainties. These uncertainties causes peaks in the transfer functions.

From closed loop transfers, we have seen that a large attenuation (-70 [dB]) occurs for the reference signal to the lateral deviations. However, the bandwidth of this sensitivity function is "small" for the front lateral deviation (up to 2 [rad/sec]) and for the rear (4 [rad/sec]). The maximal reference curvature can be a potential bottleneck with respect to the lateral deviations.

With multiple controllers, mentioned above, we have to switch between them, if the speed is gaining, or when the speed decays.

This switching has to be done "smooth" which means that the states of the previous controller has to be taken over fast by the next controller. This action can only be done, if there is a some kind of a guard mechanism or a mechanism which "warms-up" the next controller to be used. This mechanism is the "Bumpless transfer method". This is a very useful method to make a smooth switching and it has also proven it's 'anti- windup' property, which means that this method clamps the controller input to the process, if the control signal grows beyond the maximal input to the actuator. This growth is caused by the integrating property of the controller.

With simulations of the nominal process, we have verified the design specifications. However the performance (lateral deviations) at higher speeds (and maximal acceleration) above 20 [m/sec] is less, but still acceptable (about 14 [cm]).
With the simulations of the parameter uncertainties, we see that the process is susceptible for the adhesion factor $\mu$ (t); the system becomes less damped. This is also true for the velocity at higher speeds; since the zeros of the system move to the imaginary axis, the system will have a low absolute damping.
We have seen in the case of a wind disturbance, that the steering angle rates are the determinative factor for appropriate response. Angle rates below 41.11 [deg/sec] are not allowed, since the system is then not controllable.

If the center of gravity is shifted, to the rear then the rear steering system becomes more active. If the center of gravity moves to the front, then the front steering system would be more active.

The simulations results for the bumpless transfer method can be discussed as follows:

Suppose that we should not use this method, then simulations shows that, during switching, errors will arise, which are much larger then the desired values. This is of course not favorable. If we should use this method, with only a high gain constant feed back, then the results are much better. But still, if we should look at the error in the feedback loop during a switch in the lines; there is a high frequent noise, with large spikes about 40 [-] order of magnitude. This is improved by using an active filter in the feed back loop, in series with the constant high gain. Then results shows us, that with this "smoothing filter" the high frequent noise is suppressed, and also the large spikes are gone.

From these results, we can conclude that the use of a bumpless transfer method is inevitable.

Recommendations:

The results may be improved by using an other controller design approach, which is a refinement of the $H_\infty$-controller theory: $\mu$-analysis/synthesis technique (here, the symbol $\mu$ is *not* our adhesion factor).
In this method all the uncertainties are brought into a diagonal form which is, as it were pulled out of the rest of the configuration. This method is less conservative as the $H_\infty$-controller design method where, the $H_\infty$-norm of the *maximal* singular value has been shaped by proper choice of the weighting filters. With this method , $\mu$-analysis/synthesis, a specific frequency band can be selected by proper choice of the weighting filters, were the unmodelled dynamics are most disturbing. But, this is of course, at the cost of controller complexity since filters have to be used to characterize the disturbances. This results in more states for the controller.

The $H_\infty$-controller technique or $\mu$-analysis/synthesis may be also used to control multiple carriages.

May be the suspension dynamics, (mass-damper-spring model) /integrated suspension (hydraulic, spring, mass damper) systems can be used to improve passenger comfort. The control system can be developed with $H_\infty$-controller technique.

It is also recommended to look if it is possible to use a few (3 or 4) controllers. This can be done by proper division of the uncertainty area (μ,v) for each controller. It is unlikely to use only one controller.

# *References*

*[1] **Bosch***, P.P.J van den ; Hendrix, W.H.A.
CONTROL OF THE LATERAL AND LONGITIDUNAL POSITION OF THE BUS.
IFAC Transportation systems
Ghania, Greece, 1997

*[2] **Bruin***, D. de; van den Bosch, P.P.J.
LATERAL CONTROL OF A FOUR- WHEEL STEERED VEHICLE.
IFAC Transportation systems
Sevilla, Spain, 1998

*[3] **Engelaar***, P. J.
MODELING AND CONTROLLING AN ARTICULATED VEHICLE.
Master thesis, august 1997.
Eindhoven University of Technology

*[4] **Riekert***, P. And Schunk, T.E.
ZUR FAHRMECHANIK DES GUMMIBEREIFTEN KRAFTFAHRZEUGS.
Ingenieur-archiv, band 1940, pp210-223.

*[5] **Ackerman***, J. and A. Bartlett; D. Kaesbauer; W. Sienel, R. Steinhauser, V.I. Utkin
ROBUST CONTROL. 'Systems with Uncertain Physical Parameters'
Springer- Verlag London, 1993

*[6] **Ackermann***, J and J. Guldner; R. Steinhauser, V.I. Utkin.
LINEAR AND NONLINEAR CONTROLER DESIGN FOR ROBUST AUTOMATIC STEERING.
In: IEEE Transactions on Control Systems Technology, Special Issue on Automotive Control
Vol.3, No.1, march 1995, p. 132-142.

*[7] **Chao***, P.C.
THE LATERAL CONTROL OF A VEHICLE.
Master thesis, 24 april 1997.
Eindhoven University of Technology.

*[8] **Damen***, D. and Weiland, S.
ROBUST CONTROL.
Measurement and control group
Eindhoven University of Technology, 1996

*[9] **Zhou***, K.; Doyle, J.C. and Glover, K.
ROBUST AND OPTIMAL CONTROL.
Prentice- Hall
Upper Saddle River, New Jersey 1996

*[10] **Skogestad***, S.; Postlewaite, I.
MULTIVARIABLE FEEDBACK CONTROL
Analysis and Design.
John Wiley & Sons
New York, USA

*[11] **Hanus***, R; Kinnaert, M and J.L. Henrotte.
CONDITIONING TECHNIQUE, A GENERAL ANTI-WINDUP AND BUMPLES TRANFER METHOD.
Automatica, 23 (6):729-739, 1987.

*[12] **Falkus***, H.M., A.A.H Damen
MULTIVARIABLE H-infinity CCONTROL DESIGN TOOLBOX
Measurement and control group
Eindhoven University of Technology, 1994